Hydrothermal Alteration and Mineral Exploration of Zn-Pb Skarn Deposits of the Kamioka Mine, Central Japan

Hiroyasu MURAKAMI

January, 2001

Hydrothermal Alteration and Mineral Exploration of Zn-Pb Skarn Deposits of the Kamioka Mine, Central Japan

Hiroyasu MURAKAMI

A dissertation submitted to the Doctoral Program
in Geoscience, the University of Tsukuba
in partial fulfillment of the requirements
for the degree of Doctor of Philosophy (Science)

January, 2001

ABSTRACT

Skarn deposits occur throughout the world and have been mined for a variety of elements. Skarn is generally developed around or in the vicinity of limestone, and is mainly composed of Ca-dominant minerals (i.e. garnet, pyroxene, epidote) due to addition of Ca from the limestone. Since the mineral assemblage of skarn is mappable in the field and serves as the alteration envelope around a potential ore body, details of skarn mineralogy and zonation can provide key information regarding the genesis of skarn deposit and in planning exploration programs. Despite a common occurrence, limestone in skarn deposit has not been studied owing to its relative uniformity in mineral assemblage and elemental composition. Recent studies, however, have demonstrated the zonal anomaly of $\delta^{18}O$ and $\delta^{13}C$ values in limestone around ore body. Although the isotope method is noted to be promising in detecting hydrothermally-altered limestone and as a new exploration tool, detailed mineralogical and geochemical studies have not yet been done on the limestone with the isotopic anomaly. Extensive exploration has been conducted in the past decade in the Sako-nishi area of the Kamioka Zn-Pb-Ag skarn mine, central Japan. Analysis of stable isotope data shows that the $\delta^{18}O$ and $\delta^{13}C$ values of crystalline limestone ranged widely between -2.5 and +21.1‰ and between -5.9 and +5.3‰, respectively, due to interaction with hydrothermal fluids with a dominant meteoric water component. The present report addresses the mineralogical and elemental composition of isotopically altered limestone in the Sako-nishi area, and presents potential indicators applicable to the mineral exploration of skarn deposits.

The Sako-nishi limestone is classified into four groups as A, B, C, and D in 5‰ interval by oxygen isotopic composition. A decrease of $\delta^{18}O$ value correlated with; (1) increasing transparent fine-grained and veinlets calcite, (2) dominance of hydrothermal calcite which is enriched in Mn, depleted in Sr, and has bright cathodoluminescence image, (3) progressing hydrothermal alteration where clinopyroxene of original limestone altered into actinolite within weakly altered

zone, developing more alteration, chlorite within strongly altered zone, (4) dominance of hydrothermal chlorite in altered limestone which has $\delta^{18}O$ value of less than 10‰ and is enriched in Fe and small amounts of Mn content compared to mafic minerals within unaltered limestone. The enrichment of Fe and Mn was more conspicuous in calcite and chlorite in skarn deposits; the Mn content of hydrothermal calcite developed as a vein and showing bright luminescence image is 1 wt.% in maximum while that of calcite in skarn reaches maximum 2 wt.% or greater and is also characterized by low Sr content (300 ± 100 ppm). It was calculated using chlorite geothermometer that chlorite formed at temperatures around 200-250 ℃, which is compatible with the homogenization temperature of fluid inclusion and is lower than the formation temperature of skarn clinopyroxene around 300-350 ℃. The occurrence and chemical composition of hydrothermal minerals in the limestone, skarn, and ore indicate that the ^{18}O-depleted zones were formed in the later stage from fluids, which were responsible for mineralization and skarnization, and for Fe and Mn enrichment.

In dissolution experiments on limestone, acetic acid dissolves carbonate while hydrochloric acid dissolves the carbonate and chlorite selectively. The concentration of Al, Mn, Fe, and Zn in hydrochloric acid leachate increase with decreasing $\delta^{18}O$ value, and but Mg does not change conspicuously while only slight changes are observed in Mg and Sr. It is thought that this change is caused by chemical composition of a hydrothermal chlorite and calcite. The Al content (~ 0.1%), Mn content (~ 300ppm), Fe content (~ 0.3%), Fe/Mg ratio (~ 2.0) and Al/Mg ratio (~ 1.0) of hydrochloric acid leachate are effective for identifying altered limestone in the Sako-nishi area. According to exploration of outcrops in the Sako-nishi area, four mineralization zones are known. Hydrochloric acid leachate of limestone from these areas has a high Mn/Sr ratio and low Mg value. Interestingly however, limestone depleted in $\delta^{18}O$ does not correlate with the currently known distribution of mineralization zones. Possible causes may include weathering or isotope fractionation at low temperature. An index which combines

elemental composition with stable isotopic composition is more effective for specification of mineralization. The indexes used here in are a clearly anomalous along the 7-GOHI fault and the Atotsu-1GO fault. Accordingly, results show that these faults played a major role in facilitating the passage of hydrothermal fluid responsible for mineralization. This structure indicates that the skarn deposits of the Sako-nishi area belong to Mozumi-type Zn-Pb skarn deposits. It is suggested that isotope alteration zones are produced by sudden precipitation of fine-grained calcite from the hydrothermal fluid in the minute cracks which developed in limestone, and isotope exchange reaction between limestone and Mn-Fe rich hydrothermal fluid which developed during the latter stages of skarnization.

The hydrothermal alteration is also observed in silicate rocks (Inishi-rock and gneiss) where chlorite, calcite, quartz, pyrite, epidote, and prehnite occur as vein or replacement of plagioclase and mafic silicates. The leachates of silicate rocks using aqua-regia solution show a systematic increase of Ca, Sr, and Mn due to hydrothermal calcite and that of Fe and S due to pyrite as the $\delta^{18}O$ value of associated limestone decreases. The Fe/Al and Ca/Na ratios were effective for the separation of hydrothermally-altered silicate rocks from unaltered ones. Mineral assemblages observed in altered rock of the Sako-nishi area, such as high Mn calcite and high Fe chlorite, closely resemble chloritic and propylitic alteration hosted by silicate rocks recognized in Zn-Pb type vein deposits. Accordingly, analysis of acetic acid and hydrochloric acid leachate in addition to cathodoluminescence image provides an effective tool for identifying hydrothermally altered rock of Zn-Pb type deposits including skarn type because it makes possible the detection of the elemental composition of hydrothermal minerals such as chlorite and carbonate and because of the rapidity and convenience of analysis.

Key words; Kamioka mine, skarn deposit, limestone, oxygen isotopic composition, geochemical indicator, cathodoluminescence, mineral exploration

CONTENTS

LIST OF TABLES

LIST OF FIGURES

Chapter 1 INTRODUCTION

Hydrothermal alteration is commonly and widely developed around ore deposit. The style of the alteration is variable dependent on the type of hydrothermal ore deposit such that information regarding the petrography, mineralogy, and geochemistry of the altered rock is crucial in understanding the genesis of mineral deposit and in planning mineral exploration. Skarn deposit is characterized by the presence of Ca-dominant minerals. Mineral and chemical zoning is so widespread in skarn deposit that it has been applied in the past decade in exploration for skarn ore deposits (Meinert, 1992). In contrast, limestone, the major host rock of skarn deposits, has not been paid much attention owing to its homogeneous nature in the mineral assemblage and chemical composition.

Shallow intrusives and country rocks in their vicinity are subject to oxygen isotope alteration between rock and fluid associated with hydrothermal activity (Taylor, 1973; Matsuhisa et al., 1980; Criss et al., 1991). In the case of skarn hydrothermal systems, limestone is depleted in ^{13}C as well as ^{18}O around skarn ore deposits (Shimazaki et al., 1986; Fu et al., 1991; Sakurai and Shimazaki, 1993). This isotope anomaly is so sensitive in detecting the location and magnitude of fossil hydrothermal activities that stable isotope techniques, particularly those for $\delta^{18}O$, have been increasingly applied in the past decade in exploration for hydrothermal ore deposits (Nesbitt, 1996).

The Kamioka mine is a world class zinc-lead skarn deposit located within the Pre-Jurassic Hida metamorphic belt of central Japan. The mine has produced 82 million tons of ore (the average grade 5.0%Zn, 0.7%Pb, 33g/tAg) (Sakurai and Shimazaki, 1993). Various ideas have been proposed for the origin of the Kamioka deposit (Shiobara, 1961; Sakai, 1963; Akiyama, 1980). Shimazaki and Kusakabe (1990a) advocated a genetic model where the deposit formed at relatively shallow depths (Shimizu and Shimazaki, 1981), involving a large-scale convection system dominated by meteoric water and driven by large felsic intrusions at depth of late Cretaceous age. Oxygen-carbon isotope (Wada, 1978; Shimazaki et al., 1986),

hydrogen isotope (Shimazaki and Kusakabe, 1990b), and lead isotope (Sasaki et al., 1982) data support this meteoric water circulation hypothesis. According to the hydrothermal circulation model, the isotopic composition of limestone originally-enriched in ^{18}O and ^{13}C contents becomes low toward the center of hydrothermal activity. In 1991, the Metal Mining Agency of Japan (hereafter MMAJ) and Mitsui Mining & Smelting Co. Ltd. (hereafter MMS) utilized the isotope technique based on the meteoric water circulation model in the Sako-nishi area of Kamioka. Exploration succeeded in identifying high-grade zinc ore (Zn:13 %) over 40 m in width in limestone characterized by low $\delta^{18}O$ and $\delta^{13}C$ values (Hirokawa et al., 1995; Naito et al., 1995).

Like this, much geochemical data of stable isotopic composition of limestone in the vicinity of the Kamioka deposits have been accumulated during these past 10 years. Kano (1998) has also made the comprehensive research on the limestone in the Hida belt. Notably however, most of the studies have not petrographically and geochemically described limestone around deposits focusing on especially occurrences and feature of hydrothermal mineral which are expected existence in altered limestone, and so have not addressed either these sources of variation of stable isotopic composition.

Limestone is known to contain minor and trace elements such as Mg, Mn, Sr, and P (e.g., Fujinuki, 1973). The chemical composition of limestone varies depending on the depositional environment and to be altered by geological processes after deposition. For example, during diagenetic alteration, carbonates generally show an increase in Mn, Fe, and Zn with a decrease in Sr and Na (Brand and Veizer, 1980). According to Schuiling and Oosterom (1966), concentrations of Sr and Ba in regionally metamorphosed limestone on Naxos in Greece decrease with increasing metamorphic grade. In a hydrothermal system located in northwestern Sicily, mineralized limestone is enriched in Sr as well as Fe and Mn. It is, therefore, expected that the limestone in skarn deposits would vary in composition with a change in carbon and oxygen isotope ratios. It is prospective that geochemical and mineralogical information of limestone which have isotopic

variation connect with restoration of the hydrothermal system which participated in the skarn deposit formation and development of more highly precise exploration method. However, such comparisons have not yet been attempted.

In this context, I examined the relationship between isotopic composition and constituent minerals, texture, bulk chemical composition, and mineral chemistry of limestone and accompanying rock from outcrop and core samples in the Sako-nishi area, and evaluated the utility of geochemical methods as a survey tool for exploration for Zn-Pb hydrothermal ore deposits.

Chapter 2 Geology

2.1. Kamioka area

The Hida belt was regionally metamorphosed to amphibolite facies (Nozawa et al., 1975) in the pre-Jurassic. Previous studies (Kano, 1973, 1982; Sohma and Akiyama, 1984) have suggested that the belt can be divided into three blocks, eastern, central, and western masses, in terms of variation in occurrence and deformation mode. The Kamioka mine is located within the central mass. Figure 1 shows the geology in the vicinity of the Kamioka mine which has been clarified by many studies (MITI, 1978; Akiyama, 1980, 1981; Kawasaki et al., 1985).

The Hida metamorphic rocks in the Kamioka mining area are composed of gneiss, limestone, and "Inishi rock." They generally strikes NE-SW to N-S and dips 60-70° to the NW. The limestone of the central mass is equigranular as a result of recrystallization during the Hida metamorphism (Fujinuki, 1973; Kano, 1998) and contains graphite, diopsidic clinopyroxene, and olivine. The limestone was pale gray to black in color and occurred as massive or lenticular form within Inishi rock. Limestone varied in thickness from a few centimeters to several meters.

Inishi rock, which was named originally as Inishi syenite rock by Nozawa (1952), consists mainly of plagioclase and diopsidic clinopyroxene with variable amounts of K-feldspar, quartz, and titanite. This rock occurs as blocks or lenses in form between limestone and gneiss around skarn deposits. Funatsu granite of Jurassic age intrudes the Hida metamorphic rocks southeast of the Kamioka mine. The Tetori Supergroup of Jurassic-Cretaceous age crops out at the northern margin of the area and occurs in fault contact with the Hida metamorphic rocks (Fig. 1).

Cretaceous-Paleogene dike swarms, composed mainly of quartz and granitic porphyry, are present around ore deposits throughout the Kamioka mine. The K-Ar age of these hypabyssal rocks has been reported as 65 Ma (Sakurai and Shiokawa, 1993; MITI, 1998a). The K-Ar ages on the alteration minerals, sericite and hastingsite, from skarn deposits indicate that mineralization took place during the Late Cretaceous to Paleogene between 63.8 and 67.5 Ma (Nagasawa and Shibata,

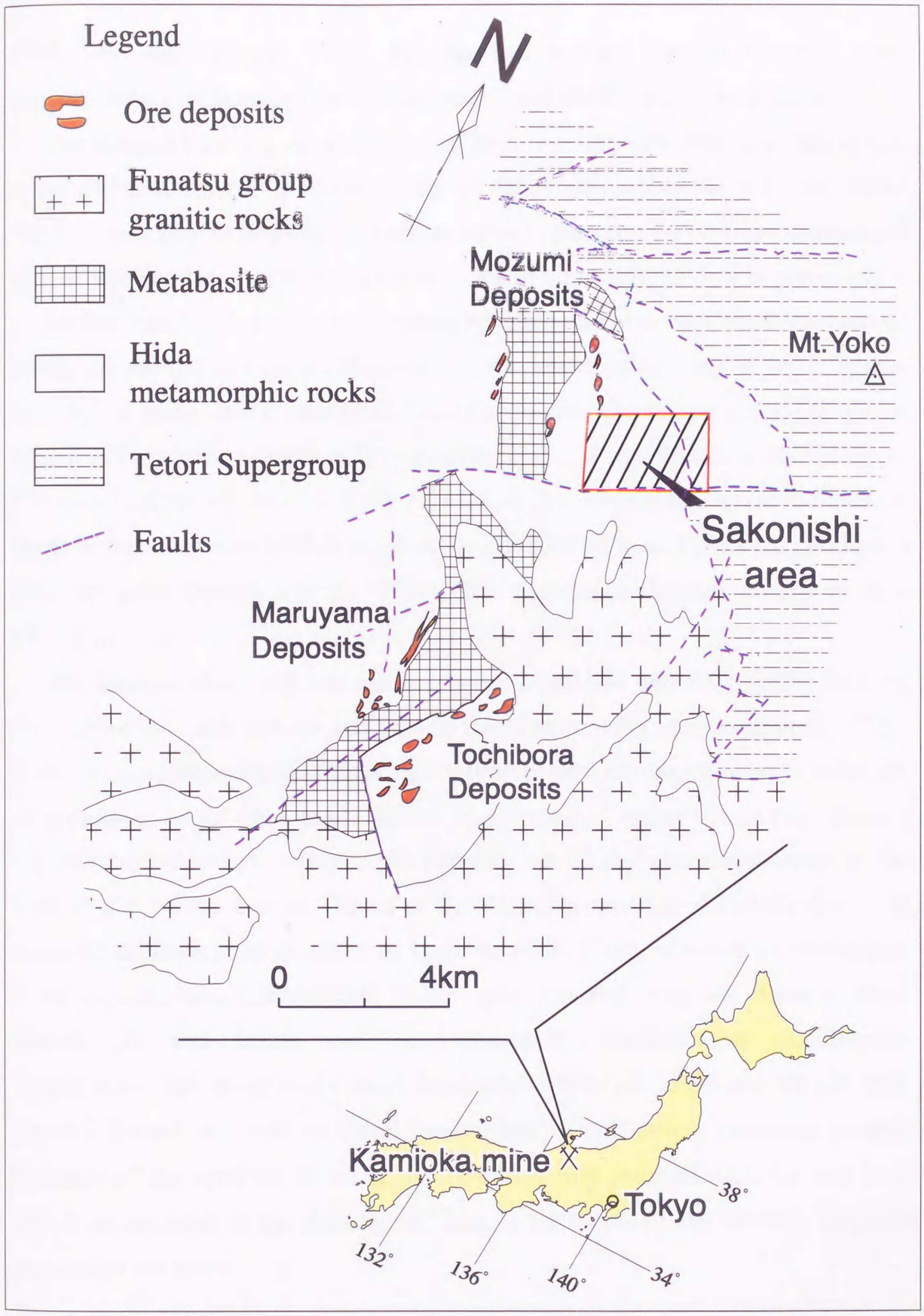

Fig.1. Geological map of the Kamioka mining area (modified after Sakurai et al., (1993), Hirokawa et al., (1995), and Naito et al., (1995)).

1985; Sato and Uchiumi, 1990). The age data indicate that the Kamioka skarn deposits formed at the same time as the intrusion of the felsic hypabyssal dikes.

The Kamioka mining area consists of three ore deposits, Mozumi, Maruyama and Tochibora, from north to south (Fig. 1). There are roughly two ore types called "Mokuji ore" and "Shiroji-ore", which are named after their occurrences. Mokuji ore is most abundant and is characterized as being of large-volume, low in grade, and is composed mainly of prismatic hedenbergitic clinopyroxene with small amounts of sphalerite, galena, and garnet. Shiroji ore is characterized as being of small-volume and high in grade, and is composed mainly of calcite, quartz, sphalerite, and galena with small amounts of sericite. The average grade of representative Shiroji ore is 7.8% Zn, 2.65% Pb, and 27g/t Ag (Tochibora No.9 orebody), while the average grade of representative Mokuji ore is 4.6% Zn, 0.43% Pb, and 29g/t Ag (Tochibora No.2 orebody) (Machida et al., 1987). The Maruyama deposits consist of only Mokuji ore.

The Mozumi skarn deposits are developed along NW and NS trending faults at the intersections of limestone and fissures (Nitta et al., 1971; Kawasaki et al., 1985). In the Mozumi deposits, the following zonation pattern for ore elements is observed, in ascending order from lower levels: iron→copper→zinc→lead. The Mozumi deposits are composed mainly of Mokuji ore, but Shiroji ore predominates in the shallow part of the deposits (Hama et al., 1975; Kawasaki et al., 1985). Owing to observed differences in occurrence, Machida et al. (1987) reported two ore types, silver deposits and disseminated Pb-Zn type deposits; both are different from Mokuji ore and Shiroji ore. Epidotization-chloritization and silicification-sericitization are particularly well-developed within disseminated Pb-Zn type deposits hosted in Inishi rock and gneiss, and exhibit strong structural control. Deposits of this type are found in the Tochibora and Mozumi deposits, and have also been reported in the Atotsugawa area, 2 km south of the Mozumi deposits (Sakurai et al., 1993).

2.2. Sako-nishi area

The Sako-nishi area is located 2 km southeast of the Mozumi deposits and 1.5 km east of the Atotsugawa area (Fig. 1). The Hida metamorphic rocks in this area are a sequence 10 to 100 meters thick of monocline structure intercalated predominantly with limestone, Inishi rock, and gneiss striking N30-40°E and dipping 50-70° to the W. Many faults, the Atotsu-1GO, N20GO, S8GO, and Atostugawa faults, distribute in the area. Of these, the Atotsu-1GO fault striking NE-SW in the southern part of the Sako-nishi area, is considered to have been the main conduit for hydrothermal fluid flow (Naito et al., 1995). The Atotsugawa right-lateral fault occurring at the southern margin of the area has been active in the Quaternary and is a post-mineralization one (Matsuda and Okada, 1968).

In the Sako-nishi area, the MMAJ and MMS have been conducting exploration since 1991. Exploration drilling in 1993 resulted in the discovery of high grade Zn-Pb mineralization (Fig. 2), with one of the holes (5MAHS-7) intersecting 44.4 m of 13.4% Zn at depths ranging from 250 to 280 meters above sea level (MMAJ, 1994). Mineralization here mainly occurs as disseminated Pb-Zn ore along with the Mokuji ore (Hirokawa et al., 1995). Ore is dominated by sphalerite and accompanied with small amounts of galena, chalcopyrite, and pyrite.

The exploration of outcrops led to the identification of four mineralized zones in the Sako-nishi area (Fig. 2) characterized by disseminated sphalerite in limestone. Zone I is distributed around the Atotsu-1GO fault where Shiroji and Mokuji ores composed over is 12 m long and 3.5 m wide, grading 4.6% Zn, 1.0% Pb and 16g/t Ag in limestone layers which strike N35°E and dip 50°W (MITI, 1982). In addition, promising mineralization has been identified east and west of zone I (Sakurai et al., 1993; Hirokawa et al., 1995). Zone II is distributed around the Tochisako old pit that formerly mined Shiroji ore grading 0.8% Zn, 1.1% Pb, and 23g/t Ag (MITI, 1982). Zone III is characterized by soil anomalies with maximum Zn of 712 ppm, Pb of 766 ppm, and Ag of 2.8g/t (MITI, 1997). To date, however, three drill holes have not intersected significant mineralized zone at the deeper parts of either zone II or III. In zone IV, disseminated Zn-Pb mineralization

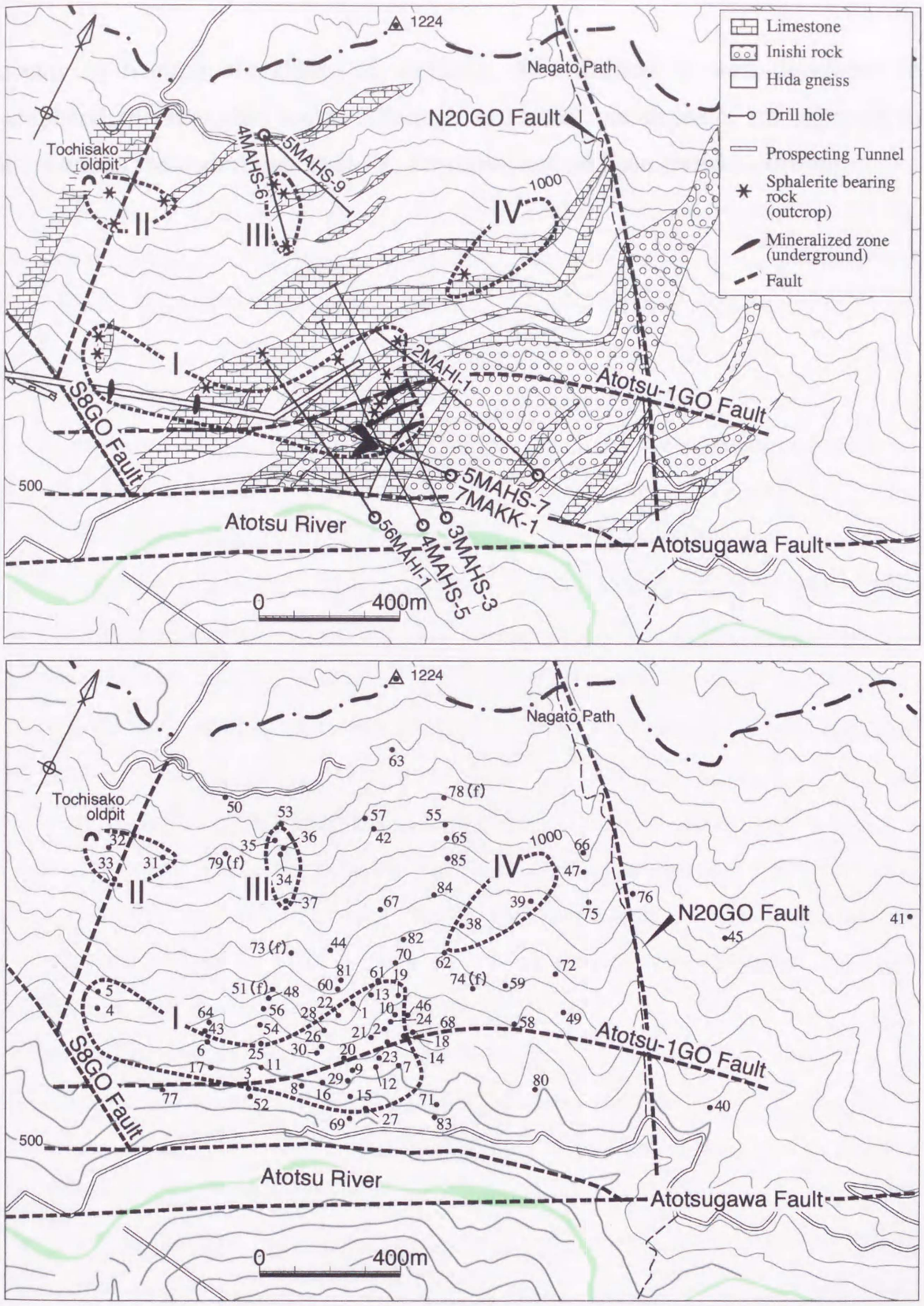

Fig.2. Geological map of the Sako-nishi area (modified after Sakurai et al. (1993), Hirokawa et al. (1995), and Naito et al. (1995)) and locations of mineralized zones, bore holes, and sampling points used for analyses. Mineralized zones from I to IV are indicated by thick broken lines. Asterisks show the location of sphalerite-bearing rocks. Sample numbers are the same as in Table 4. (f) denotes float rock.

occurs in outcropping skarn. In addition, chloritization is well developed in peripheral metamorphic rocks. Although concealed ore deposits are expected to distribute in the underlying zone IV, they have not yet been tested by drilling.

Chapter 3 SAMPLES AND ANALYTICAL PROCEDURES

A total of two hundred seventy-one (271) samples was collected from drilled cores, underground, and outcrops (Table 1). Drilled core samples used for the present study were collected by the MMAJ (56MAHI-1, 2MAHI-1, 3MAHS-3, 4MAHS-5, 4MAHS-6, 5MAHS-7, 5MAHS-9, 7MAKK-1) (Fig. 2). These cores mainly consist of limestone, Inishi rock, biotite gneiss, and hornblende gneiss. Fifty carbonate and fifty-seven silicate rock samples were selected to cover as wide a range of isotopic ratios as possible, consisting of forty-five samples of limestone, three samples of vein calcites, two samples of brecciated carbonates, forty-five samples of Inishi rock, and twelve samples of gneiss (Tables 2 and 3).

Seventy-eight samples were collected from outcropping limestone, and Seventy-three samples from Inishi rock, gneiss, and calc-silicate rocks outcrop (Fig. 2, Table 4). The calc-silicate rocks are mainly composed of calcite and calcium-bearing silicates such as diopsidic clinopyroxene, wollastonite, plagioclase, and titanite, and are considered to have been formed by regional or contact metamorphism of impure limestone (Kano, 1998). In addition, thirteen samples of skarn calcite and limestone samples were collected from deposits in the Kamioka mine including the Sako-nishi area (Table 5). Skarn calcite, named by Shimazaki et al. (1986) for calcite in skarn deposits, was generally white in color, but skarn calcite occurring as druse tended to be pale pink.

The carbon and oxygen isotope ratios have been determined for more than four hundred one carbonate samples, consisting of two hundred fifty-one samples of limestone, ninety-five samples of vein calcite, fifty-five samples of skarn calcite at the University of Tokyo by decomposing carbonate with phosphoric acid (Tables 6, 7, and 8). The isotopic composition of these samples are reported as per mil (‰) in terms of δ notation of $^{18}O/^{16}O$ and $^{13}C/^{12}C$ ratios relative to SMOW and PDB, respectively. Analytical errors are ±0.2‰ for $\delta^{18}O$ and ±0.1‰ for $\delta^{13}C$. The $\delta^{18}O$ value of carbonate from the core tends to decrease with depth, and the ^{18}O depletion is significant below 350 m.a.s.l. where hydrothermal mineral

Table 1 Number of samples for analyses.

	Sakonishi area					Kamioka mining area	
	Ls	carbonate**	Cs	Gn	In	Ls	skarn calcite
Total	78 (296)	(155)	7	51 (12)	15 (45)	4	9
Analyses							
Isotope	78 (251)	(150)	4	4			
ICP-OES							
HOAc	77 (3)		4	4		4	9
HCl	77 (3)		4	4		4	9
Aqua regia	78 (45)	(5)	7	51 (12)	15 (45)		
XRF	78		7	51 (12)	15 (45)		

* ( ) denote collected from drill hole core.

Table 2. Sample descriptions and chemical compositions of carbonate rocks in the Sako-nishi area

Drilling No.	depth	level	rock	group	$\delta^{13}C_{PDB}$	$\delta^{18}O_{SMOW}$	S	Al	Ca	Fe	Mg	K	Na	Mn	P	Sr	Zn
					(‰)	(‰)	(%)	(%)	(%)	(%)	(%)	(%)	(%)	(ppm)	(ppm)	(ppm)	(ppm)
3MAHS-3	123.8m	380mL	Ls	C	2.5	9.6	0.03	0.44	15.00	0.26	0.13	0.01	0.01	320	490	364	20
	136.3m	380mL	Ls	B	0.3	10.4	0.01	0.05	15.00	0.07	0.14	0.01	0.01	105	50	326	6
	153.1m	370mL	Ls	A	1.2	16.1	0.04	0.07	15.00	0.12	0.15	0.01	0.01	90	200	220	22
	192.9m	360mL	Ls	B	0.5	12.3	0.01	0.01	15.00	0.04	0.05	0.01	0.01	50	10	335	6
	444.1m	270mL	vein	V	-2.3	2.2	0.01	0.27	1.69	0.12	0.05	0.07	0.06	75	10	58	84
	583.8m	220mL	Ls	IP-Ls	-6.2	3.0	0.07	0.45	11.00	0.52	0.14	0.05	0.01	540	500	462	238
	636.3m	200mL	Ls	IP-Ls	-3.6	2.2	0.01	1.36	15.00	1.28	0.54	0.27	0.07	1,175	160	638	38
	709.6m	170mL	vein	V	-6.4	0.6	0.01	0.61	1.87	0.31	0.07	0.18	0.05	145	140	158	18
4MAHS-5	98.8m	390mL	Ls	D	0.1	4.5	0.05	0.72	15.00	0.53	0.34	0.01	0.01	155	350	726	58
	110.0m	390mL	Ls	B	2.7	14.1	0.01	0.41	15.00	0.33	0.19	0.01	0.01	70	200	766	20
	112.5m	390mL	Ls	C	1.6	5.4	0.10	0.23	15.00	0.35	0.06	0.01	0.01	250	450	618	24
	117.5m	390mL	Ls	D	0.6	4.5	0.03	0.27	15.00	0.27	0.15	0.04	0.01	195	160	502	66
	120.5m	390mL	Ls	IP-Ls	-1.0	4.9	0.16	1.24	12.05	0.46	0.23	0.01	0.01	150	830	109	60
	224.5m	350mL	Ls	IP-Ls	-1.6	12.3	0.06	1.67	15.00	0.23	0.05	0.04	0.01	270	10	348	22
	444.5m	270mL	Ls	D	-4.3	4.0	0.01	0.83	15.00	0.08	0.01	0.01	0.01	90	260	515	160
	461.0m	260mL	Ls	D	-2.9	4.0	0.01	0.18	15.00	0.09	0.04	0.01	0.01	165	230	461	8
	500.0m	250mL	Ls	D	-1.7	2.6	0.01	0.77	15.00	0.48	0.24	0.10	0.02	205	350	606	56
	506.8m	250mL	Ls	D	-6.3	1.0	0.05	0.63	15.00	0.89	0.40	0.12	0.01	435	240	544	50
	606.2m	210mL	Ls	C	-0.5	5.8	0.02	0.10	15.00	0.05	0.01	0.01	0.01	105	80	630	18
4MAHS-6	51.9m	1110mL	Ls	A	3.8	16.1	0.09	0.02	15.00	0.14	0.34	0.01	0.01	125	10	813	12
	78.5m	1080mL	Ls	B	-2.0	13.2	0.16	0.18	15.00	0.59	0.47	0.11	0.01	245	120	709	20
	85.8m	1070mL	Ls	A	3.3	16.6	0.02	0.03	15.00	0.09	0.17	0.01	0.01	185	10	1,020	10
	110.2m	1050mL	Ls	B	3.1	14.4	0.09	0.15	15.00	0.25	0.32	0.01	0.01	275	10	702	10
	145.5m	1020mL	Ls	A	3.3	16.3	0.02	0.03	15.00	0.20	0.23	0.01	0.01	195	10	953	6
	178.5m	990mL	Ls	B	3.9	13.9	0.01	0.01	15.00	0.16	0.34	0.01	0.01	285	10	496	8
	314.6m	860mL	Ls	IP-Ls	2.6	15.9	0.05	0.68	4.13	1.09	0.12	0.02	0.01	300	100	39	40
	599.4m	600mL	Ls	B	3.6	10.8	0.07	0.14	15.00	0.37	0.29	0.01	0.01	275	70	801	16
	785.2m	420mL	Ls	B	-2.8	10.8	0.04	0.31	15.00	0.20	0.13	0.01	0.01	120	360	517	18
5MAHS-7	74.5m	470mL	Ls	A	4.0	18.7	0.01	0.10	15.00	0.10	0.54	0.01	0.01	100	10	761	48
	84.1m	460mL	Ls	A	3.6	20.4	0.05	0.01	15.00	0.07	0.24	0.01	0.01	95	20	692	30
	89.3m	460mL	Ls	A	4.2	17.1	0.02	0.06	15.00	0.19	0.22	0.01	0.01	245	70	415	12
	111.0m	450mL	Breccia	D	-5.8	4.8	0.01	0.94	15.00	1.85	0.30	0.07	0.01	1,235	210	704	44
	146.5m	430mL	Ls	IP-Ls	-1.6	5.6	0.08	4.55	8.80	1.70	0.48	0.01	0.01	415	240	103	130
	181.8m	410mL	Ls	IP-Ls	1.6	10.0	0.26	4.38	7.43	1.00	0.25	0.01	0.01	170	700	40	40
	190.5m	400mL	Ls	C	1.3	8.3	0.02	0.22	15.00	0.10	0.06	0.01	0.01	130	250	380	12
	206.7m	390mL	Ls	IP-Ls	-0.4	10.3	0.01	2.72	15.00	0.21	0.06	0.01	0.01	120	10	227	16
	231.0m	370mL	Ls	A	-0.5	17.2	0.03	0.02	15.00	0.07	0.07	0.01	0.01	40	30	290	14
	245.7m	370mL	Ls	C	-0.5	9.9	0.02	0.18	15.00	0.12	0.11	0.06	0.01	135	50	255	18
	328.4m	310mL	Ls	D	2.3	4.5	0.09	0.28	15.00	0.51	0.28	0.01	0.01	790	60	459	1,815
5MAHS-9	541.4m	650mL	Ls lens	C	1.4	6.5	0.01	0.06	15.00	0.10	0.12	0.01	0.01	330	10	792	64
	564.8m	630mL	Ls lens	B	3.7	14.5	0.01	0.01	15.00	0.11	0.29	0.01	0.01	330	20	522	234
	588.6m	600mL	Ls lens	A	4.5	18.9	0.01	0.01	15.00	0.07	0.26	0.01	0.01	105	30	755	40
	601.5m	590mL	Ls lens	A	3.9	17.1	0.01	0.01	15.00	0.09	0.16	0.01	0.01	170	20	726	22
	606.2m	590mL	Inishi rock/Ls	C	-1.1	9.4	0.01	0.12	15.00	0.09	0.04	0.01	0.01	145	280	554	34
	907.0m	300mL	Inishi rock/Ls	IP-Ls	-6.5	3.7	0.02	1.84	12.35	2.81	1.21	0.07	0.01	1,005	280	1,020	58
7MAKK-1	280.1m	320mL	Ls lens	B	1.0	12.4	0.01	0.23	15.00	0.16	0.11	0.01	0.01	215	10	350	8
	300.5m	300mL	vein	V	-2.0	1.5	0.02	0.39	14.45	0.90	0.29	0.01	0.01	1,665	90	195	328
	300.7m	300mL	Ls lens	C	2.7	8.0	0.02	0.43	15.00	0.27	0.07	0.01	0.01	220	260	453	32
	392.0m	230mL	Ls lens	D	1.6	1.4	0.01	0.91	15.00	1.31	0.35	0.01	0.01	1,170	80	342	68
	427.1m	210mL	breccia zone?	IP-Ls	-3.0	2.2	0.65	0.65	12.60	3.70	0.28	0.01	0.01	5,830	30	297	9,700

mean composition for each group	Mg/Fe	Mg*	Al/Mg	Al/Sr	$\delta^{13}C_{PDB}$	$\delta^{18}O_{SMOW}$	S	Al	Ca	Fe	Mg	K	Na	Mn	P	Sr	Zn
					(‰)	(‰)	(%)	(%)	(%)	(%)	(%)	(%)	(%)	(ppm)	(ppm)	(ppm)	(ppm)
Group-A Ls	2.32	0.48	0.17	0.8	3.10	17.45	0.03	0.04	15.00	0.11	0.24	0.01	0.01	135	41	665	22
Group-B Ls	1.28	0.35	0.86	2.7	1.40	12.68	0.04	0.15	15.00	0.23	0.23	0.02	0.01	197	86	552	35
Group-C Ls	0.54	0.17	4.02	5.3	0.90	7.86	0.03	0.22	15.00	0.17	0.08	0.02	0.01	204	234	506	28
Group-D Ls	0.41	0.18	11.44	11.7	-1.82	3.48	0.03	0.61	15.00	0.67	0.23	0.04	0.01	493	216	540	258
Impure Ls	0.28	0.15	12.64	206.4	-2.00	7.01	0.14	1.95	11.00	1.30	0.34	0.05	0.01	998	286	328	1,034
calcite vein	0.32	0.15	6.61	96.1	-3.60	1.43	0.01	0.42	6.00	0.44	0.14	0.09	0.04	628	80	137	143

carbon and oxygen isotope data are taken from MITI (1996).

abbreviations; Ls: limestone, IP-Ls: impure limestone (<15% Ca or >1% Al), V:vein carbonate.

A, B, C, and D are limestone based on $\delta^{18}O$, >15‰, 10-15‰, 5-10‰, <5‰, respectively.

Table 3 Mineral assemblage of Inishi rock and gneiss in the Sako-nishi area.

Sample No	Rock type	G	$\delta^{13}C$ ‰	$\delta^{18}O$ ‰	Texture C	F	V	V.M	Sausuritized	Primary mineral Cal	Qz	Cpx	Pl	Kf	Tit	Wol	Hb	Hydrothermal mineral T-A	Chl	Preh	Ser	Kf	Cz	Ep	Gnt	Sph	Cp	Py	Mgt
56HI-1 278.60m	In	B	0.1	12.5																									
56HI-1 283.70m	In	B	0.1	12.5																									
56HI-1 292.30m	In	C	-0.3	7.9																									
56HI-1 314.60m	In	C	-2.3	9.1					partly	△		◎	◎	△	△			×	×	○	△		○	×			×	×	
56HI-1 351.90m	In	B	-1.5	11.2					partly			○	◎	○	△			×		○	×								
56HI-1 393.80m	In	B	-0.7	12.5																									
56HI-1 452.20m	In	B	3.4	14.8																									
56HI-1 503.00m	In	A	3.9	15.8	○		○	Preh			◎	○	△	○	△			△	×	○						×	×	×	×
56HI-1 534.60m	Gn	D	2.1	3.6	○						◎		△	△					○	◎									
56HI-1 537.70m	Gn	D	0.7	1.2																									
2HI-1 25.00m	In	B	2.8	12.8																									
2HI-1 60.40m	In	C	0.6	9.3			○	Cal		○	○			◎	○			×	○	△			×					×	
2HI-1 127.40m	In	B	1.1	12.5			○	Cz			○		◎		○				△				△					△	×
2HI-1 180.30m	In	B	1.6	11.8																									
2HI-1 378.85m	In	B	-4.2	10.5																									
2HI-1 688.10m	Gn	C	-2.8	5.5																									
3HS-3 101.50m	In	C	1.1	7.9						◎	○	△				○				○			△		△			×	
3HS-3 140.60m	In	B	0.3	10.4																									
3HS-3 155.50m	In	A	1.2	16.1					All			○	○		○			×	×	×			×						
3HS-3 363.30m	In	D	-4.0	4.6																									
3HS-3 366.80m	In	D	-4.0	4.6																									
3HS-3 426.90m	In	C	-3.1	8.4																									
3HS-3 515.55m	In	D	-3.9	1.8					vein like		○	○	○	○	○				△	○	△		×	△				×	
3HS-3 584.50m	Gn	C	-5.7	5.2			○	Cal		◎						×			△					○		○			
3HS-3 636.40m	Gn	D	-6.3	2.5																									
3HS-3 697.40m	Gn	D	-6.5	4.1			○	Ep,Chl		○	○					△			○					○					×
4HS-5 113.30m	In	C	2.2	8.5																									
4HS-5 117.40m	In	D	0.6	4.5																									
4HS-5 123.80m	In	D	-1.0	4.9																									
4HS-5 600.70m	Gn	C	0.2	5.4																									
4HS-5 605.30m	In	C	-0.3	6.9																									
4HS-6 44.00m	Gn	B	3.6	14.8																									
4HS-6 120.80m	In	B	3.6	13.8																									
4HS-6 169.00m	In	B	2.4	11.5			○	Cal	vein like	×	○	◎	◎	△	○			×					×						
4HS-6 309.50m	Gn	B	1.5	11.3																									
4HS-6 530.90m	In	B	-0.4	11.2																									
4HS-6 622.60m	Gn	C	2.2	6.7																									
4HS-6 672.70m	In	C	-0.9	7.4					partly		○		○	△					○		△			×				△	
4HS-6 786.40m	In	B	-2.5	11.6																									
5HS-7 74.50m	In	A	3.9	17.2			○	Cz	All				○		○			△	×				△			×		×	
5HS-7 92.80m	Gn	B	3.3	13.3																									
5HS-7 131.70m	In	C	0.0	6.7																									
5HS-7 326.50m	In	D	2.3	4.5																									
5HS-7 329.70m	In	D	2.3	4.5					All	○	△	○	◎	△	○			×	×				○	×				×	
5HS-7 394.60m	In	D	-2.4	1.4																									
5HS-7 411.70m	In	D	-2.0	2.1																									
5HS-9 525.20m	Gn	B	1.1	11			○	Preh	partly	○		○	○	△	×			×		◎	△		△					×	×
5HS-9 566.80m	In	B	3.5	14.1																									
5HS-9 591.20m	In	A	4.3	16.5																									
5HS-9 603.20m	In	A	3.9	17.1																									
7KK-1 204.80m	In	B	1.0	11.7					All		△	○	○	△	△			×	×										
7KK-1 283.40m	In	B	1.2	12.2			○	Ep, Preh	All			△	○		○						△		×	△				×	
7KK-1 302.90m	In	C	2.3	7.2																									
7KK-1 315.10m	In	D	-2.6	1.6																									
7KK-1 391.20m	In	D	1.9	2.7					Skarn	○	△								○					○					
7KK-1 430.60m	In	D	-1.3	4.6																									
7KK-1 447.20m	In	A	-0.7	16.4						○	×	○	○	×	○						△		×	△				×	×
7KK-1 525.50m	In	C	-0.4	6																									

*Symbols: ◎=abundant; ○=common; △=rare; and ×=trace

**Abbreviations: G=group of alteration; Gn=gneiss; In=Inishi rock; C=coarse-grained; F=fine-grained; V=veinlet; V.M=mineral in vein; Cal=calcite; Qz=quartz; Cpx=clinopyroxene; Pl=plagioclase; Kf=K-feldspar; Tit=titanite; Bt=biotite; Hb=hornblende; T-A=tremorite-actinolite; Chl=chlorite; Preh=prehnite; Ser=sericite; Cz=clinozoisite; Ep=epidote; Gnt=garnet; Sph=sphalerite; Cp=chalcopyrite; Py=pyrite; Mgt=magnetite.

Table 4 Mineral assemblage of carbonate rock and silicate rock in the Sako-nishi area.

No.	Sample No	Z	Rock type	G	$\delta^{18}O$ ‰	$\delta^{13}C$ ‰	Texture				Primary mineral									Hydrothermal mineral										
							C	F	V		Cal	Gra	Qz	Cpx	Pl	Kf	Tit	Bt	Hb	T-A	Chl	Preh	Ser	Kf	Cz	Ep	Gnt	Sph	Cp	Py	Po	Limo
1	RK3106	I	Ls	C	8.3	3.3	○	○	×	Cal. V	◎	×	△																		
2	RK3105	I	Ls	C	8.9	3.2		○	○	Chl. V	◎		△							×	△										
3	RM0618	I	Gn	C	9.7	0.2	○	○		mortalic	◎			×															×		
4	RS0112	I	Ls	B	10.2	2.5		○	△		◎									△	△							×			
5	RS0111	I	Ls	B	10.6	2.8	○		△		◎			×	×		×			△	△							×			
6	RS0405	I	Ls	B	10.6	3.2	○	○	△		◎		×							△								×			
7	RS0802	I	Ls	B	11.2	2.8	○			mortalic	◎		×	×							×									×	
8	RK2502	I	Cs	B	11.3	-0.1	○				◎		△	○	×		△		△	○					△						
9	RK3103	I	Ls	B	11.6	1.3	○				◎	×								×											
10	RK2106	I	Gn	B	11.9	1.8	○				×		△		○						△			○							
11	RK1003	I	Ls	B	12.1	2.3	○		×	Cal. V	◎			×						△									×		
12	RK2102	I	Ls	B	12.2	1.3	○	○	×		◎									×	×							×			
13	RK2509	I	Ls	B	12.2	1.0	○				◎		×	○	×																
14	RK2104	I	Ls	B	12.6	3.9	○		×		◎		×								×									×	
15	RK0702	I	Ls	B	13.1	4.4		○	×	banded	◎	×	△	△							×										
16	RK2514	I	Ls	B	13.2	0.5	○				◎		△	△	×		×			×	×										
17	RK3112	I	Ls	B	13.4	4.6		○		mylonitic	◎		×	△						×											
18	RS0403	I	Ls	B	13.4	1.8	○		×	Preh. V	◎		△									×									
19	RK2107	I	Ls	B	13.5	2.2	○			mortalic	◎	×	×																		
20	RK0704	I	Ls	B	13.8	4.0	○				◎		×	△																	
21	RK0705	I	Ls	B	14.3	3.1	○				○		○	○	◎		○			×					○					×	
22	RK2507	I	Ls	B	14.6	3.8	○				◎	×	△															×	×	×	
23	RK1006	I	Ls	B	14.7	3.0	○				×		○	○	○		△				△										
24	RK2105	I	Ls	A	15.1	4.8	○				◎	×	×	×																	
25	RM0616	I	Ls	A	15.1	4.1	○				◎	×																			
26	RK2505	I	Ls	A	16.6	3.1	○				◎		△	△																	
27	RK1004	I	Ls	A	16.8	0.1		○		mylonitic	◎						×				×									×	
28	RK2506	I	Ls	A	17.4	3.8	○				◎			△																	
29	RK0703	I	Cs	A	18.0	3.5	○				◎		×	○						○										△	
30	RK2504	I	Ls	A	18.5	3.9	○				◎		×								△									×	
31	RM0302	II	Ls	C	8.1	0.2		○			◎																	×			
32	RS0104	II	Ls	C	8.3	0.2	○	○	△	mylonitic	◎		×							×	×							×		×	×
33	RS0106	II	Ls	C	9.6	2.1	○	○	△	mylonitic	◎																	×			
34	RM0603	III	Ls	B	12.5	2.0	○		×		◎		×		×						×										
35	RM0604	III	Ls	B	13.6	3.5	○		×		◎		×	×						×	×							×			

*Symbols: ◎=abundant; ○=common; △=rare; and ×=trace

**Abbreviations: Z=zone of mineralization; G=group of limestone; Ls=limestone; Cs=calc-silicate; In=Inishi rock; Gn=gneiss; C=coarse-grained; F=fine-grained; V=veinlet; Cal=calcite; Gra=graphite; Qz=quartz; Cpx=clinopyroxene; Pl=plagioclase; Kf=K-feldspar; Tit=titanite; Bt=biotite; Hb=hornblende; T-A=tremorite-actinolite; Chl=chlorite; Preh=prehnite; Ser=sericite; Cz=clinozoisite; Ep=epidote; Gnt=garnet; Sph=sphalerite; Cp=chalcopyrite; Py=pyrite; Po=pyrrhotite; Limo=limonite.

Table 4 *(continued)*

No.	Sample No	Z	Rock type	G	$\delta^{18}O$ ‰	$\delta^{13}C$ ‰	Texture C	F	V		Primary mineral Cal	Gra	Qz	Cpx	Pl	Kf	Tit	Bt	Hb	Hydrothermal mineral T-A	Chl	Preh	Ser	Kf	Cz	Ep	Gnt	Sph	Cp	Py	Po	Limo
36	RM0605	III	Ls	B	13.8	4.3	○	○	△		◎		×							△	△							×		×	×	
37	RK0701	III	Ls	A	15.9	3.3	○			polygonal	◎	×	×	×						×	△		×									
38	RK3109	IV	Gn	B	10.3	-7.8	○				△		○		○					△	△			×				×				
39	RK2103	IV	Ls	B	14.7	2.4	○	○	×		◎									×	×							×				
40	RS1701		Cs	C	7.2	0.2		○	○	mylonitic	◎				○															×		×
41	RS1710		Ls	C	9.7	1.2	○		○	Cal. V	◎			×			×													×		
42	RK2513		Ls	C	9.8	-1.0	○			mylonitic	◎			○	△		×															
43	RS0406		Ls	B	10.6	3.2	○				◎	×	×								×											
44	RK2512		Ls	B	10.9	0.3	○	○		mylonitic	◎			○	×		×															
45	RM1503		Ls	B	11.0	1.6	○				◎			△					△												×		
46	RK3111		Cs	B	11.7	2.1	○				◎		△	△	△		×			△	△										×		
47	RS1104		Ls	B	11.9	3.4	○			polygonal	◎	×	×																			×
48	RM0613		Ls	B	12.0	4.1	○		○	Qz. V	◎		△																		×		
49	RM0617		Ls	B	12.1	2.0	○				◎										×											
50	RS0419		Ls	B	12.1	2.9		○		mylonitic	◎																					
51	RM0612		Ls	B	12.3	2.5	○			mortalic	◎																					
52	RM0619		Ls	B	12.4	0.9		○		mortalic	◎									×												
53	RM0606		Ls	B	12.5	4.8	○				◎									△												
54	RM0615		Ls	B	12.9	3.3	○				◎			△																		
55	RS0810		Ls	B	13.0	3.6		○	○	mylonitic	◎	×	○	×							×											
56	RM0614		Ls	B	13.1	3.5	○				◎										×								×			
57	RK3102		Ls	B	13.2	2.8	○				◎			△							×											
58	RM0911		Ls	B	13.3	3.0	○			polygonal	◎	×	×								×											
59	RM0910		Ls	B	13.6	3.9	○		△	Cal.-Ser. V	◎	×	×							×	×		△									
60	RK3107		Ls	B	13.7	2.5	○				◎		△	×			×				×		×									
61	RK2510		Ls	B	14.0	3.4		○			◎	×		△																		
62	RS0805		Ls	B	14.3	3.3	○			polygonal	◎	△	×	△																×	×		×
63	RS0812		Ls	B	14.7	3.9	○			polygonal	◎		×								△												×
64	RS0408		Ls	A	15.0	4.5	○				◎																					
65	RS0809		Ls	A	15.3	3.5	○				◎								×													
66	RS1103		Ls	A	15.4	3.8	○			polygonal	◎	×	×	△						×	×											
67	RK0706		Ls	A	15.8	5.1	○			mortalic	◎		△	×			×			×	×									×		
68	RS0804		Gn	A	15.8	-0.1	○				×		×	△	◎							△										
69	RM0608		Ls	A	15.9	4.8	○				◎		×	×						×	×								×			
70	RK2108		Ls	A	16.3	4.3	○			mortalic	◎	×	×	△							×											

*Symbols: ◎=abundant; ○=common; △=rare; and ×=trace

**Abbreviations: Z=zone of mineralization; G=group of limestone; Ls=limestone; Cs=calc-silicate; In=Inishi rock; Gn=gneiss; C=coarse-grained; F=fine-grained; V=veinlet; Cal=calcite; Gra=graphite; Qz=quartz; Cpx=clinopyroxene; Pl=plagioclase; Kf=K-feldspar; Tit=titanite; Bt=biotite; Hb=hornblende; T-A=tremorite-actinolite; Chl=chlorite; Preh=prehnite; Ser=sericite; Cz=clinozoisite; Ep=epidote; Gnt=garnet; Sph=sphalerite; Cp=chalcopyrite; Py=pyrite; Po=pyrrhotite; Limo=limonite.

Table 4 *(continued)*

No.	Sample No	Z	Rock type	G	$\delta^{18}O$ ‰	$\delta^{13}C$ ‰	Texture C	F	V		Primary mineral Cal	Gra	Qz	Cpx	Pl	Kf	Tit	Bt	Hb	Hydrothermal mineral T-A	Chl	Preh	Ser	Kf	Cz	Ep	Gnt	Sph	Cp	Py	Po	Limo
71	RS2408		Ls	A	16.6	3.5	○				◎		×		×				○		△											
72	RS0801		Ls	A	16.8	4.6	○			mortalic	◎		×	×						△												
73	RM0610		Ls	A	17.1	1.4	○				◎																					
74	RM2302		Ls	A	17.1	3.5	○				◎																					
75	RS1106		Ls	A	17.2	3.9	○			polygonal	◎		×								×										
76	RM1207		Ls	A	17.3	3.6	○			polygonal	◎	△	×		×		×				×		×								
77	RM0311		Ls	A	17.6	4.2	○				◎																					
78	RS0811		Ls	A	17.7	4.4	○			polygonal	◎		△	×						△	△										
79	RS0416		Ls	A	17.9	4.4	○				◎		×																			
80	RM0915		Ls	A	18.6	3.3	○			polygonal	◎	△	×							×											
81	RK2511		Ls	A	18.7	3.3	○	○		mylonitic	◎		×								×		△							×	
82	RK3108		Ls	A	19.0	5.3	○				◎																					
83	RS2410		Ls	A	19.5	4.4	○				◎	×	×				×				×									×	
84	RS0807		Ls	A	20.0	4.0	○			polygonal	◎	△	×	○																×	×
85	RS0808		Ls	A	21.1	4.4	○			polygonal	◎	△	×	○																	
	RK0707		Gn				○		×				○		◎					×	×		×		△			×			
	RK1001		In				○		×	Chl.-Preh. V			△	△	◎	△	△			×	×	×	△								
	RK1002		Gn				○						○		◎	△	△			×	○	×	△		△						
	RK1005		In				○		○	Preh. V			○	×	◎		△			○	○	◎	△		△			△		×	×
	RK2101		In				○		○	Ser. V			○	×	◎	△	△			×	△	×	○		△	×					
	RK2109		Gn				○		○	Qz. V	×		◎		×					×	△		○	△							
	RK2201		Cs				○		○	Cal.-Ser. V	○		△	○						×		△									
	RK2202		Gn				○		○	Cal. V	△		○		○	△					×		×								
	RK2501		Gn				○						◎								△	◎									
	RK2503		Gn				○		○	Qz. V			○	×	△	△				△	×			△	×			△		×	
	RK3101		Gn				○		×	Ser. V			○		△	○	×				△		×	○				×			
	RK3104		In								×		○	×	○	○	△			△	×		×		×						
	RK3110		Ls				○				◎			△						△			×						×	×	
	RM0301		In				○		○	Preh. V				△	○	×	△			△	×	○	△		×						
	RM0303		Gn				○							○	○	○				△	×	△	×								
	RM0304		Gn				○							○	○					○	×		×					×			
	RM0305		Gn				○						◎		○	×					△		×								
	RM0306		Gn				○		○	Chl.-T-A V			○		○	○				△	○		×					×		△	△
	RM0307		Gn				○		○	Chl.-Preh. V			○		○	○				×	○	△	×							△	△
	RM0308		Gn				○		×	Ser. V			○	×	○	△					△		△								

*Symbols: ◎=abundant; ○=common; △=rare; and ×=trace

**Abbreviations: Z=zone of mineralization; G=group of limestone; Ls=limestone; Cs=calc-silicate; In=Inishi rock; Gn=gneiss; C=coarse-grained; F=fine-grained; V=veinlet; Cal=calcite; Gra=graphite; Qz=quartz; Cpx=clinopyroxene; Pl=plagioclase; Kf=K-feldspar; Tit=titanite; Bt=biotite; Hb=hornblende; T-A=tremorite-actinolite; Chl=chlorite; Preh=prehnite; Ser=sericite; Cz=clinozoisite; Ep=epidote; Gnt=garnet; Sph=sphalerite; Cp=chalcopyrite; Py=pyrite; Po=pyrrhotite; Limo=limonite.

Table 4 *(continued)*

No.	Sample No	Z	Rock type	G	$\delta^{18}O$ ‰	$\delta^{13}C$ ‰	Texture C	F	V		Primary mineral Cal	Gra	Qz	Cpx	Pl	Kf	Tit	Bt	Hb	Hydrothermal mineral T-A	Chl	Preh	Ser	Kf	Cz	Ep	Gnt	Sph	Cp	Py	Po	Limo
	RM0309		Gn				○		×	Chl. V			△								△		×	◎				×				
	RM0310		Gn				○		○	T-A V			○		○	△				○	×		×					×				
	RM0312		Gn				○		○	Cal.-Preh. V	△		◎									○										
	RM0601		In				○						○	△	○	△	△			×	×		△		×							
	RM0602		In				○		×	Ser. V					○	△	○				△		△									
	RM0607		Gn				○		△	Preh. V			○		○	○	×				×	△	×					×				
	RM0609		Cs				○				△		○		△	△												×				
	RM0611		Gn					○	×	Qz. V			△	×								◎					×					
	RM0901		Gn				○						◎		△	△					△	△	×									
	RM0902		Gn				○						◎		△	○					△		△									
	RM0903		Gn					○					○	×		×					○	◎								×	△	
	RM0904		Gn				○			banded			◎			△						△										
	RM0905		In				○						○	×	△	○	○			△	△		△									
	RM0906		Gn					○					○		○	○					△		△					x				
	RM0907		Gn				○		○	Preh.-Ser. V			○		△	○	△			△	△	△	×									
	RM0908		Gn				○		×	Preh. V			○			○	◎			△	×	△	△									
	RM0909		Gn				○						○			○	◎				△	×	△	○				△		x		
	RM0912		In					○	×	Preh. V			○		◎	×	◎			△	○	△	×		○							
	RM0913		Gn				○						◎				×				○		○		×	○						
	RM0914		In				○		△	Cz. V	△		○	△	◎	×	○			△	○		△		×			×				
	RM1201		In					○	△	Cal. V	×		○		◎	×	○				○					△						
	RM1202		Gn				○						×		◎	△				△	○	△						△	△	×		
	RM1203		Gn				○						×		△	◎					×	○					×	×				
	RM1204		Gn					○			△		○		○					×	×		×						×	×		
	RM1205		In				○						○	△	◎	○	△			×	×	○										
	RM1206		Cs					○			○		△	△	△					×		○										
	RM1208		In				○						○		△	○	△			×	△		△	△				△				
	RM1209		In				○		○	Preh. V			○	△	○	○	○				△	○						△				
	RM1210		Gn				○			mylmekitic			○		△	○					△		△	△				△				
	RM1211		Gn				○						○		△	◎				△	△	○		×				×				
	RM1212		Gn				○			mylmekitic	○		○	○	△	○					×	△		△	△			×				
	RM1213		In					○			△		○	×	○	○	○			○	△							×	×			
	RM1401		Gn				○			mylmekitic			○		△	◎							○	◎				×				
	RM1402		Gn				○			mylmekitic			○		△	◎					△			△								
	RM1403		Gn				○		○	Ser. V			○		△	◎					×		○	○				×				

*Symbols: ◎=abundant; ○=common; △=rare; and ×=trace

**Abbreviations: Z=zone of mineralization; G=group of limestone; Ls=limestone; Cs=calc-silicate; In=Inishi rock; Gn=gneiss; C=coarse-grained; F=fine-grained; V=veinlet; Cal=calcite; Gra=graphite; Qz=quartz; Cpx=clinopyroxene; Pl=plagioclase; Kf=K-feldspar; Tit=titanite; Bt=biotite; Hb=hornblende; T-A=tremorite-actinolite; Chl=chlorite; Preh=prehnite; Ser=sericite; Cz=clinozoisite; Ep=epidote; Gnt=garnet; Sph=sphalerite; Cp=chalcopyrite; Py=pyrite; Po=pyrrhotite; Limo=limonite.

Table 4 *(continued)*

No.	Sample No	Z	Rock type	G	$\delta^{18}O$ ‰	$\delta^{13}C$ ‰	Texture				Primary mineral									Hydrothermal mineral											
							C	F	V		Cal	Gra	Qz	Cpx	Pl	Kf	Tit	Bt	Hb	T-A	Chl	Preh	Ser	Kf	Cz	Ep	Gnt	Sph	Cp	Py	Po	Limo
	RM1404		Gn					○	○	Preh.-Chl. V	△		○		△	◎				△	△	○						×			
	RM1405		Gn				○		○	Preh.-Chl. V			○		△	◎					△	○		◎							
	RM1501		Gn				○						○		○	○					△	×	△								
	RM1502		Gn				○		△	Preh.-Chl. V			○		○	◎	△				×	△									
	RM1504		Gn				○						○		○	○	△				×	○									
	RM1505		Gn					○					◎		○	○				×	△	○	×								
	RM2301		Gn				○		○	Preh. V			○		○	○				○	△	△	×		×		×			
	RM2303		Gn				○		×	Chl. V	×		○		◎	△					○		△				○				
	RS0803		Gn				○				△		○			○						○									
	RS0806		Gn				○				×		◎		○	△		×			△		△								
	RS1108		Gn				○						○		○	○						◎		×							

*Symbols: ◎=abundant; ○=common; △=rare; and ×=trace

**Abbreviations: Z=zone of mineralization; G=group of limestone; Ls=limestone; Cs=calc-silicate; In=Inishi rock; Gn=gneiss; C=coarse-grained; F=fine-grained; V=veinlet; Cal=calcite; Gra=graphite; Qz=quartz; Cpx=clinopyroxene; Pl=plagioclase; Kf=K-feldspar; Tit=titanite; Bt=biotite; Hb=hornblende; T-A=tremorite-actinolite; Chl=chlorite; Preh=prehnite; Ser=sericite; Cz=clinozoisite; Ep=epidote; Gnt=garnet; Sph=sphalerite; Cp=chalcopyrite; Py=pyrite; Po=pyrrhotite; Limo=limonite.

Table 5 Sampling localities and descriptions of limestone and skarn calcite of the Mokuji and Shiroji ores in the Kamioka mine.

Type of rock	Sample No.	Deposit	Ore body	Level	Rock type	Description
Limestone	98729-5B	Mozimi	East No.4	-320m	limestone near Shiroji ore	pinkish calcite and chlorite vein
	98729-1F	Mozumi	North No.20	-500m	"NAKAISHI" in Mokuji ore	fine grained and chlorite vein
	5O-10	Tochibora	No.5 OTSU	-300m	limestone near Shiroji ore	chlorite patches
	98728-3E	Tochibora	No.9	-360m	"NAKAISHI" in Mokuji ore	graphite+chlorite
Shiroji ore	98729-4A	Mozumi	North No.20	-130m	Shiroji ore	
	98729-5A	Mozimi	East No.4	-320m	Shiroji ore	calcite+chlorite
	2-7-B	Tochibora	No.5 OTSU	-300m	skarn calcite in Shiroji	megacryst calcite
	9-340	Tochibora	No.9	-340m	skarn calcite in banded Shiroji	high grade ore
	9MAHSU-1	Sako-nishi	Sako-nishi	335.5m	megacryst calcite	around Shiroji ore
Mokuji ore	2-12-B	Mozumi	East No.4	-320m	skarn calcite in Mokuji	megacryst calcite
	98729-1D	Mozumi	North No.20	-500m	calcite vein in porphyry dyke	prehnite
	98728-2	Tochibora	No.9	-230m	skarn calcite in druse	around Mokuji ore
	2-6	Tochibora	Shiragane	-250m	skarn calcite in Mokuji	pinkish in colour, include galena

The -500 levels is corresponding to an elevation of 367m above sea level.

Table 6 Oxygen and carbon isotope ratios of limestone in the Sako-nishi area.

Drilling No.	depth	rock	occurrence	$\delta^{18}O$ (‰)	$\delta^{13}C$ (‰)
2MAHI-1	9.00m	Ls	Ls	-0.1	10.6
2MAHI-1	12.90m	Ls	Ls	-1.7	5.1
2MAHI-1	14.60m	Ls	Ls	-3.1	4.0
2MAHI-1	24.40m	Ls	Ls	2.8	12.8
2MAHI-1	25.00m	Ls	f. Ls	-2.1	4.6
2MAHI-1	39.50m	Ls	Ls	-0.7	9.7
2MAHI-1	62.40m	Ls	Ls	0.7	9.2
2MAHI-1	76.30m	Ls	Ls	0.8	11.2
2MAHI-1	79.50m	Ls	f. Ls	1.6	16.9
2MAHI-1	120.90m	Ls	f. Ls	2.3	11.1
2MAHI-1	124.50m	Ls	Ls	1.0	12.1
2MAHI-1	135.30m	Ls	Ls	1.1	12.8
2MAHI-1	148.50m	Ls	f. Ls	0.7	9.6
2MAHI-1	164.85m	Ls	Ls	2.2	11.8
2MAHI-1	172.00m	Ls	Ls	1.0	11.8
2MAHI-1	186.90m	Ls	f. Ls	-0.6	9.3
2MAHI-1	193.10m	Ls	f. Ls	-0.2	10.1
2MAHI-1	278.40m	Ls	Ls	-3.6	5.8
2MAHI-1	408.00m	Ls	f. Ls	-0.9	6.6
3MAHS-1	153.80m	Ls	f. Ls	-0.4	3.7
3MAHS-1	163.50m	Ls	Ls	1.8	10.2
3MAHS-1	166.00m	Ls	Ls	0.5	7.7
3MAHS-1	169.25m	Ls	Ls	2.2	10.4
3MAHS-2	129.35m	Ls	Ls	2.9	14.3
3MAHS-2	194.80m	Ls	Ls	3.4	2.9
3MAHS-2	344.20m	Ls	f. Ls	-4.6	-2.5
3MAHS-2	344.30m	Ls	Ls	-2.3	-0.3
3MAHS-3	91.60m	Ls	f. Ls	-0.1	6.1
3MAHS-3	105.50m	Ls	Ls	1.1	7.9
3MAHS-3	123.80m	Ls	Ls	2.5	9.6
3MAHS-3	153.10m	Ls	Ls	1.2	16.1
3MAHS-3	192.90m	Ls	f. Ls	0.5	12.3
3MAHS-3	636.30m	Ls	f. Ls	-3.6	2.2
3MAHS-3	713.00m	Ls	Ls lens	-6.2	4.0
3MAHS-3	719.40m	Ls	Ls lens	-4.7	0.8
3MAHS-3	725.00m	Ls	Ls	-0.7	1.3
3MAHS-3	725.15m	Ls	Ls lens	-6.9	-1.0
3MAHS-3	148.80m	Ls	Ls	1.5	10.3
3MAHS-3	170.80m	Ls	f. Ls	0.1	11.6
3MAHS-3	196.00m	Ls	f. Ls	-0.2	10.3
3MAHS-3	427.60m	Ls	Ls	-2.9	0.9
3MAHS-4	118.60m	Ls	Ls	-3.5	3.0
4MAHS-5	98.80m	Ls	Ls	0.1	4.5
4MAHS-5	101.40m	Ls	Ls	2.6	7.6
4MAHS-5	102.20m	Ls	Ls	1.2	8.1
4MAHS-5	103.50m	Ls	Ls	-3.5	8.3
4MAHS-5	107.50m	Ls	Ls	2.2	10.3
4MAHS-5	108.50m	Ls	Ls	1.8	6.6
4MAHS-5	110.00m	Ls	Ls	2.7	14.1
4MAHS-5	111.50m	Ls	Ls	2.0	7.5
4MAHS-5	112.50m	Ls	Ls	1.6	5.4
4MAHS-5	113.50m	Ls	Ls	2.7	11.5
4MAHS-5	115.50m	Ls	Ls	2.5	5.0

*Abbreviations: Ls=limestone; f=fine-grained.

Table 6 *(continued)*

Drilling No.	depth	rock	occurrence	$\delta^{18}O$ (‰)	$\delta^{13}C$ (‰)
4MAHS-5	117.50m	Ls	Ls	0.6	4.5
4MAHS-5	118.50m	Ls	Ls	-1.1	4.8
4MAHS-5	120.50m	Ls	Ls	-1.0	4.9
4MAHS-5	224.50m	Ls	Ls	-1.6	12.3
4MAHS-5	444.50m	Ls	Ls	-4.3	4.0
4MAHS-5	449.20m	Ls	Ls	-4.0	2.1
4MAHS-5	459.60m	Ls	Ls	-4.4	13.0
4MAHS-5	461.00m	Ls	Ls	-2.9	4.0
4MAHS-5	474.00m	Ls	Ls	-1.7	4.7
4MAHS-5	500.00m	Ls	Ls	-1.7	2.6
4MAHS-5	501.40m	Ls	Ls	-3.3	1.8
4MAHS-5	506.80m	Ls	Ls	-6.3	1.0
4MAHS-5	507.70m	Ls	Ls	-5.9	1.8
4MAHS-5	604.80m	Ls	Ls	0.2	5.4
4MAHS-5	605.70m	Ls	Ls	0.1	8.0
4MAHS-5	606.20m	Ls	Ls	-0.5	5.8
4MAHS-6	40.30m	Ls	Ls	10.6	18.2
4MAHS-6	43.50m	Ls	Ls	3.4	14.3
4MAHS-6	46.00m	Ls	Ls	4.0	15.3
4MAHS-6	49.00m	Ls	Ls	4.1	16.9
4MAHS-6	51.90m	Ls	Ls	3.8	16.1
4MAHS-6	56.70m	Ls	Ls	3.9	15.2
4MAHS-6	59.00m	Ls	Ls	4.0	15.1
4MAHS-6	65.40m	Ls	Ls	4.0	13.6
4MAHS-6	69.00m	Ls	Ls	3.9	14.1
4MAHS-6	76.30m	Ls	Ls	2.9	15.1
4MAHS-6	78.50m	Ls	Ls	-2.0	13.2
4MAHS-6	80.10m	Ls	Ls	0.0	13.3
4MAHS-6	82.30m	Ls	Ls	3.2	14.6
4MAHS-6	84.50m	Ls	Ls	3.3	14.3
4MAHS-6	85.80m	Ls	Ls	3.3	16.6
4MAHS-6	87.40m	Ls	Ls	2.5	14.2
4MAHS-6	91.30m	Ls	Ls	3.4	13.2
4MAHS-6	92.90m	Ls	Ls	3.1	14.6
4MAHS-6	96.50m	Ls	Ls	2.7	13.9
4MAHS-6	101.20m	Ls	Ls	3.7	15.0
4MAHS-6	104.30m	Ls	Ls	3.3	11.3
4MAHS-6	106.80m	Ls	Ls	4.0	12.8
4MAHS-6	110.20m	Ls	Ls	3.1	14.4
4MAHS-6	114.50m	Ls	Ls	3.2	14.3
4MAHS-6	123.30m	Ls	Ls	3.9	13.2
4MAHS-6	135.80m	Ls	Ls	2.7	13.7
4MAHS-6	145.50m	Ls	Ls	3.3	16.3
4MAHS-6	154.70m	Ls	Ls	2.7	13.9
4MAHS-6	155.80m	Ls	Ls	3.3	14.0
4MAHS-6	159.90m	Ls	Ls	2.5	13.9
4MAHS-6	164.40m	Ls	Ls	3.7	14.0
4MAHS-6	165.90m	Ls	Ls	2.6	13.6
4MAHS-6	168.20m	Ls	Ls	3.1	11.3
4MAHS-6	169.80m	Ls	Ls	1.7	11.7
4MAHS-6	173.90m	Ls	Ls	3.0	13.2
4MAHS-6	178.50m	Ls	Ls	3.9	13.9
4MAHS-6	312.90m	Ls	Ls	0.8	10.7
4MAHS-6	313.60m	Ls	Ls	2.1	11.8

*Abbreviations: Ls=limestone; f=fine-grained.

Table 6 *(continued)*

Drilling No.	depth	rock	occurrence	$\delta^{18}O$ (‰)	$\delta^{13}C$ (‰)
4MAHS-6	314.60m	Ls	Ls	2.6	15.9
4MAHS-6	342.00m	Ls	Ls	1.3	11.4
4MAHS-6	593.10m	Ls	Ls	2.0	12.2
4MAHS-6	593.70m	Ls	Ls	0.6	8.7
4MAHS-6	595.90m	Ls	Ls	2.9	9.0
4MAHS-6	599.40m	Ls	Ls	3.6	10.8
4MAHS-6	601.70m	Ls	Ls	3.2	6.7
4MAHS-6	603.80m	Ls	Ls	2.7	7.5
4MAHS-6	613.90m	Ls	Ls	3.1	13.1
4MAHS-6	622.90m	Ls	Ls	2.2	6.7
4MAHS-6	784.10m	Ls	Ls	-2.1	12.4
4MAHS-6	785.20m	Ls	Ls	-2.8	10.8
4MAHS-6	825.50m	Ls	Ls	-1.4	12.4
4MAHS-6	826.50m	Ls	Ls	0.9	13.2
56MAHI-1	282.80m	Ls	f. Ls	-0.6	6.6
56MAHI-1	285.10m	Ls	Ls	0.1	9.2
56MAHI-1	301.00m	Ls	Ls	-1.9	8.8
56MAHI-1	301.15m	Ls	Ls	-1.9	8.7
56MAHI-1	349.65m	Ls	Ls	-1.6	10.9
56MAHI-1	350.65m	Ls	Ls	-0.4	10.5
56MAHI-1	357.50m	Ls	Ls	-1.0	13.2
56MAHI-1	370.50m	Ls	Ls	-0.7	12.4
56MAHI-1	377.30m	Ls	Ls	-0.6	12.5
56MAHI-1	393.60m	Ls	Ls	0.1	12.5
56MAHI-1	402.50m	Ls	Ls	3.0	12.9
56MAHI-1	408.40m	Ls	Ls	2.3	12.5
56MAHI-1	409.85m	Ls	Ls	-1.2	12.5
56MAHI-1	429.50m	Ls	Ls	3.6	13.1
56MAHI-1	429.80m	Ls	Ls	4.3	13.6
56MAHI-1	438.20m	Ls	Ls	3.2	13.1
56MAHI-1	444.40m	Ls	Ls	3.6	16.1
56MAHI-1	451.90m	Ls	Ls	3.6	14.6
56MAHI-1	453.80m	Ls	Ls	3.1	15.0
56MAHI-1	460.50m	Ls	Ls	4.3	19.5
56MAHI-1	466.70m	Ls	Ls	2.6	13.7
56MAHI-1	476.90m	Ls	Ls	3.9	15.1
56MAHI-1	478.90m	Ls	Ls	3.8	14.3
56MAHI-1	482.00m	Ls	Ls	3.9	13.6
56MAHI-1	483.70m	Ls	Ls	3.5	13.2
56MAHI-1	488.20m	Ls	Ls	2.9	16.2
56MAHI-1	495.20m	Ls	Ls	3.5	14.2
56MAHI-1	495.90m	Ls	Ls	3.3	17.2
56MAHI-1	496.30m	Ls	Ls	3.7	16.2
56MAHI-1	502.05m	Ls	Ls	4.1	16.6
56MAHI-1	513.60m	Ls	Ls	3.6	15.0
56MAHI-1	519.50m	Ls	Ls	3.9	13.3
56MAHI-1	520.30m	Ls	Ls	1.8	10.0
56MAHI-1	528.50m	Ls	Ls	4.2	10.2
56MAHI-1	528.90m	Ls	Ls	2.7	5.1
56MAHI-1	531.90m	Ls	Ls	3.3	12.3
56MAHI-1	534.90m	Ls	Ls	3.4	5.9
56MAHI-1	535.80m	Ls	f. Ls	0.7	1.2
56MAHI-2	124.00m	Ls	Ls	1.6	9.8
56MAHI-2	141.10m	Ls	Ls	2.5	9.5

*Abbreviations: Ls=limestone; f=fine-grained.

Table 6 *(continued)*

Drilling No.	depth	rock	occurrence	$\delta^{18}O$ (‰)	$\delta^{13}C$ (‰)
56MAHI-2	143.70m	Ls	Ls	0.7	3.2
56MAHI-2	283.30m	Ls	Ls	0.5	12.9
56MAHI-2	286.30m	Ls	Ls	2.3	13.6
56MAHI-2	293.80m	Ls	Ls	3.7	12.9
56MAHI-2	313.40m	Ls	Ls	3.1	13.2
56MAHI-2	315.80m	Ls	Ls	1.9	9.1
56MAHI-2	319.30m	Ls	Ls	1.6	6.1
56MAHI-2	323.20m	Ls	Ls	1.4	4.9
56MAHI-2	327.60m	Ls	Ls	0.0	3.9
56MAHI-2	331.50m	Ls	Ls	4.1	13.8
56MAHI-2	336.20m	Ls	Ls	3.4	9.3
56MAHI-2	339.90m	Ls	Ls	4.5	17.2
56MAHI-2	344.30m	Ls	Ls	2.1	10.3
56MAHI-2	345.80m	Ls	f. Ls	2.0	3.3
56MAHI-2	353.80m	Ls	Ls	3.3	8.2
56MAHI-2	412.85m	Ls	f. Ls	2.2	1.4
56MAHI-2	415.70m	Ls	f. Ls	0.0	2.0
56MAHI-2	417.40m	Ls	Ls	-0.4	5.9
56MAHI-2	430.75m	Ls	Ls	1.5	6.8
5MAHS-7	73.40m	Ls	Ls	4.6	18.2
5MAHS-7	74.50m	Ls	Ls	4.0	18.7
5MAHS-7	78.40m	Ls	Ls	2.7	14.0
5MAHS-7	84.10m	Ls	Ls	3.6	20.4
5MAHS-7	89.30m	Ls	Ls	4.2	17.1
5MAHS-7	91.70m	Ls	Ls	4.5	15.6
5MAHS-7	138.70m	Ls	Ls	0.0	6.7
5MAHS-7	140.10m	Ls	Ls	-0.2	6.3
5MAHS-7	146.50m	Ls	Ls	-1.6	5.6
5MAHS-7	173.10m	Ls	Ls	0.5	8.7
5MAHS-7	174.60m	Ls	Ls	0.2	7.7
5MAHS-7	181.80m	Ls	Ls	1.6	10.0
5MAHS-7	183.70m	Ls	Ls	-0.7	8.9
5MAHS-7	185.90m	Ls	Ls	0.8	7.7
5MAHS-7	188.90m	Ls	Ls	1.3	9.0
5MAHS-7	190.50m	Ls	Ls	1.3	8.3
5MAHS-7	192.50m	Ls	Ls	1.8	12.1
5MAHS-7	202.30m	Ls	Ls	0.0	12.4
5MAHS-7	205.10m	Ls	Ls	0.8	13.2
5MAHS-7	206.70m	Ls	Ls	-0.4	10.3
5MAHS-7	209.30m	Ls	Ls	0.1	11.1
5MAHS-7	214.00m	Ls	Ls	0.6	15.9
5MAHS-7	220.90m	Ls	Ls	0.3	12.5
5MAHS-7	224.40m	Ls	Ls	-0.9	9.1
5MAHS-7	229.00m	Ls	Ls	-0.7	14.0
5MAHS-7	231.00m	Ls	Ls	-0.5	17.2
5MAHS-7	233.20m	Ls	Ls	0.2	15.7
5MAHS-7	235.90m	Ls	Ls	-0.4	12.9
5MAHS-7	243.70m	Ls	Ls	-0.8	11.4
5MAHS-7	245.70m	Ls	Ls	-0.5	9.9
5MAHS-7	328.40m	Ls	Ls	2.3	4.5
5MAHS-9	522.45m	Ls	Ls lens	1.1	11.0
5MAHS-9	541.40m	Ls	f. Ls	1.4	6.5
5MAHS-9	550.80m	Ls	Ls lens	3.5	6.7
5MAHS-9	554.40m	Ls	Ls lens	4.2	14.1

*Abbreviations: Ls=limestone; f=fine-grained.

Table 6 *(continued)*

Drilling No.	depth	rock	occurrence	$\delta^{18}O$ (‰)	$\delta^{13}C$ (‰)
5MAHS-9	564.80m	Ls	Ls lens	3.7	14.5
5MAHS-9	570.30m	Ls	Ls lens	3.2	13.6
5MAHS-9	579.50m	Ls	Ls lens	3.4	12.3
5MAHS-9	588.55m	Ls	Ls lens	4.5	18.9
5MAHS-9	595.55m	Ls	Ls lens	4.1	14.0
5MAHS-9	601.50m	Ls	Ls lens	3.9	17.1
7MAKK-1	207.25m	Ls	f. Ls	1.0	11.7
7MAKK-1	209.40m	Ls	f. Ls	1.1	11.8
7MAKK-1	209.50m	Ls	Ls	0.5	10.4
7MAKK-1	212.35m	Ls	f. Ls	1.2	11.4
7MAKK-1	280.10m	Ls	Ls lens	1.0	12.4
7MAKK-1	280.75m	Ls	Ls	1.4	12.0
7MAKK-1	282.10m	Ls	Ls	0.3	8.2
7MAKK-1	282.30m	Ls	Ls	0.6	10.0
7MAKK-1	300.65m	Ls	Ls lens	2.7	8.0
7MAKK-1	303.85m	Ls	Ls lens	1.9	6.4
7MAKK-1	306.90	Ls	Ls	-0.5	8.5
7MAKK-1	389.20m	Ls	Ls lens	2.1	4.0
7MAKK-1	392.00m	Ls	Ls lens	1.6	1.4
7MAKK-1	393.20m	Ls	Ls lens	0.9	2.7
7MAKK-1	427.80m	Ls	Ls lens	-0.8	7.1
7MAKK-1	438.90m	Ls	Ls	-1.7	2.1
7MAKK-1	439.30m	Ls	Ls	0.9	19.2
7MAKK-1	440.65m	Ls	Ls	-0.2	12.9
7MAKK-1	443.80m	Ls	Ls	0.5	15.4
7MAKK-1	445.10m	Ls	Ls	-0.5	12.8
7MAKK-1	446.50m	Ls	Ls	1.0	13.7
7MAKK-1	447.10m	Ls	Ls	-0.6	17.2
7MAKK-1	447.50m	Ls	Ls	-0.8	15.5
7MAKK-1	449.60m	Ls	Ls	0.6	16.1
7MAKK-1	451.45m	Ls	Ls	1.0	12.3
7MAKK-1	454.70m	Ls	Ls	-0.3	1.8
7MAKK-1	520.80m	Ls	Ls	-0.1	5.7
7MAKK-1	521.30m	Ls	Ls	1.3	8.7
7MAKK-1	523.80m	Ls	Ls	-1.4	9.0
7MAKK-1	525.20m	Ls	Ls	-0.4	6.0

*Abbreviations: Ls=limestone; f=fine-grained.

Table 7 Oxygen and carbon isotope ratios of vein calcite in the Sako-nishi area.

Drilling No.	depth	rock	occurrence	$\delta^{18}O$ (‰)	$\delta^{13}C$ (‰)
2MAHI-1	331.50m	Inishi rock	Cal. v	-5.0	9.0
2MAHI-1	339.40m	alt. Inishi rock?	Cal. v	-6.1	4.0
2MAHI-1	378.85m	alt. Inishi rock	Cal. v	-4.2	10.5
3MAHS-2	297.90m	Hb. gneiss	Cal. v	-3.8	3.3
3MAHS-2	304.10m	Hb. gneiss	Cal. v	-3.4	1.7
3MAHS-2	438.50m	alt. gneiss?	Cal. v	-5.1	-1.0
3MAHS-2	440.90m	alt. gneiss	Cal. v	-4.9	9.9
3MAHS-2	539.60m	alt. Inishi rock	Cal. v	-3.7	-0.4
3MAHS-2	540.80m	felsic gneiss	Cal. v	-3.8	0.2
3MAHS-2	553.40m	alt. Inishi rock	Cal. v	-4.8	9.4
3MAHS-3	362.00m	felsic Inishi rock?	Cal. v	-5.6	15.6
3MAHS-3	365.20m	alt. Inishi rock	Cal. v	-4.1	5.5
3MAHS-3	444.10m	gneiss with Ep.-v	Cal. v	-2.3	2.2
3MAHS-3	520.90m	Inishi-gneiss?	Cal. v	-3.9	1.8
3MAHS-3	684.50m	Cal.v	Cal. v	-7.3	0.7
3MAHS-3	709.60m	gneiss with Ser.-v	Cal. v	-6.4	0.6
3MAHS-4	127.10m	felsic Inishi rock?	Cal. v	-8.0	0.9
3MAHS-4	130.60m	felsic Inishi rock?	Cal. v	-5.4	5.8
3MAHS-4	256.30m	alt. Inishi rock?	Cal. v	-4.3	10.6
4MAHS-5	203.50m	Inishi rock	Cal. v (?)	-4.0	8.8
4MAHS-5	242.00m	gneiss	Cal. v	-4.0	3.5
4MAHS-5	287.50m	Inishi rock	Cal. v (?)	-3.9	9.6
4MAHS-5	380.70m	gneiss	Cal. v	-2.9	0.8
4MAHS-5	426.90m	Inishi rock	Cal. v	-5.6	1.0
4MAHS-5	514.60m	Inishi rock	Cal. v (?)	-3.3	3.7
4MAHS-5	522.50m	Inishi rock	Cal. v (?)	-4.5	8.7
4MAHS-5	543.40m	Inishi rock	Cal. v	-3.9	1.4
4MAHS-5	551.70m	gneiss	Cal. v	-4.5	1.5
4MAHS-5	557.10m	Inishi rock	Cal. v	-6.1	3.0
4MAHS-5	611.10m	gneiss	Cal. v	-5.3	4.4
4MAHS-5	617.40m	gneiss	Cal. v	-6.5	1.1
4MAHS-5	636.10m	Inishi rock	Cal. v (?)	-5.8	0.8
4MAHS-5	636.60m	Inishi rock	Cal. v (?)	-6.4	0.5
4MAHS-5	687.20m	Inishi rock	Cal. v	-6.9	1.9
4MAHS-5	695.40m	Inishi rock	Cal. v	-6.6	4.7
4MAHS-5	696.70m	Inishi rock	Cal. v	-6.1	2.7
4MAHS-6	190.40m	gneiss	Cal. v	-5.0	15.4
4MAHS-6	210.00m	Inishi rock	Cal. v (?)	-5.1	10.7
4MAHS-6	240.50m	gneiss	Cal. v	-4.1	12.2
4MAHS-6	251.20m	gneiss	Cal. v	-6.3	14.5
4MAHS-6	253.30m	gneiss	Cal. v	-5.6	14.8
4MAHS-6	263.70m	gneiss	Cal. v (?)	-5.7	10.0
4MAHS-6	264.20m	gneiss	Cal. v (?)	-6.6	11.0
4MAHS-6	325.10m	gneiss	Cal. v (?)	1.8	10.7
4MAHS-6	453.00m	gneiss	Cal. v	-1.5	8.4
4MAHS-6	466.80m	gneiss	Cal. v (?)	0.6	11.8
4MAHS-6	469.50m	gneiss	Cal. v	-3.9	5.9
4MAHS-6	469.90m	gneiss	Cal. v	-4.9	4.7

*Abbreviations: V=veinlet; alt=alteration; Ep=epidote; Cal=calcite; Hb=hornblende; Ser=sericite.

Table 7 *(continued)*

Drilling No.	depth	rock	occurrence	$\delta^{18}O$ (‰)	$\delta^{13}C$ (‰)
4MAHS-6	511.30m	gneiss	Cal. v	-5.4	11.1
4MAHS-6	647.80m	felsic dike	Cal. v	-7.5	12.9
4MAHS-6	658.50m	gneiss	Cal. v	-7.9	3.8
4MAHS-6	660.60m	gneiss	Cal. v	-7.3	6.7
4MAHS-6	664.30m	gneiss	Cal. v	-6.9	7.2
4MAHS-6	685.30m	Inishi rock	Cal. v	-6.2	0.0
4MAHS-6	693.80m	gneiss	Cal. v	-6.1	10.5
4MAHS-6	706.00m	Inishi rock	Cal. v (?)	-6.5	8.4
4MAHS-6	712.20m	Inishi rock	Cal. v	-3.8	9.6
4MAHS-6	719.30m	gneiss	Cal. v	-6.7	7.2
4MAHS-6	722.20m	Inishi rock	Cal. v	-5.8	2.0
4MAHS-6	724.30m	Inishi rock	Cal. v	-5.6	3.3
4MAHS-6	734.50m	Inishi rock	Cal. v	-6.6	3.3
4MAHS-6	742.40m	gneiss	Cal. v	-6.3	-1.3
4MAHS-6	748.50m	Inishi rock	Cal. v (?)	-7.0	4.7
4MAHS-6	753.90m	Inishi rock	Cal. v (?)	-6.1	9.5
4MAHS-6	801.10m	Inishi rock	Cal. v (?)	-6.1	10.9
4MAHS-6	817.00m	Inishi rock	Cal. v (?)	-2.5	12.6
4MAHS-6	818.60m	Inishi rock	Cal. v	-5.8	11.2
4MAHS-6	822.80m	Inishi rock	Cal. v (?)	-2.5	11.8
4MAHS-6	823.10m	Inishi rock	Cal. v	-6.1	10.7
4MAHS-6	849.50m	Inishi rock	Cal. v	-5.5	8.3
4MAHS-6	851.20m	Inishi rock	Cal. v	-5.3	12.1
4MAHS-6	883.30m	Inishi rock	Cal. v	-6.3	7.7
4MAHS-6	897.30m	Inishi rock	Cal. v	-6.2	10.1
56MAHI-1	138.30m	gneiss	Cal. v	-5.8	11.6
56MAHI-1	288.40m	Inishi rock	Cal. v	-1.7	2.7
56MAHI-2	238.50m	gneiss	Cal. v	-3.6	2.3
56MAHI-2	254.80m	Inishi rock	Cal. v	-1.6	15.5
5MAHS-7	167.70m	Inishi rock	Cal. v	-5.5	11.4
5MAHS-7	179.80m	Inishi rock	Cal. v	-6.0	10.2
5MAHS-7	260.30m	Inishi rock	Cal. v	-4.5	12.4
5MAHS-7	291.20m	Inishi rock	Cal. v	-1.8	1.0
5MAHS-7	309.90m	alt. Inishi rock	Cal. v	-3.6	1.7
5MAHS-7	353.60m	gneiss	Cal. v	-2.5	1.3
5MAHS-7	414.50m	Ep. Skarn	Cal. v	-2.7	1.0
5MAHS-7	422.10m	alt. Inishi rock	Cal. v	-3.0	3.2
5MAHS-7	438.20m	Ep. Skarn	Cal patch	-4.1	2.2
5MAHS-7	445.00m	gneiss	Cal. v	-2.6	3.9
5MAHS-7	451.00m	gneiss	Cal. v	-2.3	5.1
5MAHS-9	827.55m	alt. Inishi rock?	Cal. v	-5.9	6.6
5MAHS-9	905.00m	alt. Inishi rock	Cal. v	-6.8	-0.1
5MAHS-9	910.30m	alt. Inishi rock	Cal. v	-6.3	6.2
5MAHS-9	978.90m	alt. gneiss?	Cal. v	-7.3	1.2
5MAHS-9	983.40m	alt. gneiss?	Cal. v	-6.7	7.4
5MAHS-9	1001.90m	alt. gneiss?	Cal. v	-7.0	5.3
7MAKK-1	401.90m	Inishi rock ?	Cal. v	-3.6	12.0

*Abbreviations: V=veinlet; alt=alteration; Ep=epidote; Cal=calcite; Hb=hornblende; Ser=sericite.

Table 8 Oxygen and carbon isotope ratios of skarn calcite in the Sako-nishi area.

Drilling No.	depth	rock	occurrence	$\delta^{18}O$ (‰)	$\delta^{13}C$ (‰)
2MAHI-1	374.50m	skarn?	aggregate	-3.5	8.4
2MAHI-1	542.50m	alt. skarn	aggregate	-7.5	-5.1
2MAHI-1	547.65m	alt. skarn	thin vein	-3.1	0.0
2MAHI-1	549.60m	alt. skarn	thin vein	-3.4	0.2
2MAHI-1	674.10m	alt. skarn?	patch	-6.7	-4.3
2MAHI-1	683.80m	alt. skarn	patch	-7.3	-4.8
2MAHI-1	688.10m	alt. rock	vein	-2.8	5.5
3MAHS-1	139.60m	skarn	aggregate	-2.1	-0.3
3MAHS-1	146.60m	skarn	aggregate	-3.4	-1.6
3MAHS-1	148.30m	skarn	aggregate	-4.1	-2.0
3MAHS-1	291.70m	skarn?	aggregate	-6.8	-5.8
3MAHS-1	295.00m	Chl. skarn?	aggregate	-7.6	-3.7
3MAHS-1	297.70m	Chl. skarn?	aggregate	-7.8	-4.2
3MAHS-1	431.80m	skarn?	irregular vein	-5.4	-3.1
3MAHS-1	433.40m	skarn	thin vein	-4.7	2.8
3MAHS-1	435.45m	skarn	aggregate	-6.0	0.7
3MAHS-2	432.60m	skarn	aggregate	-5.7	-0.5
3MAHS-3	427.80m	mineralized gneiss	Cal. spot	-3.1	8.4
4MAHS-5	357.80m	ore	matrix	-3.0	0.8
4MAHS-5	368.40m	skarn	Ls remnant	-1.1	-0.2
56MAHI-1	145.10m	skarn	patch	-5.8	4.5
56MAHI-1	293.10m	skarn	patch	-2.6	9.3
5MAHS-7	324.30m	Ep. skarn	Cal. aggregate	-0.6	-0.6
5MAHS-7	335.30m	alt. skarn	Cal. aggregate	-2.4	0.7
5MAHS-7	340.40m	skarn	Cal. aggregate	-3.0	1.4
5MAHS-7	344.20m	skarn	Ls lens	-3.9	2.3
5MAHS-7	366.30m	ore	Cal. aggregate	-3.1	2.7
5MAHS-7	367.50m	ore	Cal. aggregate	-2.9	2.4
5MAHS-7	371.50m	ore	Cal. aggregate	-3.2	1.2
5MAHS-7	374.80m	ore	Cal. aggregate	-3.3	1.3
5MAHS-7	379.30m	ore	Cal. aggregate	-2.7	1.5
5MAHS-7	391.40m	ore	Cal. aggregate	-2.4	1.4
5MAHS-7	398.70m	alt. skarn	Cal. aggregate	-2.8	1.8
5MAHS-7	407.80m	ore	Cal. aggregate	-2.0	2.1
5MAHS-7	415.40m	skarn	Ls lens	-3.6	-1.3
5MAHS-7	419.70m	alt. skarn	matrix	-2.8	3.6
5MAHS-7	427.00m	skarn	Cal. aggregate	-1.8	1.4
5MAHS-7	433.70m	skarn	Cal. aggregate	-2.0	0.9
5MAHS-9	833.80m	skarn?	vein-lens	-7.0	10.7
5MAHS-9	836.40m	skarn?	vein	-7.0	6.8
62MAHI-1	106.30m	skarn	patch	-2.1	-1.5
62MAHI-1	108.10m	alt. skarn	aggregate	-2.6	1.3
62MAHI-1	219.90m	alt. skarn	vein	-4.8	10.4
62MAHI-1	222.20m	alt. skarn?	vein	-5.3	10.5
62MAHI-1	225.50m	alt. skarn?	vein	-4.2	12.4
62MAHI-1	307.00m	alt. skarn	thin vein	-4.4	7.7
62MAHI-1	310.20m	alt. skarn?	vein	-4.6	10.7
62MAHI-1	323.40m	skarn	thin vein	-7.1	-4.8
62MAHI-1	409.00m	skarn	vein	-2.2	1.6
62MAHI-1	412.60m	alt. rock	vein	-2.9	1.9
62MAHI-1	418.20m	alt. rock	vein	-3.4	1.8
7MAKK-1	314.00m	alt. skarn	matrix	-1.8	0.5
7MAKK-1	317.60m	alt. skarn	vein	-3.4	2.7
7MAKK-1	400.50m	skarn?	vein	-3.1	1.7
7MAKK-1	403.50m	skarn	vein	-3.7	14.0

*Abbreviations: Ls=limestone; alt=alteration; Chl=chlorite; Ep=epidote; Cal=calcite.

assemblages become dominant.

Petrolographical and mineralogical observations were performed for all carbonate used for isotopic analyses and silicate rock samples collected from outcrop and some silicate rocks from core in the Sako-nishi area (Table 4).

The bulk chemical compositions of the carbonate and silicate rocks were determined by means of inductively coupled plasma-optical emission spectrometry (ICP-OES, Jarrell-Ash model 750) at the Chemical Analysis Center, the University of Tsukuba. Chemical compositions of limestone, silicate rocks (gneiss, Inishi rock, and calc-silicate rock), and skarn calcite were analyzed using approximately 0.1g of powdered samples dissolved in 5ml of 20 % hydrochloric acid or 20ml of 5% HOAc. Quantitative analysis for ten elements Fe, Al, Mg, Mn, Ca, Na, Ba, Sr, Pb, and Zn was carried out on leachates. In order to compare technique of this study with commercial technique, I employed the ICP-OES method on aqua regia leachates by Chemex Labs Ltd., British Columbia, Canada.

The chemical compositions of whole rock of carbonate and silicate rock samples were also determined by means of Phillips PW1404 wavelength sequential automatic spectrometer (XRF) at the University of Tsukuba. Mold pellets were used for all rocks by pressing 2~3g samples and 4~5g Boric Acid (H_3BO_3) powder of Merck Co. Ltd.

On several samples with distinct stable isotopic compositions, observations and determinations of mineral compositions were carried out by means of cathodoluminescence (CL) and electron probe microanalysis (EPMA), respectively. Cathodoluminescence of calcite was undertaken using a Nuclide Corporation ELM-3R Luminoscope at Hiroshima University. General operating conditions for CL were 10-15 kV potential, 0.6-1.0 mA beam current, and 5-10 mm focussed beam. The electron microscope used for analyses of silicate and carbonate mineral compositions is a JEOL 5400 with Link Systems model QX2000 energy-dispersive spectrometer at the National Science Museum. Analytical conditions were 15kV accelerating voltage, 1nA sample current, and 80-seconds counting time (Yokoyama et al., 1993). The current drift was less than 1%.

Chapter 4 RESULTS

The chemical composition of the hydrochloric acid (HCl) and acetic acid (HOAc) leachates of the carbonate rocks are given in Tables 9 and 10, and that of the leachate using hydrochloric acid (HCl) and acetic acid (HOAc) of the skarn calcite and limestone collected from the Kamioka mine are shown in Table 11. The $\delta^{13}C$-$\delta^{18}O$ diagram and the concentration of elements for HCl leachate of the carbonate rocks plotted against $\delta^{18}O$ value are also shown in Figure 3.

4.1. Stable Isotopic Composition of Carbonate

Relationship of the oxygen and carbon isotopic composition of studied carbonate rock is shown in Figure 3A. The $\delta^{18}O$ and $\delta^{13}C$ values of limestone from drill core vary widely from -2.7 to 20.4‰ and from -7.7 to 4.6‰, respectively. In comparison, unaltered limestone 5 to 10 km away from the Kamioka mine has a narrow oxygen and carbon isotopic range ($\delta^{18}O$, 17-23‰; $\delta^{13}C$, 4.0-5.0‰. Arita and Wada,1990; MITI, 1998a). Accordingly, limestones having a high $\delta^{18}O$ value, more than 15‰, is considered unaltered and unaffected by hydrothermal fluid associated with mineralization. $\delta^{18}O$ values of no more than 5‰ characterize altered limestone which has been affected strongly by hydrothermal fluid associated with mineralization.

Several authors (Wada, 1978; Shimazaki et al., 1986; Shimazaki and Kusakabe, 1990a; MITI, 1998a) have reported that skarn calcite associated with skarn and ore minerals have distinct $\delta^{18}O$ and $\delta^{13}C$ values ranging from -5.7 to 5.8‰ and from -7.8 to 0.0‰, respectively (Fig. 3A). Skarn calcite is significantly depleted in ^{18}O and ^{13}C relative to limestone. The $\delta^{18}O$ and $\delta^{13}C$ values for limestone from outcrop in the Sako-nishi area are relatively high ranging from 8.1 to 21.1‰ and from -1 to 5.3‰, respectively, while strongly altered limestone with low $\delta^{18}O$ values of 5‰ or less could not be recognized. I divided the limestone into four groups based on $\delta^{18}O$ values: A ($\delta^{18}O$:>15‰), B ($\delta^{18}O$:10-15‰), C ($\delta^{18}O$:5-10‰), and D $\delta^{18}O$:<5‰). In outcrop around the Sako-nishi area, limestone of groups A to C are

Table 9 Chemical compositions for acetic acid(HOAc) digestion of limestone and silicate rock in the Sako-nishi area.

No	Sample No.	Z	rock	G	$\delta^{18}O$ (‰)	$\delta^{13}C$ (‰)	Fe (ppm)	Al (ppm)	Mg (ppm)	Mn (ppm)	Ca (%)	Na (ppm)	Ba (ppm)	Sr (ppm)	Pb (ppm)	Zn (ppm)
1	RK3106	I	Ls	C	8.3	3.3	745	47	1350	450	38.9	84	16	972	0	39
2	RK3105	I	Ls	C	8.9	3.2	1340	307	777	399	29.2	0	14	646	0	69
3	RM0618	I	Gn	C	9.7	0.2	102	10	799	210	8.8	45	8	213	0	2
4	RS0112	I	Ls	B	10.2	2.5	1000	0	2830	648	36.6	192	631	412	169	374
5	RS0111	I	Ls	B	10.6	2.8	1770	89	661	482	41.1	52	41	400	0	13
6	RS0405	I	Ls	B	10.6	3.2	1970	244	1430	373	33.0	95	41	816	0	79
7	RS0802	I	Ls	B	11.2	2.8	2360	112	1620	542	34.7	33	20	666	0	50
8	RK2502	I	Cs	B	11.3	-0.1	1080	324	267	207	12.8	51	13	241	0	84
9	RK3103	I	Ls	B	11.6	1.3	877	27	3920	181	40.2	37	8	440	0	8
10	RK2106	I	Gn	B	11.9	1.8	363	391	255	71	6.5	66	5	137	0	65
11	RK1003	I	Ls	B	12.1	2.3	1740	92	4800	270	38.6	94	12	665	0	51
12	RK2102	I	Ls	B	12.2	1.3	1680	106	17400	1020	37.1	63	6	564	0	16
13	RK2509	I	Ls	B	12.2	1.0	420	29	99	148	34.3	9	71	539	0	26
14	RK2104	I	Ls	B	12.6	3.9	1210	30	1000	411	45.8	101	32	855	0	18
15	RK0702	I	Ls	B	13.1	4.4	608	0	1550	140	39.5	138	10	1030	718	0
16	RK2514	I	Ls	B	13.2	0.5	1060	39	1130	156	41.2	93	37	271	0	30
17	RK3112	I	Ls	B	13.4	4.6	1050	46	2850	112	38.4	66	23	780	0	25
18	RS0403	I	Ls	B	13.4	1.8	1230	80	302	363	29.9	34	13	341	0	70
19	RK2107	I	Ls	B	13.5	2.2	598	69	1720	230	22.4	70	9	253	0	29
20	RK0704	I	Ls	B	13.8	4.0	152	0	119	231	36.8	8	318	1240	0	0
21	RK0705	I	Ls	B	14.3	3.1	1910	33	3210	323	39.8	85	25	516	0	29
22	RK2507	I	Ls	B	14.6	3.8	874	125	1401	669	34.8	44	37	658	0	33
23	RK1006	I	Ls	B	14.7	3.0	694	192	420	249	20.6	46	14	578	0	38
24	RK2105	I	Ls	A	15.1	4.8	908	113	2760	146	40.4	0	88	673	265	2
25	RM0616	I	Ls	A	15.1	4.1	629	123	6580	84	40.4	80	14	661	0	47
26	RK2505	I	Ls	A	16.6	3.1	2730	192	24000	419	35.5	84	10	439	0	73
27	RK1004	I	Ls	A	16.8	0.1	880	136	671	109	39.7	79	6	347	0	14
28	RK2506	I	Ls	A	17.4	3.8	1140	0	7160	172	38.5	49	16	592	0	50
29	RK0703	I	Cs	A	18.0	3.5	1250	155	19300	136	29.8	220	14	337	0	22
30	RK2504	I	Ls	A	18.5	3.9	1490	29	2530	342	37.6	101	13	682	0	18
31	RM0302	II	Ls	C	8.1	0.2	767	22	1250	515	42.1	90	39	442	0	29
32	RS0104	II	Ls	C	8.3	0.2	1640	0	4620	595	35.3	319	13	538	0	7
33	RS0106	II	Ls	C	9.6	2.1	585	23	1340	164	41.9	45	21	280	0	33
34	RM0603	III	Ls	B	12.5	2.0	1130	84	1730	319	38.9	56	169	1350	0	41
35	RM0604	III	Ls	B	13.6	3.5	881	107	3570	210	25.5	64	459	373	0	56
36	RM0605	III	Ls	B	13.8	4.3	1960	121	909	595	39.7	0	179	885	0	53
37	RK0701	III	Ls	A	15.9	3.3	1260	77	1620	153	36.1	62	9	856	0	23
38	RK3109	IV	Gn	B	10.3	-7.8	2410	664	485	470	4.8	0	39	260	0	18
39	RK2103	IV	Ls	B	14.7	2.4	1820	96	3800	573	38.3	99	36	462	0	119
40	RS1701		Cs	C	7.2	0.2	334	0	128	192	31.4	171	5	178	117	213
41	RS1710		Ls	C	9.7	1.2	288	167	172	181	37.4	0	7	308	0	0
42	RK2513		Ls	C	9.8	-1.0	249	32	159	97	31.5	60	4	554	0	11
43	RS0406		Ls	B	10.6	3.2	1690	94	7620	161	37.1	132	19	799	0	37
44	RK2512		Ls	B	10.9	0.3	330	55	267	172	21.1	67	21	305	0	18
45	RM1503		Ls	B	11.0	1.6	473	49	2580	207	36.4	109	39	262	0	56
46	RK3111		Cs	B	11.7	2.1	1510	66	8320	562	32.8	64	14	446	0	7
47	RS1104		Ls	B	11.9	3.4	349	122	3710	122	42.0	0	22	551	0	31
48	RM0613		Ls	B	12.0	4.1	1240	42	1770	189	39.0	103	15	806	0	14
49	RM0617		Ls	B	12.1	2.0	854	118	2990	122	41.2	112	10	553	0	21
50	RS0419		Ls	B	12.1	2.9	513	134	3710	184	38.3	54	9	519	0	8
51	RM0612		Ls	B	12.3	2.5	686	164	1590	373	39.9	45	56	407	0	59
52	RM0619		Ls	B	12.4	0.9	1080	82	907	291	42.0	21	5	383	0	0
53	RM0606		Ls	B	12.5	4.8	731	4	1600	299	39.7	111	100	779	0	22
54	RM0615		Ls	B	12.9	3.3	1250	73	1460	537	32.0	101	45	636	0	88
55	RS0810		Ls	B	13.0	3.6	3040	140	5120	241	37.2	1	47	806	0	31
56	RM0614		Ls	B	13.1	3.5	1750	32	4370	335	40.7	133	45	766	0	4
57	RK3102		Ls	B	13.2	2.8	478	0	630	142	39.3	139	142	908	0	10
58	RM0911		Ls	B	13.3	3.0	1800	84	3110	383	36.8	41	17	1310	0	100
59	RM0910		Ls	B	13.6	3.9	831	152	3840	121	38.2	8	10	993	0	65
60	RK3107		Ls	B	13.7	2.5	1930	39	5570	724	38.7	111	37	446	0	0
61	RK2510		Ls	B	14.0	3.4	1860	0	1400	372	39.4	60	10	850	0	4
62	RS0805		Ls	B	14.3	3.3	2700	76	1900	521	36.7	91	51	725	0	12
63	RS0812		Ls	B	14.7	3.9	2330	16	2050	307	40.3	111	21	635	0	39
64	RS0408		Ls	A	15.0	4.5	1240	36	1850	240	40.2	135	22	725	0	53
65	RS0809		Ls	A	15.3	3.5	878	112	841	166	39.0	44	13	886	0	54
66	RS1103		Ls	A	15.4	3.8	612	156	3540	135	38.8	67	69	1060	0	14
67	RK0706		Ls	A	15.8	5.1	921	6	1700	264	38.4	128	20	535	0	43
68	RS0804		Gn	A	15.8	-0.1	86	11	82	103	11.6	73	1	73	0	0
69	RM0608		Ls	A	15.9	4.8	487	80	1510	341	38.5	60	100	701	0	25
70	RK2108		Ls	A	16.3	4.3	1050	76	1840	222	39.2	6	45	634	31	20
71	RS2408		Ls	A	16.6	3.5	1870	0	6150	187	34.4	354	19	427	5	9
72	RS0801		Ls	A	16.8	4.6	333	33	1430	76	41.7	145	15	699	0	51
73	RM0610		Ls	A	17.1	1.4	247	50	2210	135	40.9	13	89	461	0	45
74	RM2302		Ls	A	17.1	3.5	690	32	863	357	3.9	39	13	701	0	6
75	RS1106		Ls	A	17.2	3.9	751	99	2940	267	40.3	84	28	859	0	24
76	RM1207		Ls	A	17.3	3.6	2470	192	4960	193	34.1	89	20	823	0	13
77	RM0311		Ls	A	17.6	4.2	407	68	2210	82	40.0	142	18	867	0	38
78	RS0811		Ls	A	17.7	4.4	829	25	1780	169	34.4	86	8	818	0	17
79	RS0416		Ls	A	17.9	4.4	816	0	413	479	37.3	0	464	962	0	45
80	RM0915		Ls	A	18.6	3.3	2500	32	2210	325	39.9	44	13	862	0	97
81	RK2511		Ls	A	18.7	3.3	1760	93	7600	172	39.4	127	22	489	0	60
82	RK3108		Ls	A	19.0	5.3	380	139	2590	71	39.0	106	22	643	0	34
83	RS2410		Ls	A	19.5	4.4	498	187	3730	184	41.4	64	13	698	0	54
84	RS0807		Ls	A	20.0	4.0	1280	38	1360	363	37.0	48	3	842	0	10
85	RS0808		Ls	A	21.1	4.4	905	43	1780	301	38.7	57	8	939	0	0
	3HS-3		Ls	C	9.6	2.5	1070	120	715	351	34.9	97	19	362	0	11
	3HS-3		Ls	D	2.2	-3.6	1190	538	408	1016	19.6	466	16	431	0	2
	7KK-1		Ls	D	1.4	1.6	1210	241	292	776	18.2	103	2	203	0	3
	9HSU		Ls				7740	0	505	####	40.8	134	0	420	15	3

Oxygen and carbon isotopic data are taken from MITI (1998a).

Abbreviations: Z=zone of mineralization; G=group of limestone; Ls=limestone; Gn=gneiss; Cs=calc-silicate rock; In=Inishi rock.

Table 10 Chemical compositions for hydrochloric acid(HCl) leachate of limestone and silicate rock in the Sako-nishi area.

No	Sample No.	Z	rock	G	δ 18O (‰)	δ 13C (‰)	Fe (ppm)	Al (ppm)	Mg (ppm)	Mn (ppm)	Ca (%)	Na (ppm)	Ba (ppm)	Sr (ppm)	Pb (ppm)	Zn (ppm)
1	RK3106	I	Ls	C	8.3	3.3	1040	207	1250	377	31.9	67	14	804	32	27
2	RK3105	I	Ls	C	8.9	3.2	9550	10200	7030	411	21.5	71	12	486	12	64
3	RM0618	I	Gn	C	9.7	0.2	1470	337	6260	296	8.6	55	10	194	18	12
4	RS0112	I	Ls	B	10.2	2.5	2800	1120	4510	671	39.6	143	659	399	489	2190
5	RS0111	I	Ls	B	10.6	2.8	1500	228	504	325	25.7	83	29	280	27	12
6	RS0405	I	Ls	B	10.6	3.2	9370	3700	3720	316	23.9	127	33	599	60	104
7	RS0802	I	Ls	B	11.2	2.8	8380	3050	2840	469	28.0	74	20	552	55	85
8	RK2502	I	Cs	B	11.3	-0.1	11000	5370	2970	250	10.0	152	18	200	20	161
9	RK3103	I	Ls	B	11.6	1.3	1170	143	2850	137	28.4	82	8	335	64	43
10	RK2106	I	Gn	B	11.9	1.8	3460	4400	1220	111	5.8	146	6	121	39	124
11	RK1003	I	Ls	B	12.1	2.3	3100	1360	5210	243	33.0	151	12	582	41	23
12	RK2102	I	Ls	B	12.2	1.3	4600	682	11600	762	26.5	158	4	420	32	18
13	RK2509	I	Ls	B	12.2	1.0	567	291	143	164	27.7	86	56	405	15	36
14	RK2104	I	Ls	B	12.6	3.9	1120	238	1730	188	23.0	60	17	403	34	32
15	RK0702	I	Ls	B	13.1	4.4	712	136	1420	112	30.1	55	10	839	41	14
16	RK2514	I	Ls	B	13.2	0.5	875	184	960	107	27.0	121	27	204	32	68
17	RK3112	I	Ls	B	13.4	4.6	1570	772	3310	89	28.2	96	20	647	18	13
18	RS0403	I	Ls	B	13.4	1.8	2330	1160	382	272	21.2	52	9	249	23	20
19	RK2107	I	Ls	B	13.5	2.2	1290	1970	2200	218	19.4	91	9	213	11	16
20	RK0704	I	Ls	B	13.8	4.0	237	49	174	207	30.4	71	269	1020	45	20
21	RK0705	I	Ls	B	14.3	3.1	1260	358	1660	132	15.6	98	10	246	69	21
22	RK2507	I	Ls	B	14.6	3.8	1900	776	1890	508	25.1	61	28	493	12	17
23	RK1006	I	Ls	B	14.7	3.0	2040	1430	958	202	15.5	292	12	462	11	43
24	RK2105	I	Ls	A	15.1	4.8	750	134	2180	107	28.9	77	64	478	37	23
25	RM0616	I	Ls	A	15.1	4.1	510	90	4350	57	27.2	144	10	472	22	18
26	RK2505	I	Ls	A	16.6	3.1	3510	591	17700	330	26.0	156	9	331	72	100
27	RK1004	I	Ls	A	16.8	0.1	1640	646	1110	94	32.4	76	6	286	4	20
28	RK2506	I	Ls	A	17.4	3.8	935	193	3980	128	23.5	84	13	384	52	20
29	RK0703	I	Cs	A	18.0	3.5	4280	3010	23200	129	24.8	591	25	288	91	47
30	RK2504	I	Ls	A	18.5	3.9	2070	217	2480	309	32.3	73	12	45	49	24
31	RM0302	II	Ls	C	8.1	0.2	1160	246	1070	374	28.5	66	30	329	7	17
32	RS0104	II	Ls	C	8.3	0.2	3780	1830	7260	604	40.2	248	13	502	31	13
33	RS0106	II	Ls	C	9.6	2.1	731	161	1160	128	30.9	121	17	220	16	16
34	RM0603	III	Ls	B	12.5	2.0	1070	190	1450	240	27.8	141	131	1000	40	28
35	RM0604	III	Ls	B	13.6	3.5	2270	737	4950	250	28.2	92	575	448	38	152
36	RM0605	III	Ls	B	13.8	4.3	2460	133	821	505	32.3	65	159	744	100	68
37	RK0701	III	Ls	A	15.9	3.3	2680	1720	3140	130	25.9	75	8	612	38	36
38	RK3109	IV	Gn	B	10.3	-7.8	16500	6800	2340	435	4.0	61	49	209	35	54
39	RK2103	IV	Ls	B	14.7	2.4	3720	1180	4540	459	28.9	100	35	364	68	222
40	RS1701		Cs	C	7.2	0.2	6480	3410	2450	226	30.1	174	9	165	587	1480
41	RS1710		Ls	C	9.7	1.2	2200	1570	1210	165	27.0	75	7	244	7	53
42	RK2513		Ls	C	9.8	-1.0	1020	534	1560	133	19.6	56	10	270	45	23
43	RS0406		Ls	B	10.6	3.2	1900	87	6400	152	34.0	170	19	747	77	50
44	RK2512		Ls	B	10.9	0.3	1210	635	1310	415	26.5	102	24	265	20	42
45	RM1503		Ls	B	11.0	1.6	992	609	3220	182	30.3	114	50	219	24	20
46	RK3111	Cs	B		11.7	2.1	4070	2580	11700	484	27.0	197	18	372	59	111
47	RS1104	Ls	B		11.9	3.4	328	70	2520	83	28.4	97	16	384	21	32
48	RM0613	Ls	B		12.0	4.1	2240	1720	3050	161	31.1	78	14	679	61	38
49	RM0617	Ls	B		12.1	2.0	1090	419	3040	101	33.1	79	8	449	37	20
50	RS0419	Ls	B		12.1	2.9	3020	2660	6380	145	27.6	83	8	376	46	42
51	RM0612	Ls	B		12.3	2.5	667	852	1190	262	26.8	71	38	284	34	62
52	RM0619	Ls	B		12.4	0.9	1190	127	735	214	28.7	60	5	289	7	14
53	RM0606	Ls	B		12.5	4.8	742	142	1370	221	28.3	179	71	551	22	21
54	RM0615	Ls	B		12.9	3.3	1530	224	1530	425	24.0	70	37	509	8	60
55	RS0810	Ls	B		13.0	3.6	2240	197	3430	176	26.9	62	41	623	23	30
56	RM0614	Ls	B		13.1	3.5	1760	161	3280	255	29.8	95	35	566	45	21
57	RK3102	Ls	B		13.2	2.8	894	324	1060	142	42.6	105	137	839	35	27
58	RM0911	Ls	B		13.3	3.0	2130	376	2490	291	27.0	82	15	975	42	85
59	RM0910	Ls	B		13.6	3.9	911	293	3130	94	28.4	86	8	786	17	29
60	RK3107	Ls	B		13.7	2.5	2450	560	4710	559	28.3	131	29	348	55	22
61	RK2510	Ls	B		14.0	3.4	4530	517	1760	325	32.0	94	11	692	35	17
62	RS0805	Ls	B		14.3	3.3	6390	291	1840	445	29.9	72	44	602	53	53
63	RS0812	Ls	B		14.7	3.9	2900	604	2170	240	29.6	90	18	493	32	19
64	RS0408	Ls	A		15.0	4.5	1170	159	1680	194	31.6	112	19	594	35	16
65	RS0809	Ls	A		15.3	3.5	1340	384	1250	143	31.9	82	11	721	16	20
66	RS1103	Ls	A		15.4	3.8	586	314	2830	90	25.1	62	57	734	51	33
67	RK0706	Ls	A		15.8	5.1	2720	530	2420	240	32.8	81	19	485	27	46
68	RS0804	Gn	A		15.8	-0.1	524	134	2100	89	17.5	47	6	183	39	23
69	RM0608	Ls	A		15.9	4.8	897	265	1540	257	26.9	97	78	533	34	44
70	RK2108	Ls	A		16.3	4.3	1250	252	1880	190	32.5	76	39	543	55	51
71	RS2408	Ls	A		16.6	3.5	2520	1450	8380	195	39.8	361	24	416	45	38
72	RS0801	Ls	A		16.8	4.6	298	81	1200	60	31.7	73	13	553	13	27
73	RM0610	Ls	A		17.1	1.4	302	303	2030	114	33.6	73	76	383	44	31
74	RM2302	Ls	A		17.1	3.5	1300	393	1120	321	31.4	74	11	574	13	14
75	RS1106	Ls	A		17.2	3.9	1200	203	2730	240	34.2	75	26	731	21	43
76	RM1207	Ls	A		17.3	3.6	3880	2290	5300	176	29.3	602	26	722	91	45
77	RM0311	Ls	A		17.6	4.2	442	194	1740	55	25.5	123	12	569	32	28
78	RS0811	Ls	A		17.7	4.4	887	124	1610	133	26.0	62	7	636	10	30
79	RS0416	Ls	A		17.9	4.4	965	60	251	266	20.0	64	298	516	35	18
80	RM0915	Ls	A		18.6	3.3	1700	270	1260	231	23.0	102	118	530	65	27
81	RK2511	Ls	A		18.7	3.3	1460	276	4520	93	22.7	131	14	297	58	59
82	RK3108	Ls	A		19.0	5.3	641	426	2330	49	26.3	140	18	469	34	75
83	RS2410	Ls	A		19.5	4.4	884	348	3430	156	33.7	115	12	585	18	35
84	RS0807	Ls	A		20.0	4.0	5660	309	1420	307	30.0	70	4	682	51	14
85	RS0808	Ls	A		21.1	4.4	1120	147	1470	235	28.5	74	8	703	20	53
	3HS-3	Ls	C		9.6	2.5	3180	3540	1330	377	37.6	94	20	342	19	20
	3HS-3	Ls	D		2.2	-3.6	14600	12300	5110	1290	20.1	2290	100	607	39	40
	7KK-1	Ls	D		1.4	1.6	14400	7610	3280	1220	18.3	87	4	297	44	59
	9HSU	Ls					7300	46	484	9910	37.5	90	1	368	70	5

Oxygen and carbon isotopic data are taken from MITI (1998a).

Abbreviations: Z=zone of mineralization; G=group of limestone; Ls=limestone; Gn=gneiss; Cs=calc-silicate rock; In=Inishi rock.

Table 11 Chemical compositions for HOAc and HCl leachates of limestone and skarn calcite from the Kamioka mine.

Rock	Deposit	Locality orebody and drill-core	Fe (ppm)	Al (ppm)	Mg (ppm)	Mn (ppm)	Ca (%)	Na (ppm)	Ba (ppm)	Sr (ppm)	Pb (ppm)	Zn (ppm)
Acetic acid (HOAc)												
Limestone	Mozumi	East No.4	2100	0	65	2950	27.7	135	1	138	87	13
	Mozumi	North No.20	459	6	503	240	41.2	145	0	256	0	1
	Tochibora	No.5 OTSU	674	7	1910	127	39.5	259	5	797	27	2
	Tochibora	No.9	691	88	607	180	34.3	290	5	809	17	2
Shiroji ore	Mozumi	North No.20	1040	0	172	6500	42.4	148	0	276	23	25
	Mozumi	East No.4	1590	126	223	12100	30.7	139	0	176	126	193
	Tochibora	No.5 OTSU	3080	0	424	29500	39.2	135	10	528	50	5
	Tochibora	No.9	9530	25	1070	43500	38.5	336	1	396	231	36
	Sako-nishi	9MAHSU-1	7740	0	505	10600	40.8	134	0	420	15	3
Mokuji ore	Mozumi	East No.4	718	0	45	4710	41.2	199	0	249	0	2
	Mozumi	North No.20	147	63	64	3950	41.3	189	0	322	10	2
	Tochibora	No.9	36	0	4	3080	43.4	110	0	69	0	1
	Tochibora	Shiragane	418	0	35	9400	39.5	170	2	315	7	3
Hydrochloric acid (HCl)												
Limestone	Mozumi	East No.4	4080	234	155	4530	30.4	127	3	129	278	302
	Mozumi	North No.20	780	347	852	245	39.1	95	1	226	33	12
	Tochibora	No.5 OTSU	733	258	2070	119	34.5	185	5	685	40	12
	Tochibora	No.9	1990	3730	1930	217	31.1	275	7	741	36	12
Shiroji ore	Mozumi	North No.20	1050	54	183	5850	37.9	85	2	242	33	53
	Mozumi	East No.4	4200	1340	683	11200	27.9	86	1	153	583	514
	Tochibora	No.5 OTSU	2980	55	411	26800	35.3	87	11	462	74	44
	Tochibora	No.9	9060	188	1020	39000	34.3	219	2	353	852	559
	Sako-nishi	9MAHSU-1	7300	46	484	9910	37.5	90	1	368	70	5
Mokuji ore	Mozumi	East No.4	892	73	58	4500	38.1	129	1	213	27	66
	Mozumi	North No.20	184	4270	81	3690	38.6	196	2	296	35	20
	Tochibora	No.9	67	36	9	2890	40.3	65	0	60	22	13
	Tochibora	Shiragane	687	51	41	8600	35.9	112	4	271	47	48

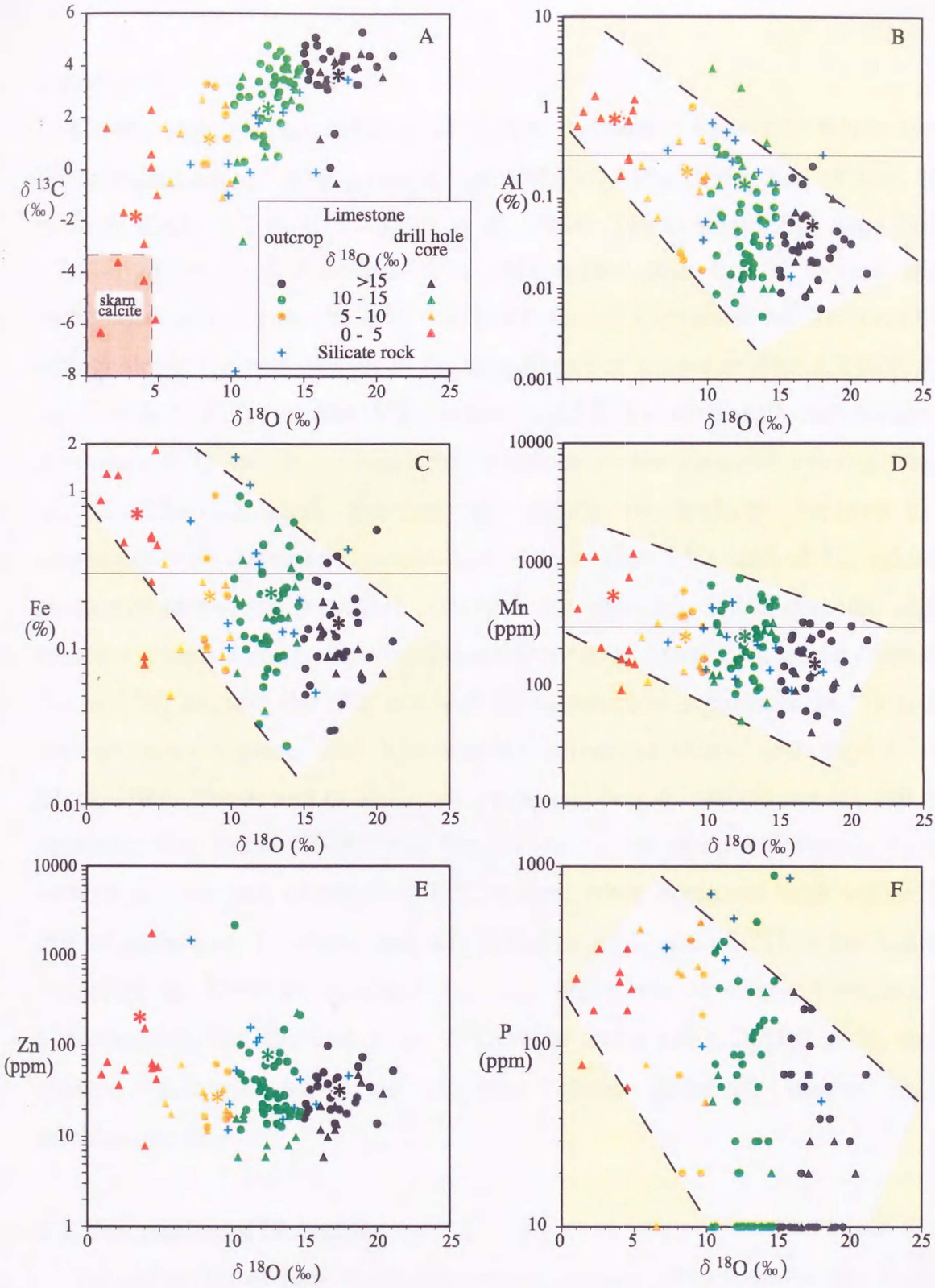

Fig 3. Scatter plots of $\delta^{13}C$, Al, Fe, Mn, Zn, and P against $\delta^{18}O$ for limestones and silicate rocks from the Sako-nishi area. The concentrations of Al, Fe, Mn, and Zn are for the HCl-leachates, that of P is for the aqua-regia leachates. The oxygen and carbon isotopic data are taken from MITI (1998a). Thin lines are recommended threshold values for the Al, Fe, and Mn contents to separate hydrothermally-altered limestone from the unaltered one in the Sako-nishi area.

distributed.

Carbon isotopic compositions of marine carbonates vary only within narrow limits regardless of their geologic age (0.56±1.55‰, Keith and Weber, 1964; mollusk shells -1.7 to 4.2‰, Keith et al., 1964). The average $\delta^{13}C$ value (3.65± 1.23‰) of group A limestone is a little higher than that of typical marine carbonates. In contrast, the $\delta^{18}O$ values of marine carbonates are known to vary with geologic age and changes in the temperature of sea water (Faure, 1986). Shieh and Taylor (1969) reported $\delta^{18}O$ values of 22-27‰ for marine carbonates. The maximum $\delta^{18}O$ values for unaltered limestone in the Kamioka mining area are around 22‰, indicating that they are slightly but distinctly depleted in ^{18}O compared with reported marine carbonates. The $\delta^{18}O$ and $\delta^{13}C$ values of metamorphic and hydrothermal carbonate are generally lower than the primary values. Carbonate rocks experiencing decarbonation reactions become depleted in ^{18}O and ^{13}C because the CO_2 released during reaction is enriched in ^{18}O and ^{13}C through metamorphism and hydrothermal alteration (Shieh and Taylor, 1969; Black, 1984; Taylor and O'Neil, 1977; Kim and Nakai, 1980; So et al., 1993). As pointed out by Wada (1978), only the $\delta^{18}O$ values of group A limestone decrease without conspicuous decrease of $\delta^{13}C$ values, when compared with values from marine carbonate. I assume that this selective depletion of ^{18}O in the unaltered limestone in Kamioka resulted from the interaction between limestone and hydrothermal fluid that had a low $\delta^{18}O$ value and a low CO_2/H_2O ratio, such as evolved meteoric water or magmatic fluid generated during regional metamorphism.

4.2. Description of Limestone

The collection of pure limestone was sometimes difficult where thin layers of the Inishi rock, gneiss, and calc-silicate rock are intercalated in limestone. However, microscopic observation shows that the limestone is clearly distinguished from the intercalating silicate rocks by the absence of plagioclase and titanite. Most of the limestone is pale gray in color with significant amounts of

disseminated black graphite. Although correlation between the $\delta^{18}O$ and $\delta^{13}C$ value and color of limestone are not distinct, it is recognized that limestone which has low isotopic composition tends to be greenish white to gray in color (Fig. 4).

4.2.1. Group A

Thirty eight carbonate samples from limestone fall within group-A. Group-A limestone is white to pale gray in color (Fig. 4A) and consists mainly of equigranular holocrystalline calcite (grain size: 0.5 to 2mm) and small amounts of diopsidic clinopyroxene, tremolite, olivine, and graphite (Fig. 5A-2). The observed boundaries between calcite grains are sharp and polygonal (Fig. 5A-1). A deformation structure develops occasionally in these calcites. Olivine is partly altered to serpentine, and diopsidic clinopyroxene to tremolite. Kano (1998) revealed that limestone of the Hida belt is extremely poor in the dolomitic component (rich in the calcic component), and limestone of the central mass exhibits coarse- to medium-grained, typical granoblastic texture without the development of any mylonitic structure, and is characterized by small amounts of diopsidic clinopyroxene, tremolite, olivine, and graphite.

4.2.2. Group B

Fifty four carbonate samples from limestone fall within group-B. The majority of the group-B limestone is pale gray to pale green in color (Fig. 4B). Coarse-grained calcite is dominant, but small aggregates or micro-veinlets (to 0.1 mm in width) of fine-grained calcite occur locally. Under the microscope, the fine-grained calcites are more transparent than the coarse-grained ones. The limestone contains diopsidic clinopyroxene, and olivine with minor actinolite, chlorite, tremolite, prehnite, pyrite, and stilpnomelane. Actinolite, chlorite, and tremolite replace primary diopsidic clinopyroxene. In some cases, actinolite replaces tremolite along the rims and cleavage of pseudomorphosed clinopyroxene (Fig. 5B-2). Chlorites is sporadically distributed and associated with actinolite. Prehnite occurs as vein with fine-grained and columnar crystals (20-100 μm in width), and is hydrothermal in

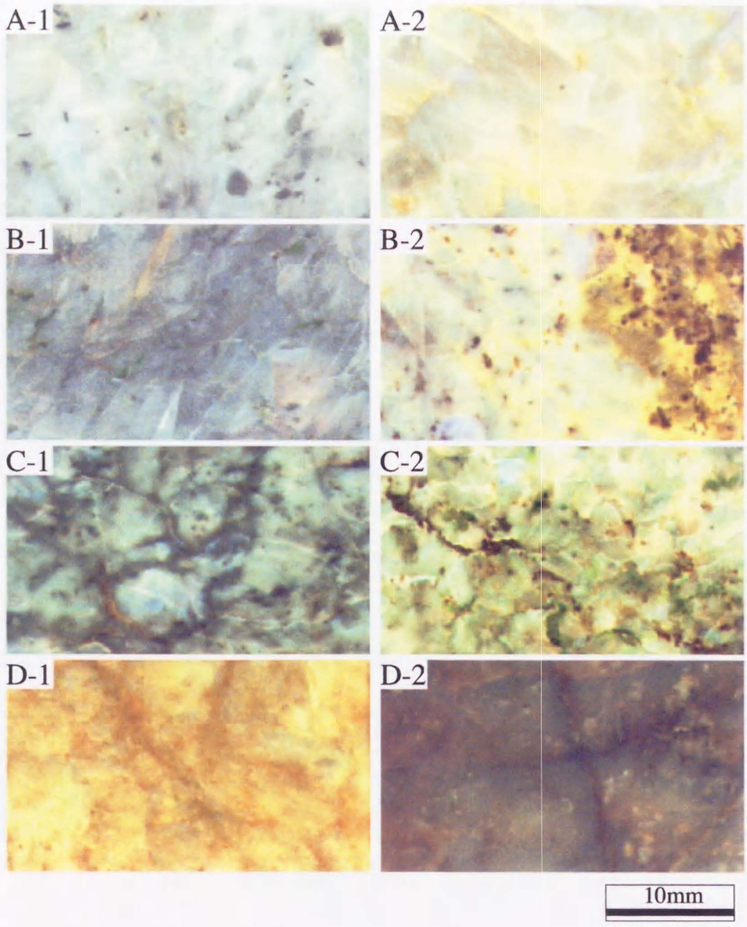

Fig. 4. Representative hand specimens of limestone in the Sako-nishi and Mozumi areas. Plate numbers of A, B, C, and D correspond to limestone of groups A, B, C, and D, respectively. A-1, sample 0808 containing graphite and showing pale gray ($\delta^{18}O$=21.1‰ and $\delta^{13}C$=4.4‰); A-2, sample 1106 composed of an aggregate of calcite with polygonal grain boundaries ($\delta^{18}O$=17.2‰ and $\delta^{13}C$=3.9‰); B-1, sample 605 containing amphibole and chlorite and showing pale green ($\delta^{18}O$=13.8‰ and $\delta^{13}C$=4.3‰); B-2, sample 2102 with dissemination of brown sphalerite and pyrite mostly oxidized into hydroxide along the rim ($\delta^{18}O$=12.2‰ and $\delta^{13}C$=1.3‰); C-1, sample 0104 with blackish veinlet of fine-grained calcite ($\delta^{18}O$=8.3‰ and $\delta^{13}C$=0.2‰); C-2, sample 0112 composed of fine-grained calcite and chlorite exhibiting amoeba-like texture or replacing mafic minerals ($\delta^{18}O$=10.2‰ and $\delta^{13}C$=2.5‰); D-1, sample RH006 with pale orange veinlets of fine-grained calcite ($\delta^{18}O$=2.9‰ and $\delta^{13}C$=–1.6‰); D-2, sample RH005 with fine-grained calcite occurring as matrix and veinlets ($\delta^{18}O$=1.1‰ and $\delta^{13}C$ =–0.5‰). Samples RH005 and RH006 are taken from MITI (1998b).

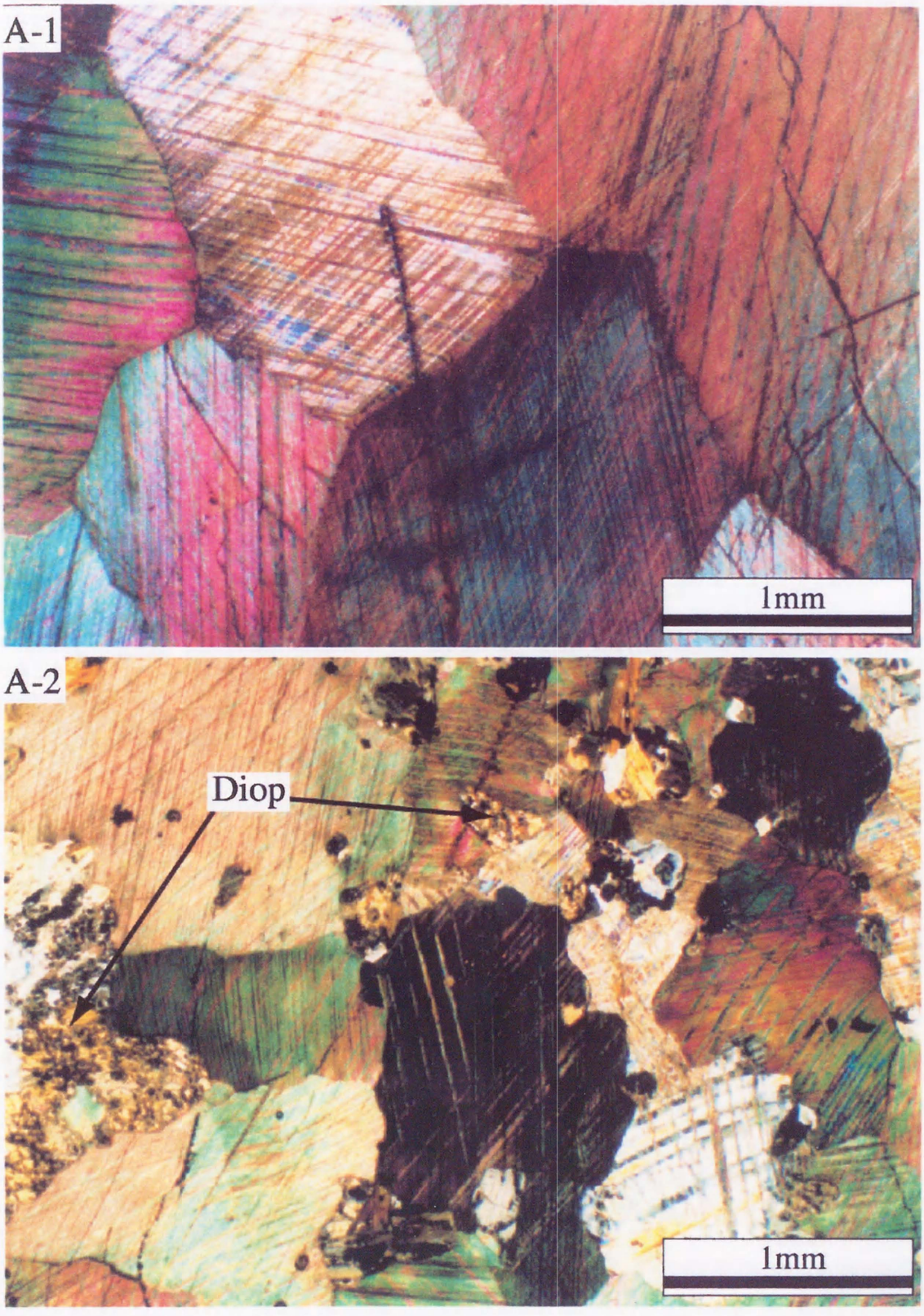

Fig. 5. Microscopic photograph of limestones in the Sako-nishi area *(see p.41)*.

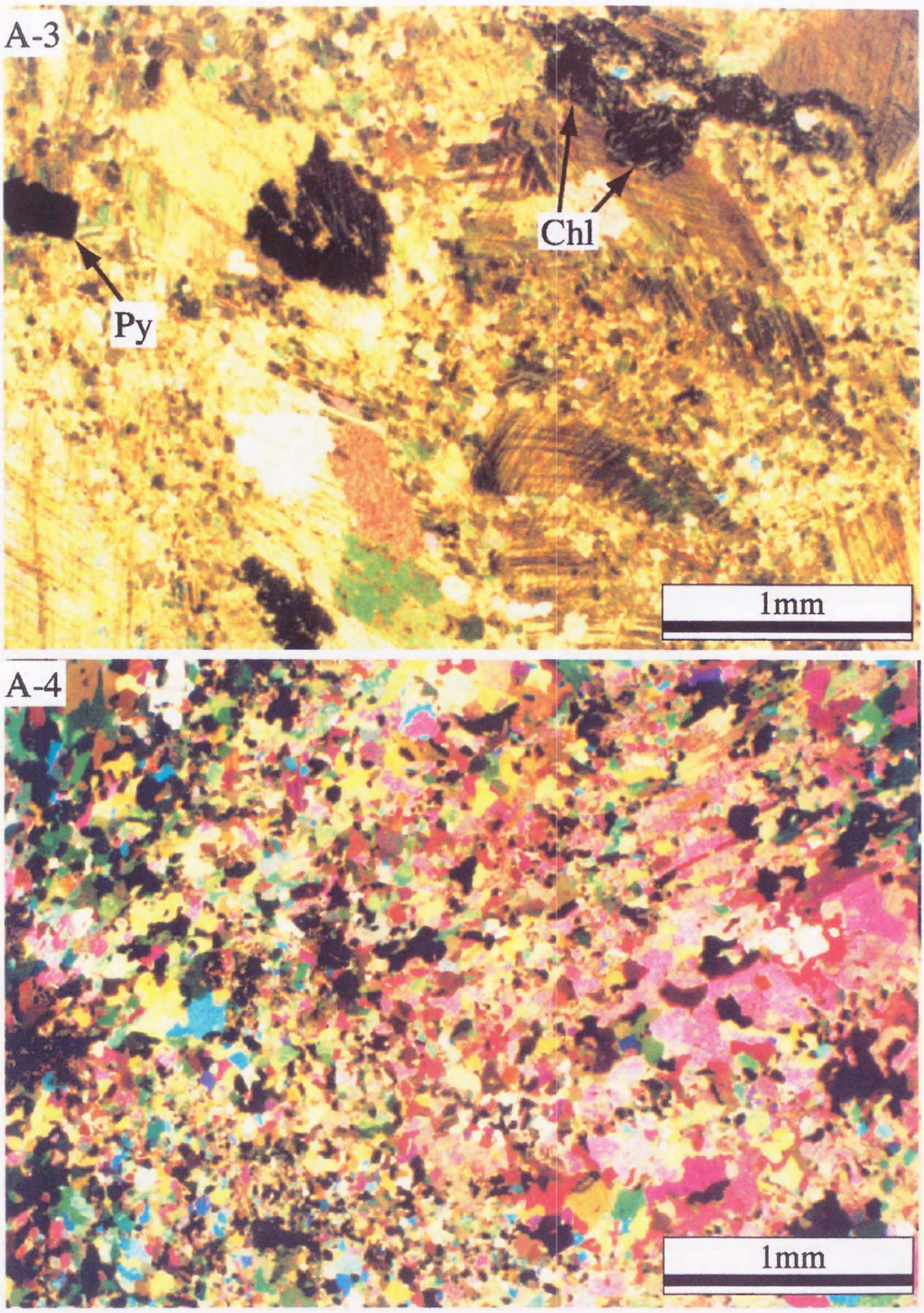

Fig. 5. *(continued)*

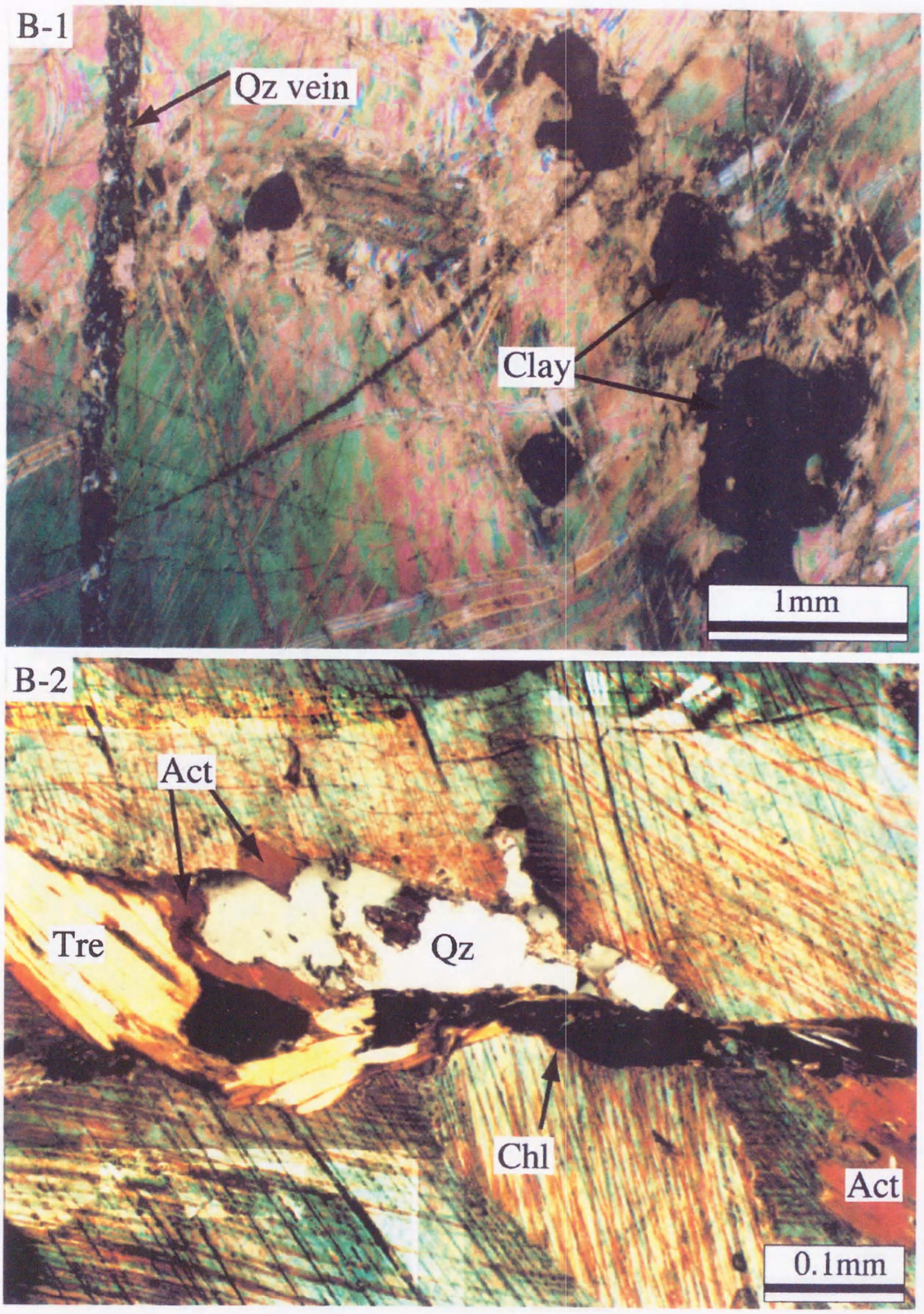

Fig. 5. *(continued)*

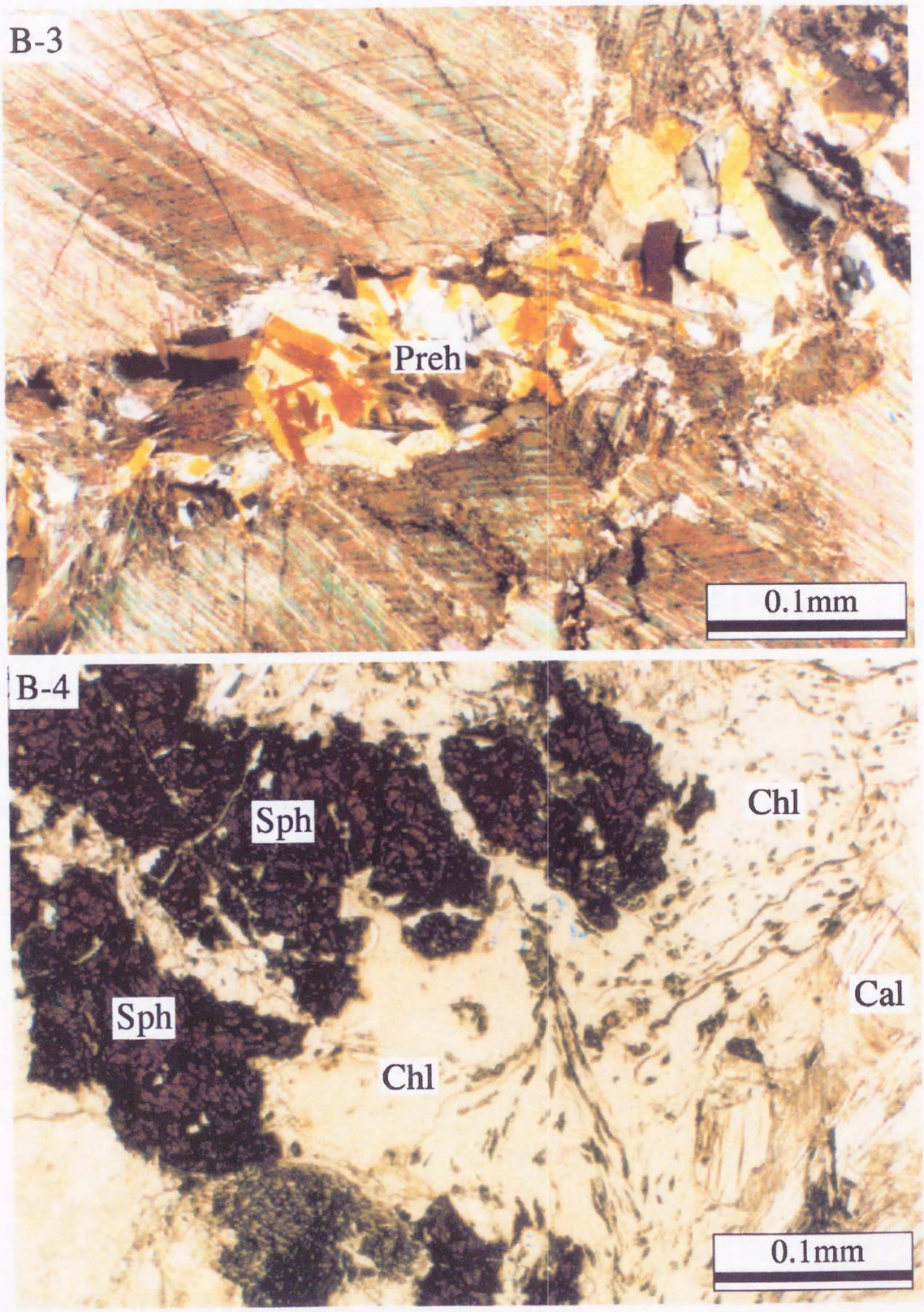

Fig. 5. *(continued)*

Fig. 5. *(continued)*

Left microphotograph (A-1 to A-4) shows the textural change of limestone and right one (B-1 to B-4) shows the occurrence of hydrothermal minerals. A-1 and A-2, sample 2408 composed of an aggregate of coarse-grained calcite with polygonal grain boundaries and containing sporadic diopsidic clinopyroxene ($\delta^{18}O$=16.6 ‰ and $\delta^{13}C$=3.5 ‰); A-3, sample 0104 composed of fine-grained calcite as veinlet or network and accompanying chlorite and pyrite ($\delta^{18}O$=8.3‰ and $\delta^{13}C$=0.2‰); A-4, sample RH006 composed of an aggregate of dominant, fine-grained calcite ($\delta^{18}O$=2.9‰ and $\delta^{13}C$=–1.6‰); B-1, sample 3102 accompanying quartz (Qz) veinlet and an aggregate of clay minerals (Clay) ($\delta^{18}O$=13.2‰ and $\delta^{13}C$=2.8‰); B-2, sample 0605 containing actinolite (Act) and chlorite (Chl) replacing tremolite (Tre) along the rim and cleavage ($\delta^{18}O$=13.8‰ and $\delta^{13}C$=4.3‰). B-3, sample 403 containing prehnite (Preh) veinlet ($\delta^{18}O$=13.4 and $\delta^{13}C$=1.8). B-4, sample 0112 with dissemination of sphalerite (Sph) and chlorite (Chl) with calcite (Cal) ($\delta^{18}O$=10.2‰ and $\delta^{13}C$=2.5‰).

origin as well as fine-grained calcite (Fig. 5B-3). These observations suggest that most chlorites result from replacement of mafic minerals within the group-A limestone. However, the chlorite seems to be hydrothermal in origin, because in some instances sphalerite occurs together with chlorite (Fig. 5B-4). Most pyrite is euhedral and oxidized into limonite along the rim.

4.2.3. Group C

Fifteen carbonate samples from limestone fall within group-C. Group-C limestone is greenish white to bluish white in color, exhibiting a speckled appearance along with a blackish vein structure due to mafic minerals such as chlorite (Fig. 4C). The ratio of the transparent fine-grained calcite to coarse-grained calcite is greater than that of group-B limestone (Fig. 5A-3). Transparent fine-grained calcite develops as veinlets or sometimes occurs as a network, and most mafic minerals originally-contained in limestone are altered into chlorite or actinolite. Anhedral chlorite exhibiting amoeba-like texture accompanies calcite veins (Fig. 5A-3). Sphalerite and pyrite tend to be locally associated with chlorite when the amount of chlorite is relatively large.

4.2.4. Group D

Ten carbonate samples from limestone fall within group-D. Group-D limestone was collected from the outcrop above the Mozumi deposits and drill cores from the Sako-nishi area (MITI, 1998a; 1998b). Group-D limestone is gray to bluish white, occasionally orange in color (Fig. 4D), and consists mainly of transparent fine-grained calcite. The amount of coarse-grained calcite is less than that of the group-C limestone (Fig. 5A-4). Anhedral chlorite exhibiting amoeba-like texture occurs in group-D limestone, and often tends to be observed along calcite veins. Mafic minerals in the group-D limestone have been completely altered to chlorite. In these altered limestones, sulfide minerals such as sphalerite and pyrite occur locally.

4.3. Description of Inishi-rock and gneiss

Samples of gneiss, Inishi-rock, and calc-silicate rock were more ore less subjected to hydrothermal alteration. Strongly altered rock is greenish due to the presence of chlorite. As a result of alteration, primary plagioclase, commonly contained in these silicate rocks, is partly altered to sericite or epidote, while primary mafic silicates of clinopyroxene and hornblende are partly altered into chlorite or actinolite. Chlorite and prehnite are dominant in silicate rocks along the Atotsu-1GO and N20GO faults. The presence of titanite is useful for the identification of the original Inishi rock or calc-silicate rock because of no alteration of this mineral even in strongly ^{18}O-depleted rock.

In the same way of grouping of limestone, Inishi rocks and gneisses were collected from drilled core were divided into four groups based on average of the $\delta^{18}O$ values of limestone layer intercalating silicate rocks: A ($\delta^{18}O$:>15‰), B ($\delta^{18}O$:10-15‰), C ($\delta^{18}O$:5-10‰), and D ($\delta^{18}O$:<5‰).

4.3.1. Group A

Inishi rock of group-A consists mainly of plagioclase, diopsidic clinopyroxene, titanite, quartz, and partly small amounts of potash feldspar (Fig. 6A-1). Diopsidic clinopyroxene shows a fresh appearance by the naked eye, however, most of it is altered to actinolite along the rim and cleavage. Chlorite is sporadically distributed and associated with actinolite. Plagioclase is generally clear, but is locally dusty due to saussuritization, which forms an aggregate of illite and calcite. Plagioclase is sometimes altered to clinozoisite along the rim and cleavage. Epidote and clinozoisite occur as veinlets or sometimes as a pseudomorphed plagioclase, and tend to be dominant in silicate rocks in the vicinity of the Sako-nishi ore body. Prehnite vein is generally observed around the Sako-nishi ore body. Sphalerite, chalcopyrite, and pyrite tend to be locally associated with veinlets of prehnite and clinozoisite.

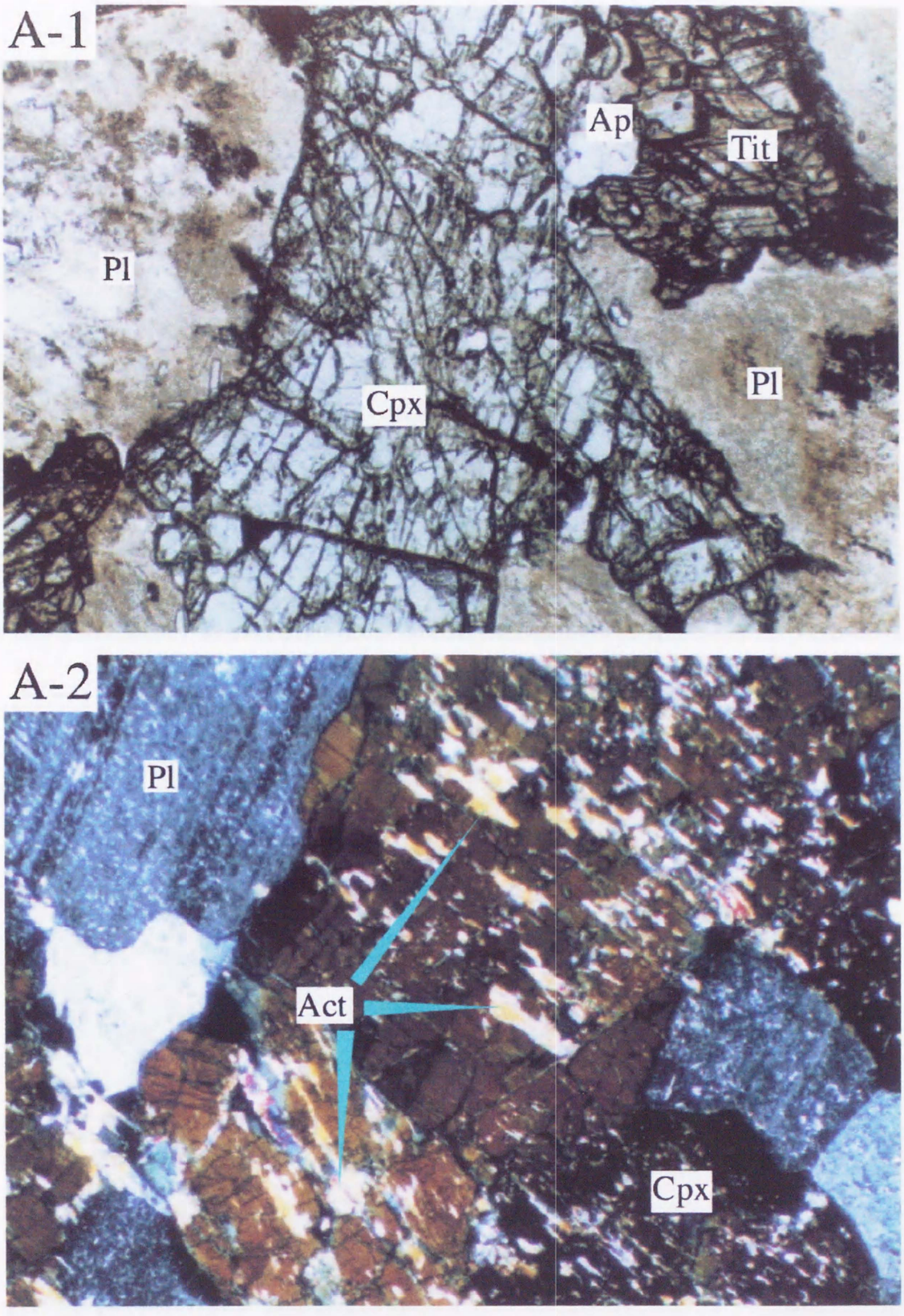

Fig. 6. Microphotograph of Inishi rock in the Sako-nishi area (*see p.48*).

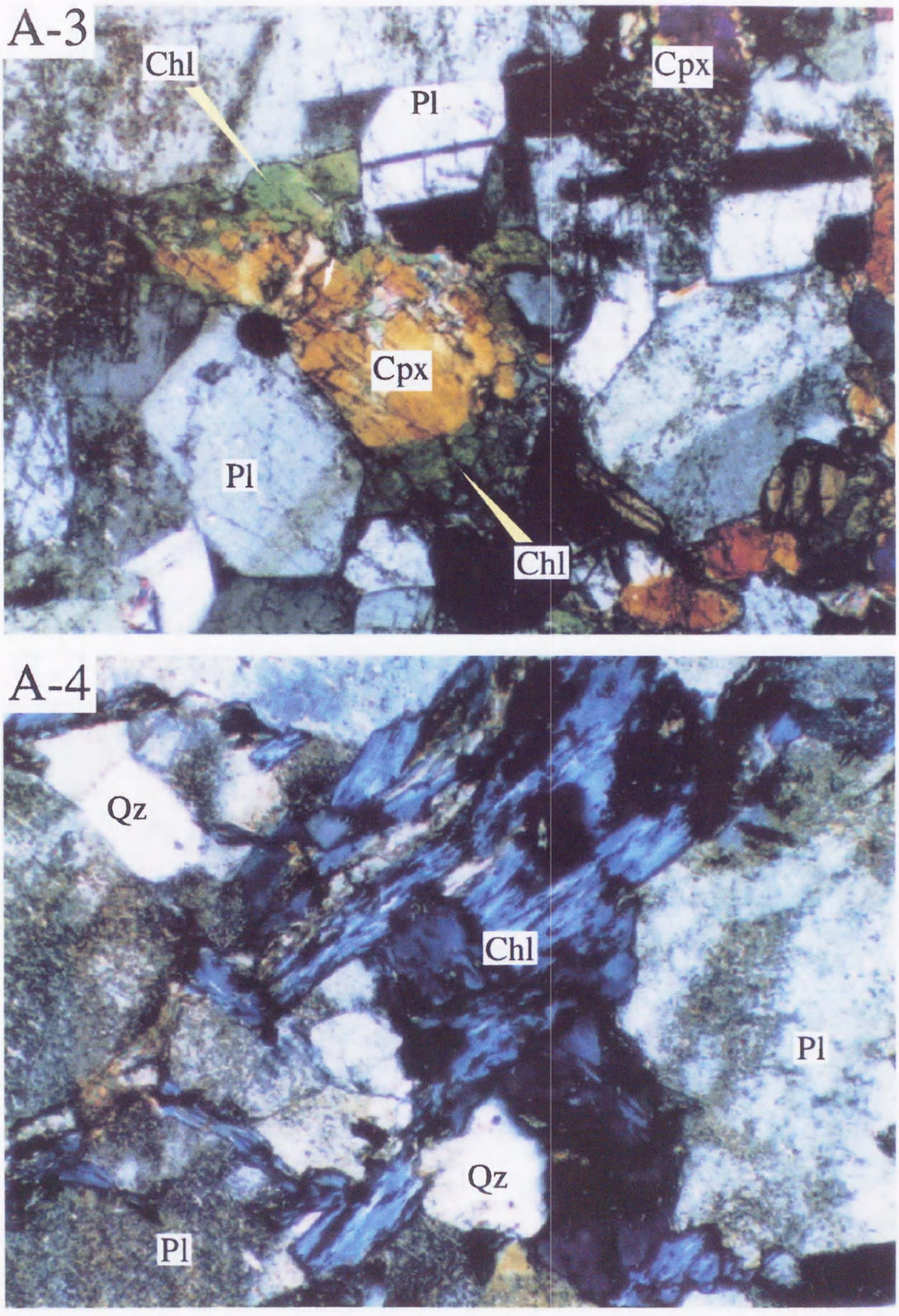

Fig. 6. *(continued)*

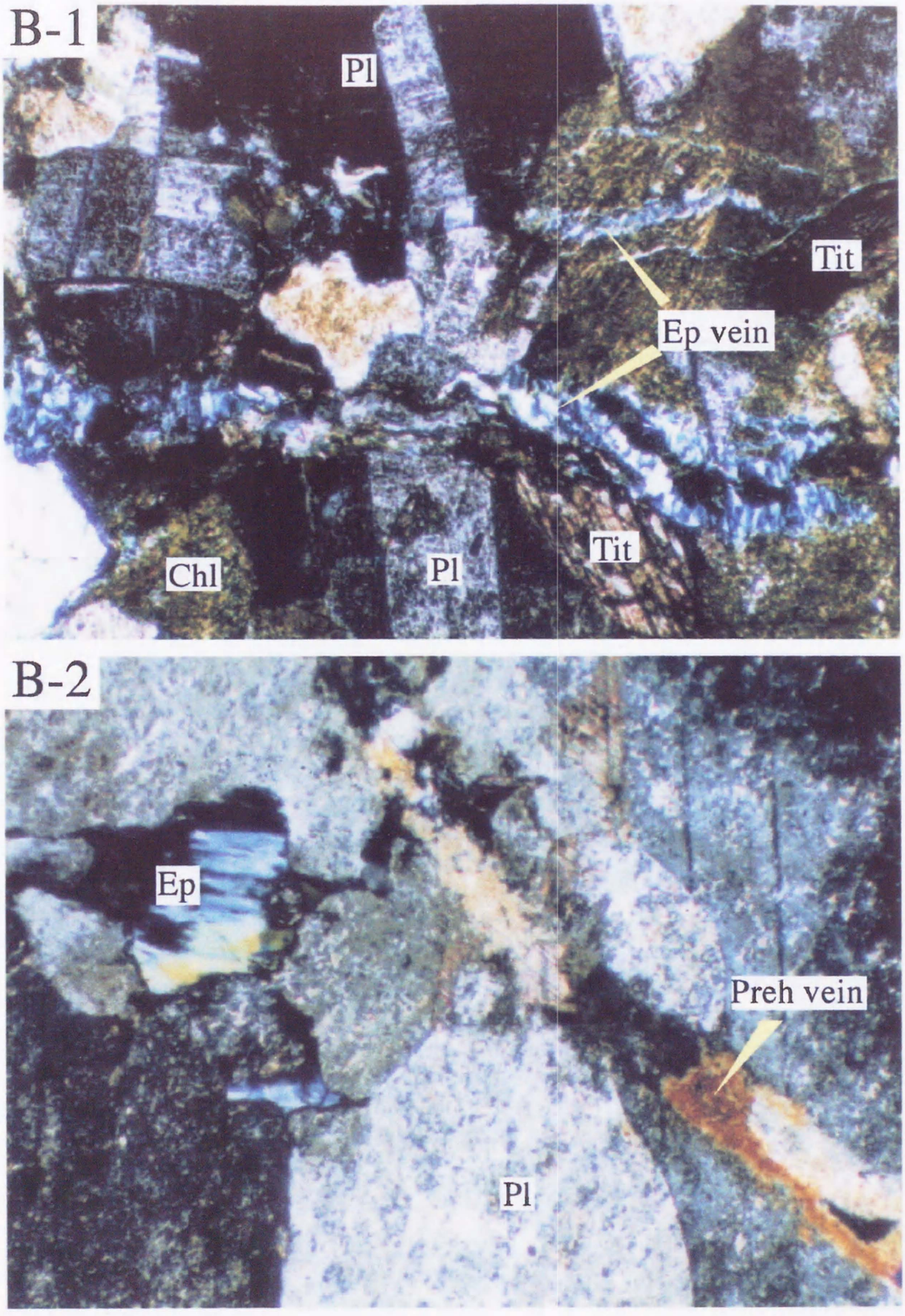

Fig. 6. *(continued)*

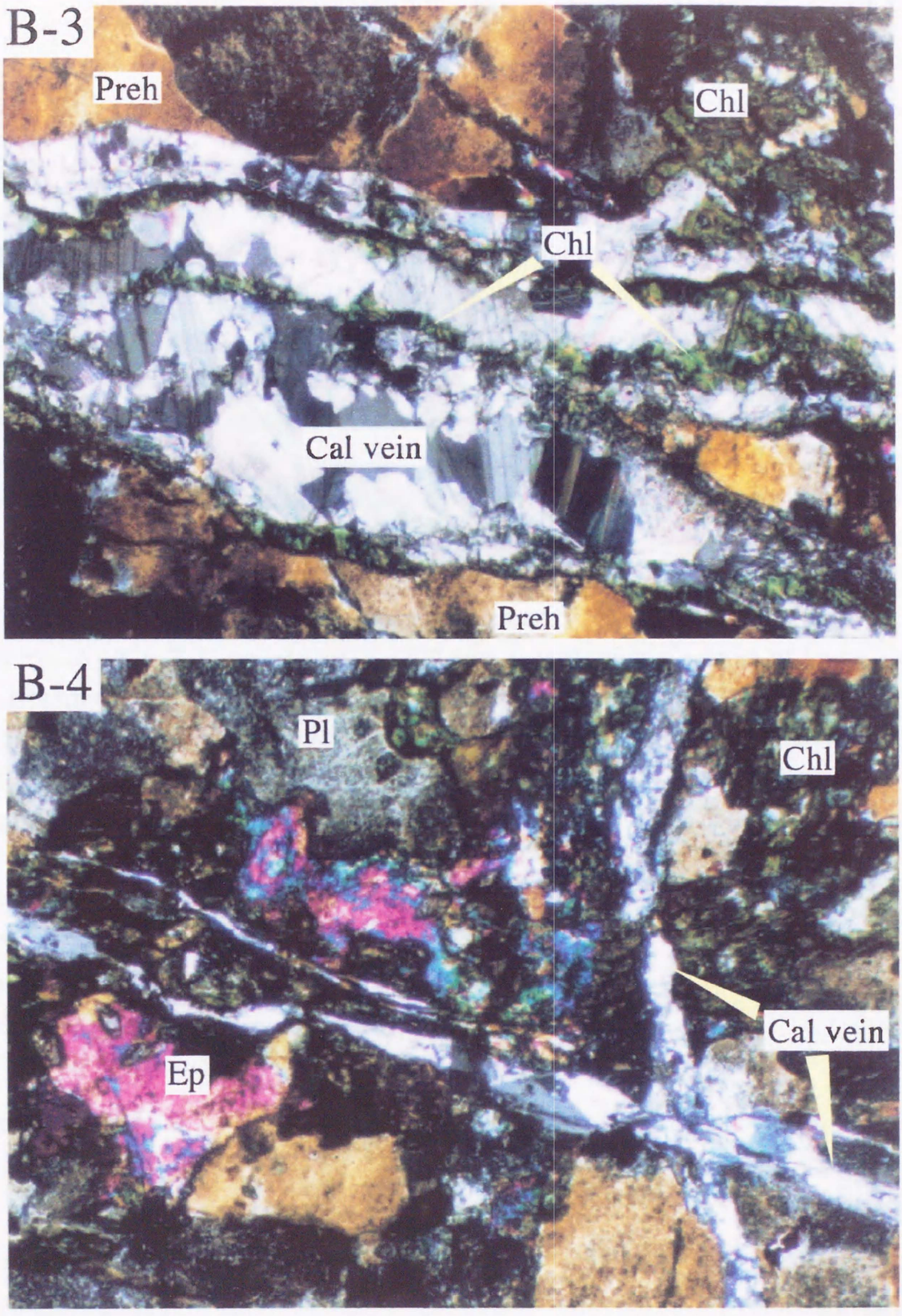

Fig. 6. *(continued)*

Fig. 6. *(continued)*

Left microphotograph (A-1 to A-4) shows the alteration of clinopyroxene, right one (B-1 to B-4) shows the occurrence of plagioclase associated with vein. A-1, sample 3HS-3 (155.5m) composed of plagioclase (Pl), clinopyroxene (Cpx), titanite (Tit), and apatite (Ap) ($\delta^{18}O$=16.1‰ and $\delta^{13}C$=1.2‰); A-2, sample 7KK-1 (204.8m) containing actinolite (Act) replacing clinopyroxene along the rim and cleavage ($\delta^{18}O$=11.7‰ and $\delta^{13}C$=1.0‰); A-3, sample 4HS-6 (169.0m) containing chlorite (Chl) replacing clinopyroxene along the rim and cleavage ($\delta^{18}O$=11.5‰ and $\delta^{13}C$=2.4‰); A-4, sample 4HS-6 (672.7m) amoeba-like chlorite completely replacing clinopyroxene accompanied quartz (Qz) ($\delta^{18}O$=7.4‰ and $\delta^{13}C$=–0.9‰); B-1, sample 2HI-1 (127.4m) accompanying epidote of high clinozoisite component (Ep) veinlet and an aggregate of chlorite ($\delta^{18}O$=12.5‰ and $\delta^{13}C$=1.1‰); B-2, sample 5HS-9 (525.0m) containing prehnite (Preh) veinlet and epidote of less clinozoisite component replacing plagioclase along the rim ($\delta^{18}O$=11.0‰ and $\delta^{13}C$=1.1‰). B-3, sample 5HS-7 (329.7m) composed of prehnite after plagioclase, chlorite after clinopyroxene, calcite (Cal) and chlorite vein ($\delta^{18}O$=4.5 and $\delta^{13}C$=2.3). B-4, sample 5HS-7 (329.7m) containing epidote of high pistacite component replacing plagioclase along the rim and calcite veinlet ($\delta^{18}O$=4.5‰ and $\delta^{13}C$=2.3‰).

4.3.2. Group B

Although the Inishi-rock of group-B has the same mineral assemblage as that of group-A, it tends to become dominant in quartz, K-feldspar, and saussuritized plagioclase. The replacement of plagioclase by clinozoisite along the rim becomes more pronounced (Fig. 6B-1,2). Except samples in drill cores along the N20GO fault, clinopyroxene is generally fresh and is weakly altered to actinolite and/or chlorite along the rim (Fig. 6A-2,3). Epidote of high clinozoisite component and prehnite is developed around the Sako-nishi deposit. Drill-core samples along the N20GO fault contain pyrite with network-like chlorite after clinopyroxene.

4.3.3. Group C

Quartz, calcite, chloritized clinopyroxene, and saussuritized plagioclase are widely observed in the group-C Inishi-rock (Fig. 6A-4). The grain size of illite in saussuritized plagioclase becomes larger. Most of the plagioclase is altered to prehnite and epidote with less clinozoisite component. Alteration to clinozoisite and dissemination of pyrite are widely observed around the Sako-nishi deposit.

4.3.4. Group D

Quartz, calcite, and K-feldspar are dominant. Plagioclase is altered to illite and epidote with high pistacite component (Fig. 6B-3,4), while the alteration of clinopyroxene to actinolite and chlorite is not so common compared to clinopyroxene in other groups. The degree of pyrite dissemination is similar to group-C Inishi-rock. Quartz, calcite, epidote after plagioclase, chlorite after mafic silicates, and veinlets of epidote and/or chlorite are predominant in gneiss than in Inishi-rock.

4.4. Cathodoluminescence Image

The cathodoluminescence signals reflect the distribution of trace metallic elements and lattice defects. The cathodoluminescence signals of carbonate minerals are red to orange, and in general are qualitatively described by the

strength of the signal as either bright, dull, or non-luminescent. It is generally considered that the Mn^{2+} concentration controls the luminescence intensity (Frank et al., 1982; Marshall, 1988). Minimum concentrations required to activate luminescence detectable to the eye are known to exceed 20 ppm of Mn^{2+} (Savard et al., 1995). On the other hand, it has been shown that Fe^{2+} decreases the intensity of the luminescence. The intensity begins to weaken when the concentration of Fe^{2+} exceeds several thousand ppm, and the sample becomes non-luminescent when it reaches levels of several tens of thousands of ppm (Savard et al., 1995).

Microscopic observation shows that carbonate minerals occurring in the limestones of the Sako-nishi area can be divided roughly into two groups: coarse-grained calcite within original crystalline limestone, and fine-grained calcite of hydrothermal origin. Generally, the cathodoluminescence image of coarse-grained calcite is dark, but that of fine-grained calcite is bright (Fig. 7A). This is illustrated in Figures 7A and 8, showing that bright luminescence zones are distributed along grain boundaries of calcite, and veinlets with strong luminescence intensity are developed across the aggregate of calcite. Areas with a bright luminescence image tend to increase with decreasing $\delta^{18}O$ and $\delta^{13}C$ values. In particular, luminescence images of fine-grained calcite veins occurring in group D limestone are characteristically bright (Figs 7B and 8). These observations indicate that the hydrothermal fluid with high Mn content replaced calcite into Mn-enriched calcite from the grain boundaries and through the aggregate of the grains.

4.5. Mineral Chemistry

4.5.1. Calcite

Coarse-grained carbonate minerals constituting crystalline limestone are nearly pure calcite, only slightly enriched in Mg (Table 12). This agrees well with the conventional result of Fujinuki (1973) and Kano (1998). On the other hand, fine-grained calcite in limestone in groups C and D and skarn calcite tend to be enriched in Mn and Fe. The Mn enrichment is significant in calcites in group D limestone. As a result, calcites in strongly ^{18}O-depleted limestone have high Mn/Fe

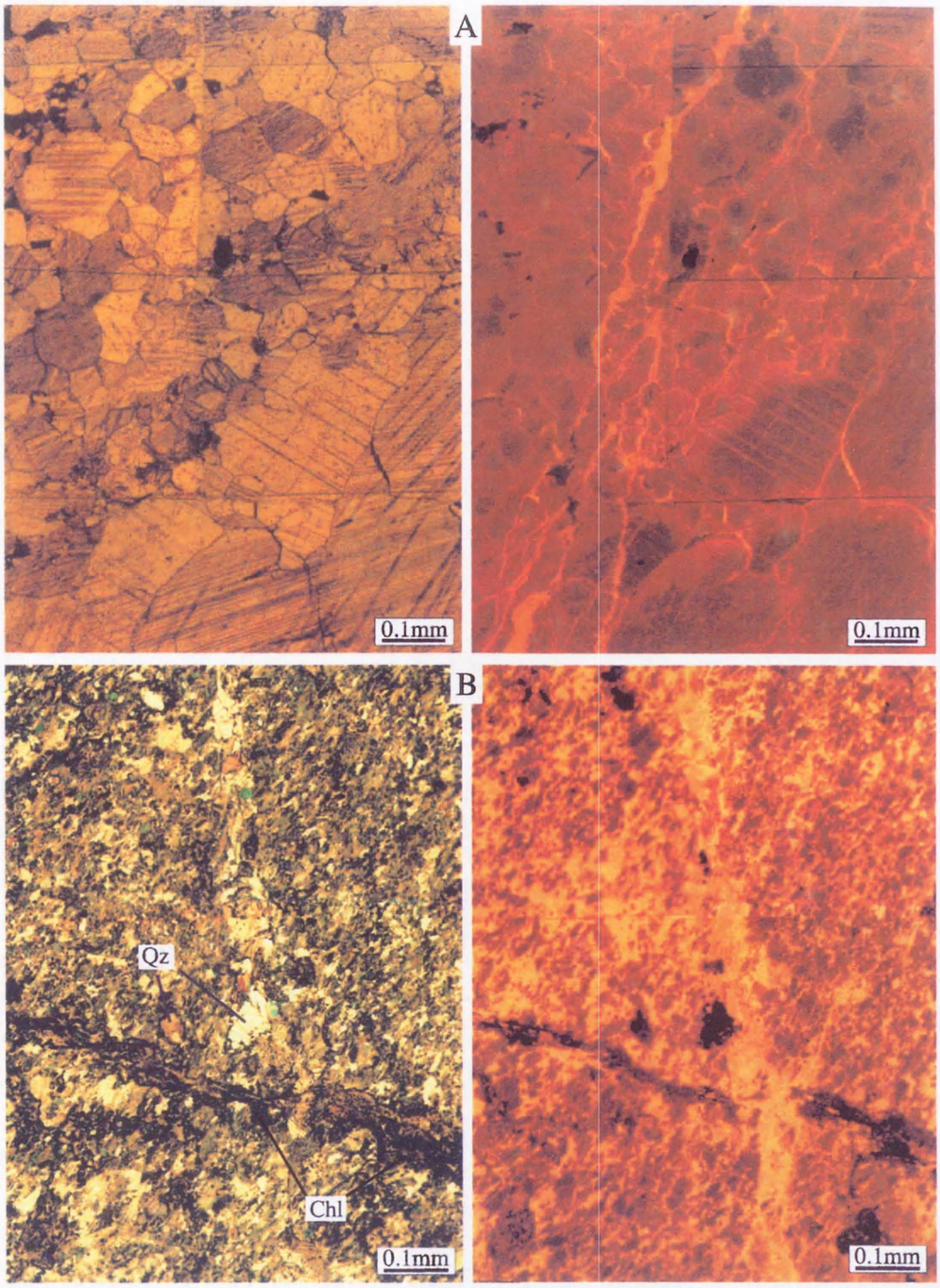

Fig. 7. Microphotograph (left) and cathodoluminescence image (right) of group-D limestone. (A): the upper sample ($\delta^{18}O$=1.4 ‰ and $\delta^{13}C$=1.6 ‰) collected from drill core (7MAKK-1) in the Sako-nishi area. (B): the lower sample ($\delta^{18}O$=1.1 ‰ and $\delta^{13}C$=–0.5 ‰) collected from an outcrop in the Mozumi area.

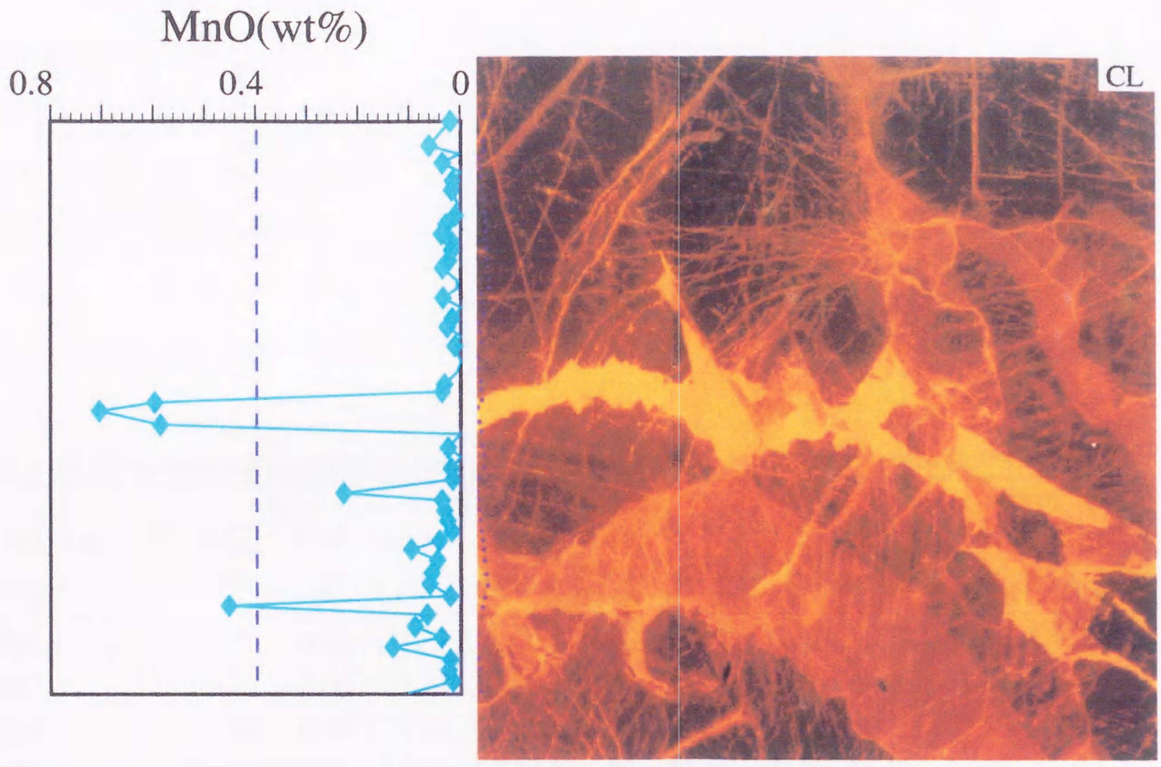

Fig. 8.
Cathodoluminescence image (upper) and microphotograph under open nicol (lower) of group-C limestone($\delta^{18}O=7.1‰$ and $\delta^{13}C=-0.8‰$) collected from the drill core of 7MAKK-1. EPMA analysis for the determination of MnO content in calcite was made along a blue line in the lower photograph.

Table 12 Representative chemical compositions of calcite in limestone and skarn.

Group	A		B		C		D		skarn	
$\delta^{18}O$ (‰)	17.6	17.6	13.8	12.6	8.4	7.1	1.1	1.1	n.d	n.d
Sample	77	77	36	14	3HS-3 427.6m	7KK-1 427.7m	RH005	RH005	7KK-1 355.8m	Mokuji
FeO*	0.00	0.09	0.27	0.00	0.46	0.08	0.33	0.33	0.30	0.43
MnO	0.01	0.00	0.12	0.00	1.02	0.71	3.86	4.07	1.81	2.47
MgO	0.00	0.36	0.26	0.00	0.07	0.01	0.70	0.82	0.00	0.03
CaO	56.90	56.05	55.19	56.77	54.35	54.21	51.48	51.21	54.97	53.34
Number of cations on the basis of 3(O)										
Fe	0.000	0.001	0.004	0.000	0.006	0.001	0.005	0.005	0.004	0.006
Mn	0.000	0.000	0.002	0.000	0.014	0.010	0.055	0.058	0.025	0.035
Mg	0.000	0.009	0.006	0.000	0.002	0.000	0.017	0.021	0.000	0.001
Ca	1.000	0.990	0.987	1.000	0.977	0.989	0.923	0.917	0.970	0.958
Mn/(Fe+Mg+Mn)	0.00	0.00	0.17	0.00	0.64	0.91	0.71	0.70	0.86	0.84

* Total Fe as FeO. n.d=not determined.

ratios (Fig. 9).

The relationship between the chemical composition of the calcite and the luminescence image for underground limestone of group C is shown in Figure 8. It is notable that points of high Mn content exhibit bright yellow to orange luminescence, whereas points of nearly pure calcite appear to be dark red. Accordingly, calcite showing bright luminescence in group C and D limestones is consistent with chemical composition data of calcite, which showed a higher concentration of Mn than of Fe.

4.5.2. Hydrothermal Silicate Minerals

Silicate minerals identified in the hydrothermal altered limestone include chlorite, actinolite, tremolite, epidote, prehnite, and stilpnomelane. Representative analytical data of several silicate minerals are shown in Table 13. Clinopyroxene in unaltered limestone is characterized by higher Mg content than skarn clinopyroxene. This result is consistent with previous data by Kano (1998) and Mariko et al. (1996). Amphiboles replace primary diopsidic clinopyroxene in limestone, and exhibit a comparatively wide compositional range from near tremolite to actinolite. In particular, the amphibole of sphalerite-bearing limestone is enriched in the actinolite component with increased amounts of Mn along the rim and cleavage. I assume that the amphibole composition becomes enriched in Fe and Mn with the advance of alteration. Epidote occurs in group D limestone. It is low in Mn content. The pistacite molecule of the epidote ranges from 20 to 30%.

Chlorite is classified into two types based on the mode of occurrence: one is resulted from the replacement of mafic minerals in crystalline limestone; the second is of hydrothermal origin showing vein texture. The crystal structure of the chlorite exhibits a wide range of element substitutions, such as Al and Si in tetrahedral sites, and Fe, Mn, Al, and Mg in octahedral sites. However, the chemical compositions of chlorites in a single sample are almost similar between the two types, indicating that the chemical composition of the chlorite is controlled through interaction with a hydrothermal fluid. Chlorite in limestone containing

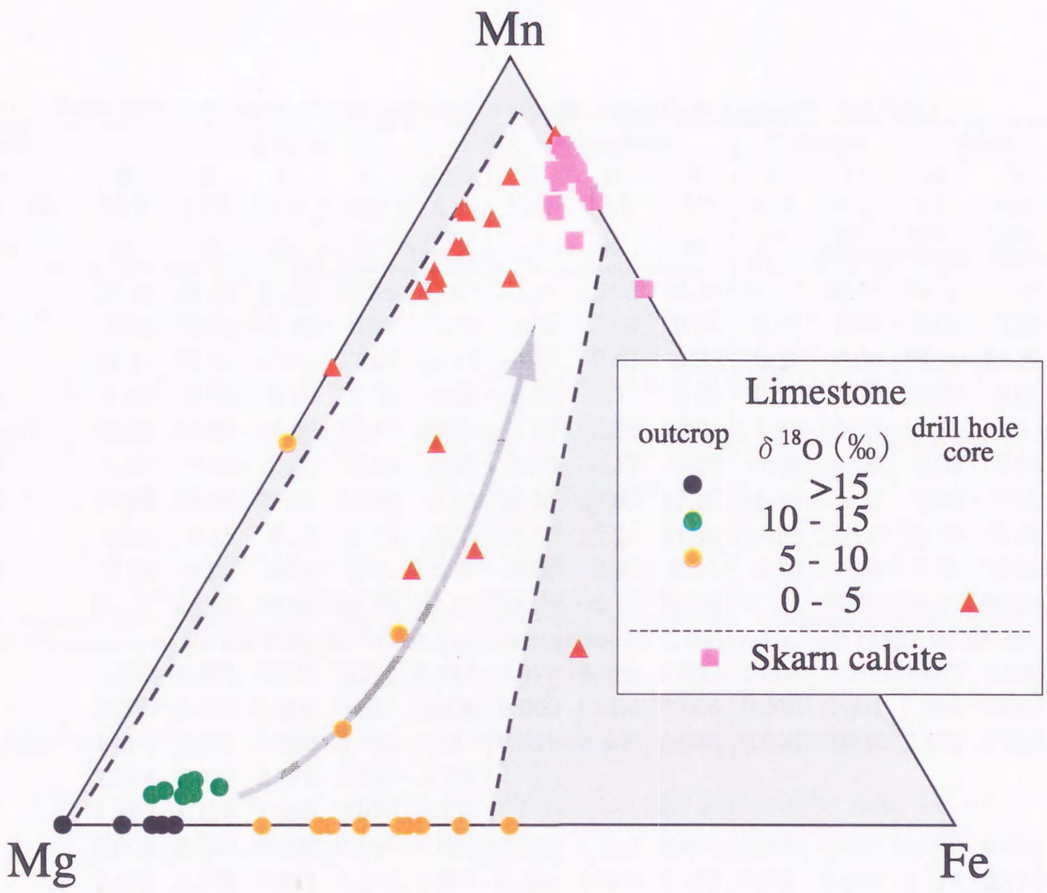

Fig. 9. Ternary plot of Mg, Mn, and Fe of calcite in the Sako-nishi limestone and skarn calcite. Some data correspond to the bright cathodoluminescence images in Fig. 8. The arrow indicates a trend of calcite compositions with decreasing $\delta^{18}O$ values.

Table 13 Representative chemical compositions of silicate minerals in limestone and skarn.

Mineral	Chlorite					Amphibole			Pyroxene		Epidote	
Group	B	B	C	C	skarn	A	B	B	A	D	D	D
$\delta^{18}O$ (‰)	12.6	13.8	8.3	8.9	n.d	16.8	13.8	13.8	16.8	4.0	4.0	4.0
sample	14	36	32	2	7KK-1 355.8m	27	36	36	27	7KK-1 388.6m	7KK-1 388.6m	7KK-1 388.6m
SiO_2	29.96	29.34	31.53	27.80	23.47	57.31	55.98	54.16	53.73	50.63	36.37	37.45
TiO_2	0.00	0.00	0.00	0.07	0.00	0.00	0.04	0.05	0.00	0.04	0.07	0.09
Al_2O_3	19.37	15.40	17.73	17.64	19.47	0.43	0.62	0.25	0.31	0.06	18.79	23.32
Cr_2O_3	0.00	0.00	0.00	0.03	0.00	0.00	0.15	0.00	0.00	0.00	0.00	0.01
Fe-total*	16.69	20.89	14.00	22.37	35.21	1.77	8.89	16.81	1.93	20.57	17.89	11.87
MnO	0.00	0.50	0.00	0.30	0.82	0.00	0.17	0.47	0.00	1.09	0.07	0.03
MgO	19.08	18.49	25.01	16.00	6.16	22.65	17.83	12.85	16.44	4.53	0.00	0.00
CaO	0.46	0.15	0.18	0.18	0.02	13.58	12.29	11.69	24.95	22.60	23.39	23.46
Na_2O	0.00	0.05	0.40	0.01	0.00	0.00	0.20	0.11	0.00	0.04	0.03	0.00
Total	85.56	85.20	88.85	84.38	85.15	95.75	96.16	96.39	97.36	99.56	96.61	96.23
Number of cations on the basis of 28(O) for chlorite, 23(O) for amphibole, 6(O) for pyroxene, and 12.5(O) for epidote												
Si	6.120	6.222	6.132	5.990	5.445	7.978	8.006	8.032	2.004	2.018	3.002	3.023
Ti	0.000	0.000	0.000	0.011	0.000	0.000	0.004	0.006	0.000	0.001	0.004	0.005
Al (total)	4.664	3.849	4.063	4.480	5.322	0.071	0.105	0.044	0.014	0.003	1.828	2.219
Al^{VI}	2.784	2.071	2.195	2.470	2.767							
Al^{IV}	1.880	1.778	1.868	2.010	2.555							
Cr	0.000	0.000	0.000	0.005	0.000	0.000	0.017	0.000	0.000	0.000	0.000	0.001
Fe	2.852	3.705	2.277	4.031	6.831	0.206	1.063	2.085	0.060	0.686	1.112	0.721
Mn	0.000	0.090	0.000	0.055	0.161	0.000	0.021	0.059	0.000	0.037	0.005	0.002
Mg	5.812	5.845	7.251	5.139	2.131	4.701	3.801	2.841	0.914	0.269	0.000	0.000
Ca	0.100	0.034	0.037	0.042	0.005	2.026	1.883	1.858	0.997	0.965	2.069	2.029
Na	0.000	0.021	0.152	0.004	0.000	0.000	0.055	0.032	0.000	0.003	0.005	0.000
Fe/(Mg+Fe)	32.92	38.79	23.90	43.96	76.22	4.20	21.86	42.33	6.18	71.81	—	—

* Total Fe as FeO for chlorite, amphibole, and pyroxene, and as Fe_2O_3 for epidote.

n.d=not determined.

sphalerite is enriched in Fe, as shown in Table 13, although a distinct relationship is not recognized between the chemical composition of chlorite and the oxygen and carbon isotopic compositions of the limestone because of the small number of samples. Although the MnO content of chlorite is low (1% or less), there is a weak positive correlation between the ratio of Fe/(Fe+Mg), designated hereafter as the Fe# value, and the MnO content (Fig. 10A).

4.6. Chemical Composition of Limestone

4.6.1. Acid Leaching of Limestone

On the basis of observations and geochemical data, it is interpreted that veinlets of chlorite and calcite in the limestone and silicate rock of the Sako-nishi area are hydrothermal in origin. According to previous experimental studies, it is known that calcite dissolves in acetic acid, while both calcite and chlorite dissolve in hydrochloric acid (Oinuma and Kobayashi, 1965; Kitano et al., 1981). A comparison of Ca, Sr, Mn, Fe, Mg, Al, and Zn contents in the HOAc and HCl leachates of the Sako-nishi limestones and skarn calcites indicates that there is no significant difference in the concentration of Sr, Mn, and Ca in either HOAc or HCl leachates (Figs 11 and 12). It is suggested then that these elements are concentrated in the calcite. On the other hand, Al, Fe, and Mg concentrations in the HCl leachate are much higher than those in the HOAc leachate. Likewise, the concentration of Zn is high in the HCl leachate. It is therefore suggested that selective leaching of these elements from chlorite occurred. Therefore, Ca, Sr, and Mn are leached using HOAc, while Fe, Mg, Al, and Zn are leached only by HCl.

Table 14 shows chemical composition in the leachates of the Sako-nishi limestones using aqua regia. There is no difference on chemical composition in the leachates of the Sako-nishi limestones between using aqua regia or using HCl (Table 14, Fig. 13). Therefore, the chemical composition of leachate with each acid seems to be consistent one with the other.

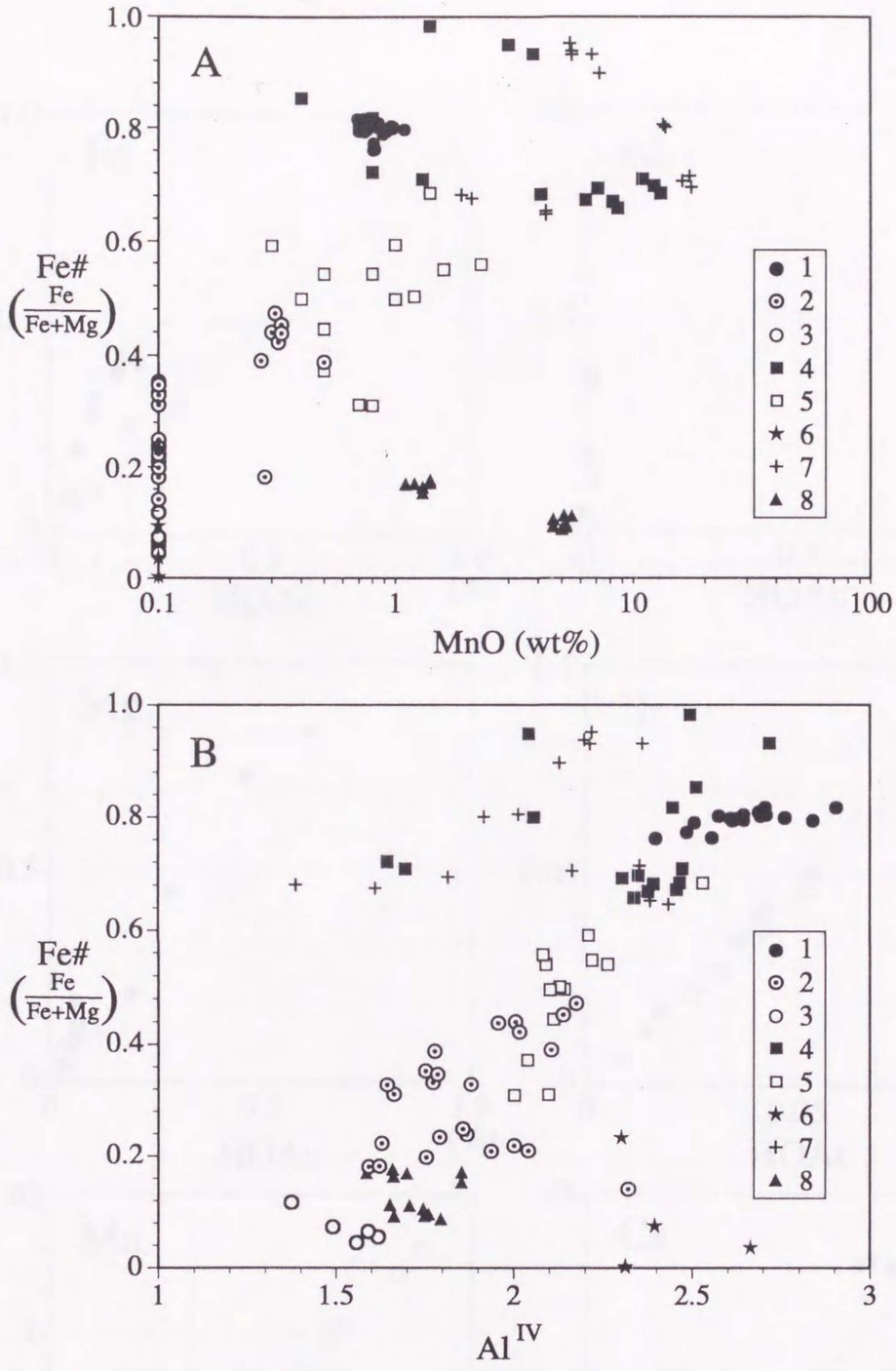

Fig. 10. (A) plot of Fe# against MnO contents and (B) plot of Fe# against tetrahedral Al contents (in atoms per formula unit) for chlorites in skarn and limestone of the Sako-nishi area (1 to 3) compared with chlorites from hydrothermal deposits and geothermal areas (4 to 8). 1=skarn; 2=group B and C limestone with sphalerite; 3=group B limestone without sphalerite; 4=polymetal vein type deposits (Abe, 1957; Sawai, 1984, 1986, 1988; Yoneda, 1989); 5=wall rocks of polymetallic vein-type deposits (Sawai, 1984, 1986, 1988); 6=Kuroko deposits (Hayashi, 1961; Sakamoto et al., 1956); 7=gold deposits in Green Tuff region (Yoneda, 1989); 8=epithermal gold deposits (Yoneda, 1989).

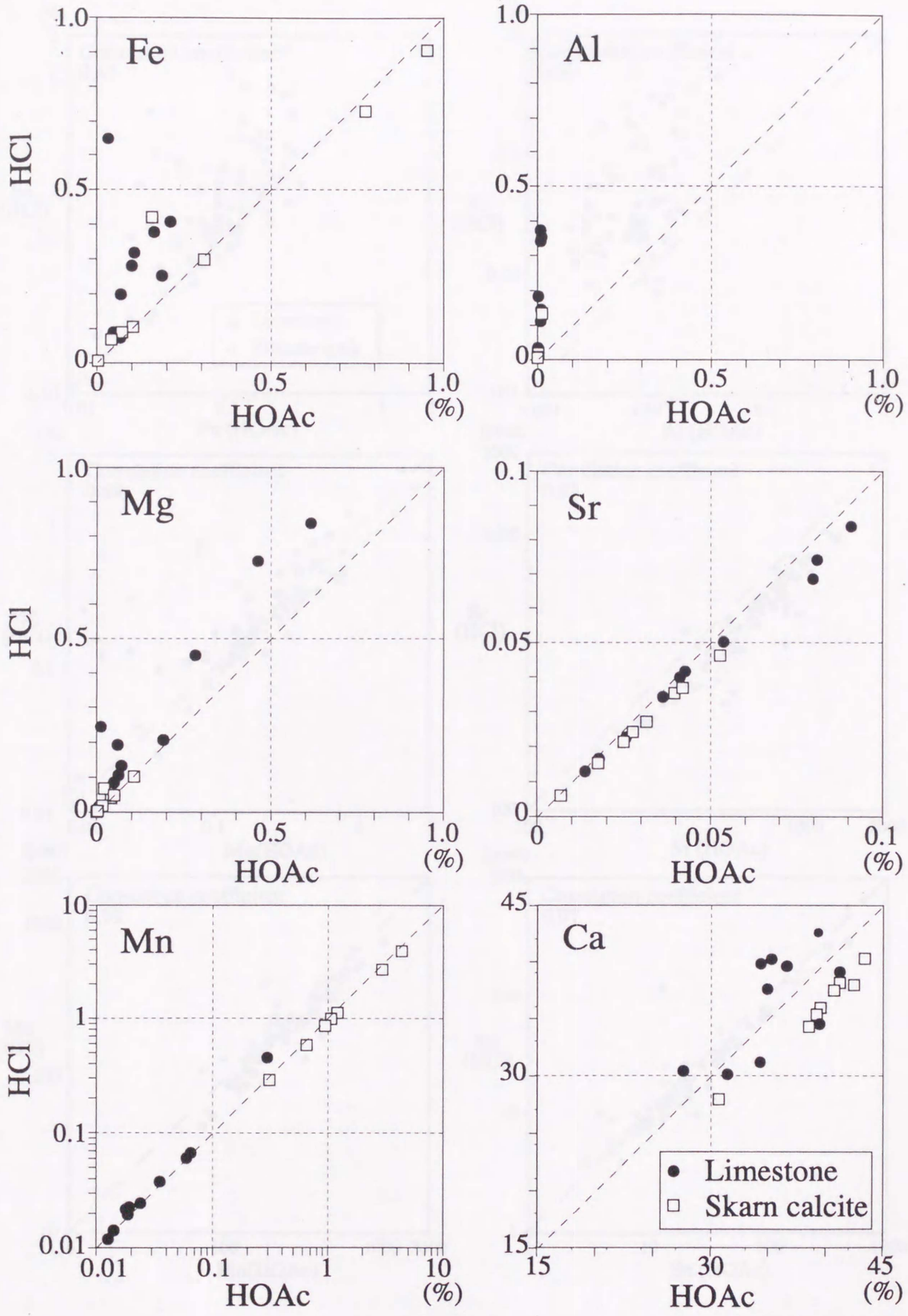

Fig.11. Comparison of Fe, Al, Mg, Sr, Mn, and Ba contents between the HOAc and HCl leachates of limestone and skarn calcite in the Kamioka mine.

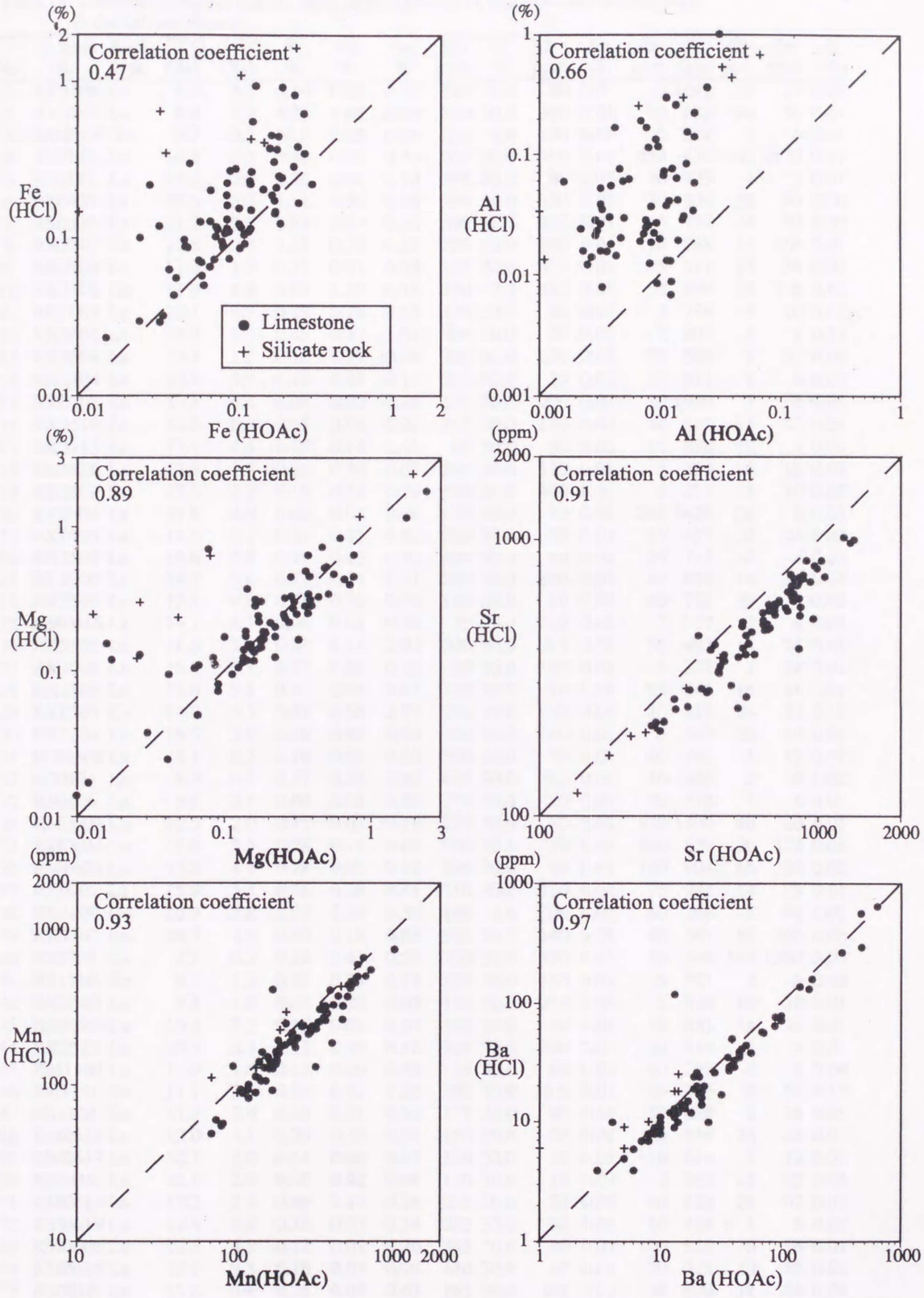

Fig.12. Comparison of Fe, Al, Mg, Sr, Mn, and Ba contents between the HOAc and HCl leachates of carbonate and silicate rocks in the Sako-nishi area.

Table 14 Chemical compositions for aqua regia digestion of limestone and silicate rock in the Sako-nishi area.

No.	Sample No.	Rock type	$\delta^{18}O$ (‰)	$\delta^{13}C$ (‰)	Fe %	Al %	Mg %	Mn ppm	Ca %	P ppm	Na %	Ba ppm	Sr ppm	Pb ppm	Zn ppm	S (%)
1	RK3106	Ls	8.3	3.3	0.10	0.03	0.12	310	30.0	20	0.01	10	1040	30	18	0.01
2	RK3105	Ls	8.9	3.2	1.00	1.63	0.88	390	30.0	390	0.01	10	683	94	50	0.01
3	RM0618	Gn	9.7	0.2	0.15	0.05	0.86	285	8.0	100	0.01	5	227	2	6	0.01
4	RS0112	Ls	10.2	2.5	0.30	0.12	0.46	530	30.0	0.5	0.01	550	473	442	2170	0.11
5	RS0111	Ls	10.6	2.8	0.20	0.06	0.10	455	30.0	80	0.01	40	435	1	2	0.01
6	RS0405	Ls	10.6	3.2	1.11	0.56	0.48	290	30.0	330	0.01	30	854	28	96	0.06
7	RS0802	Ls	11.2	2.8	0.81	0.37	0.30	395	30.0	380	0.01	10	737	44	80	0.02
8	RK2502	Cs	11.3	-0.1	1.27	0.78	0.37	250	10.9	300	0.01	10	268	12	168	0.01
9	RK3103	Ls	11.6	1.3	0.13	0.01	0.33	125	30.0	0.5	0.01	5	471	52	36	0.01
10	RK2106	Gn	11.9	1.8	0.69	1.39	0.16	160	7.8	510	0.01	5	190	26	136	0.01
11	RK1003	Ls	12.1	2.3	0.28	0.16	0.55	195	30.0	50	0.01	5	736	4	10	0.01
12	RK2102	Ls	12.2	1.3	0.45	0.12	1.59	705	30.0	20	0.01	5	601	8	8	0.11
13	RK2509	Ls	12.2	1.0	0.12	0.13	0.08	250	30.0	230	0.01	70	580	8	52	0.01
14	RK2104	Ls	12.6	3.9	0.12	0.03	0.11	255	30.0	10	0.01	20	811	8	8	0.01
15	RK0702	Ls	13.1	4.4	0.08	0.02	0.18	130	30.0	200	0.01	10	1030	1	6	0.01
16	RK2514	Ls	13.2	0.5	0.15	0.04	0.21	215	30.0	110	0.01	40	327	16	32	0.01
17	RK3112	Ls	13.4	4.6	0.17	0.15	0.43	80	30.0	30	0.01	10	886	10	4	0.01
18	RS0403	Ls	13.4	1.8	0.26	0.30	0.04	260	30.0	120	0.01	5	354	6	18	0.03
19	RK2107	Ls	13.5	2.2	0.16	0.51	0.26	190	30.0	490	0.01	5	277	4	10	0.02
20	RK0704	Ls	13.8	4.0	0.02	0.01	0.01	175	30.0	10	0.01	240	1420	28	6	0.01
21	RK0705	Ls	14.3	3.1	0.21	0.11	0.42	230	30.0	30	0.01	10	457	32	24	0.01
22	RK2507	Ls	14.6	3.8	0.19	0.10	0.22	490	30.0	10	0.01	30	713	12	8	0.01
23	RK1006	Ls	14.7	3.0	0.22	0.21	0.11	200	30.0	890	0.01	10	639	16	34	0.01
24	RK2105	Ls	15.1	4.8	0.08	0.02	0.26	100	30.0	10	0.01	60	723	20	8	0.01
25	RM0616	Ls	15.1	4.1	0.06	0.01	0.56	55	30.0	10	0.01	5	717	2	8	0.01
26	RK2505	Ls	16.6	3.1	0.38	0.15	2.92	300	30.0	0.5	0.01	10	483	14	94	0.01
27	RK1004	Ls	16.8	0.1	0.17	0.08	0.12	85	30.0	160	0.01	5	347	1	24	0.01
28	RK2506	Ls	17.4	3.8	0.11	0.04	0.67	120	30.0	10	0.01	10	646	16	14	0.01
29	RK0703	Cs	18.0	3.5	0.41	0.56	3.75	105	30.0	50	0.05	40	313	24	32	0.12
30	RK2504	Ls	18.5	3.9	0.18	0.02	0.24	240	30.0	60	0.01	5	740	20	10	0.01
31	RM0302	Ls	8.1	0.2	0.18	0.04	0.18	500	30.0	70	0.01	40	463	1	12	0.01
32	RS0104	Ls	8.3	0.2	0.37	0.23	0.80	475	30.0	0.5	0.01	10	596	2	8	0.02
33	RS0106	Ls	9.6	2.1	0.09	0.03	0.20	170	30.0	20	0.01	20	378	1	6	0.01
34	RM0603	Ls	12.5	2.0	0.11	0.03	0.18	225	30.0	10	0.01	130	1490	40	20	0.01
35	RM0604	Ls	13.6	3.5	0.28	0.11	0.61	230	30.0	30	0.01	540	629	26	174	0.06
36	RM0605	Ls	13.8	4.3	0.28	0.03	0.12	590	30.0	90	0.01	180	904	66	60	0.02
37	RK0701	Ls	15.9	3.3	0.36	0.38	0.51	140	30.0	110	0.01	5	993	14	28	0.01
38	RK3109	Gn	10.3	-7.8	2.07	1.26	0.30	440	4.4	700	0.01	60	266	6	48	0.01
39	RK2103	Ls	14.7	2.4	0.50	0.18	0.65	560	30.0	140	0.01	40	541	50	260	0.06
40	RS1701	Cs	7.2	0.2	0.62	0.41	0.26	200	30.0	350	0.01	10	208	598	1380	0.03
41	RS1710	Ls	9.7	1.2	0.25	0.28	0.13	150	30.0	150	0.01	5	321	2	6	0.03
42	RK2513	Ls	9.8	-1.0	0.05	0.32	0.03	110	30.0	250	0.01	5	620	10	16	0.01
43	RS0406	Ls	10.6	3.2	0.15	0.01	0.63	105	30.0	10	0.01	10	853	34	32	0.01
44	RK2512	Ls	10.9	0.3	0.12	0.19	0.16	395	30.0	210	0.01	20	344	1	4	0.01
45	RM1503	Ls	11.0	1.6	0.14	0.09	0.35	155	30.0	60	0.01	40	238	6	1	0.04
46	RK3111	Cs	11.7	2.1	0.54	0.41	1.55	380	30.0	0.5	0.01	20	446	8	52	0.17
47	RS1104	Ls	11.9	3.4	0.06	0.01	0.39	125	30.0	90	0.01	30	628	2	28	0.01
48	RM0613	Ls	12.0	4.1	0.20	0.23	0.34	130	30.0	30	0.01	10	855	26	28	0.01
49	RM0617	Ls	12.1	2.0	0.11	0.06	0.41	130	30.0	70	0.01	10	614	2	12	0.01
50	RS0419	Ls	12.1	2.9	0.47	0.42	0.88	130	30.0	10	0.01	5	562	12	32	0.08
51	RM0612	Ls	12.3	2.5	0.09	0.17	0.14	255	30.0	20	0.01	40	428	28	62	0.01
52	RM0619	Ls	12.4	0.9	0.16	0.03	0.14	285	30.0	90	0.01	10	438	1	6	0.01
53	RM0606	Ls	12.5	4.8	0.12	0.02	0.20	345	30.0	80	0.01	100	858	6	16	0.01
54	RM0615	Ls	12.9	3.3	0.16	0.03	0.18	410	30.0	10	0.01	30	722	10	58	0.01
55	RS0810	Ls	13.0	3.6	0.25	0.03	0.43	165	30.0	0.5	0.01	40	890	18	26	0.01
56	RM0614	Ls	13.1	3.5	0.17	0.03	0.39	235	30.0	10	0.01	30	837	22	10	0.01
57	RK3102	Ls	13.2	2.8	0.07	0.03	0.09	110	30.0	0.5	0.01	110	1000	14	20	0.01
58	RM0911	Ls	13.3	3.0	0.22	0.05	0.29	260	30.0	10	0.01	10	1390	34	84	0.01
59	RM0910	Ls	13.6	3.9	0.13	0.06	0.45	135	30.0	60	0.01	10	1035	1	22	0.01

Abbreviations: Ls=limestone; Gn=gneiss; Cs=calc-silicate rock; In=Inishi rock.

Table 14 *(continued)*

No.	Sample No.	Rock type	$\delta^{18}O$ (‰)	$\delta^{13}C$ (‰)	Fe %	Al %	Mg %	Mn ppm	Ca %	P ppm	Na %	Ba ppm	Sr ppm	Pb ppm	Zn ppm	S (%)
60	RK3107	Ls	13.7	2.5	0.33	0.09	0.71	705	30.0	130	0.01	40	505	28	22	0.02
61	RK2510	Ls	14.0	3.4	0.50	0.08	0.23	385	30.0	140	0.01	10	878	6	16	0.01
62	RS0805	Ls	14.3	3.3	0.62	0.04	0.19	365	30.0	10	0.01	40	781	52	38	0.04
63	RS0812	Ls	14.7	3.9	0.40	0.10	0.32	300	30.0	230	0.02	30	847	4	8	0.01
64	RS0408	Ls	15.0	4.5	0.12	0.02	0.19	165	30.0	10	0.01	10	801	8	6	0.01
65	RS0809	Ls	15.3	3.5	0.12	0.05	0.13	115	30.0	10	0.01	5	981	10	8	0.01
66	RS1103	Ls	15.4	3.8	0.12	0.07	0.48	150	30.0	70	0.01	80	1150	20	40	0.01
67	RK0706	Ls	15.8	5.1	0.30	0.07	0.26	195	30.0	10	0.01	10	619	24	38	0.11
68	RS0804	Gn	15.8	-0.1	0.04	0.02	0.03	100	30.0	860	0.01	5	85	2	34	0.01
69	RM0608	Ls	15.9	4.8	0.13	0.04	0.22	365	30.0	70	0.01	100	775	16	38	0.01
70	RK2108	Ls	16.3	4.3	0.11	0.03	0.19	155	30.0	0.5	0.01	30	705	30	38	0.01
71	RS2408	Ls	16.6	3.5	0.21	0.16	0.88	150	30.0	20	0.01	20	481	16	12	0.01
72	RS0801	Ls	16.8	4.6	0.06	0.01	0.17	120	30.0	60	0.01	60	812	10	10	0.01
73	RM0610	Ls	17.1	1.4	0.05	0.05	0.25	165	30.0	70	0.01	90	533	6	24	0.01
74	RM2302	Ls	17.1	3.5	0.11	0.05	0.11	255	30.0	10	0.01	5	738	8	4	0.01
75	RS1106	Ls	17.2	3.9	0.14	0.04	0.36	260	30.0	100	0.01	30	881	8	26	0.01
76	RM1207	Ls	17.3	3.6	0.35	0.29	0.57	140	30.0	160	0.03	20	934	76	32	0.01
77	RM0311	Ls	17.6	4.2	0.05	0.04	0.25	55	30.0	10	0.01	10	950	22	26	0.01
78	RS0811	Ls	17.7	4.4	0.09	0.01	0.19	120	30.0	10	0.01	5	909	12	20	0.01
79	RS0416	Ls	17.9	4.4	0.23	0.01	0.07	530	30.0	40	0.01	570	1120	22	16	0.04
80	RM0915	Ls	18.6	3.3	0.27	0.08	0.25	210	30.0	40	0.01	10	858	58	26	0.01
81	RK2511	Ls	18.7	3.3	0.34	0.11	0.92	195	30.0	110	0.01	30	553	22	112	0.04
82	RK3108	Ls	19.0	5.3	0.08	0.07	0.30	45	30.0	10	0.01	10	710	20	42	0.01
83	RS2410	Ls	19.5	4.4	0.08	0.05	0.37	125	30.0	10	0.01	10	745	8	20	0.01
84	RS0807	Ls	20.0	4.0	0.52	0.04	0.15	260	30.0	30	0.01	5	913	8	2	0.09
85	RS0808	Ls	21.1	4.4	0.14	0.02	0.22	320	30.0	70	0.01	10	973	8	1	0.01
	RK0707	Gn			0.19	0.44	0.04	35	0.7	60	0.05	5	23	1	10	0.12
	RK1001	In			0.58	0.93	0.34	105	1.0	120	0.04	40	20	2	20	0.01
	RK1002	Gn			2.06	1.60	0.65	275	0.8	590	0.01	80	40	6	74	0.01
	RK1005	In			1.73	1.35	0.58	215	1.6	240	0.03	10	28	8	48	0.01
	RK2101	In			0.64	0.45	0.21	80	1.5	370	0.01	5	26	8	46	0.01
	RK2109	Gn			0.39	0.37	0.09	105	1.4	1780	0.02	10	42	22	12	0.10
	RK2201	Cs	11.8	1.9	0.29	0.53	0.05	115	30.0	880	0.01	30	1015	24	22	0.01
	RK2202	Gn			1.38	0.81	0.54	350	2.1	200	0.03	70	133	6	36	0.01
	RK2501	Gn			0.55	2.59	0.07	70	3.6	140	0.01	5	10	10	28	0.01
	RK2503	Gn			0.67	0.31	0.06	60	0.2	590	0.01	5	6	10	18	0.08
	RK3101	Gn			0.32	0.19	0.04	105	0.4	70	0.01	190	9	24	20	0.01
	RK3104	In			0.43	1.23	0.63	155	2.6	0.5	0.01	10	27	10	54	0.01
	RK3110	Ls	15.4	0.9	0.41	0.45	2.57	630	30.0	190	0.01	30	521	22	90	0.01
	RM0301	In			0.93	1.75	0.49	305	2.4	2690	0.03	30	40	2	34	0.01
	RM0303	Gn			0.39	1.15	0.10	60	1.0	30	0.05	10	25	2	12	0.01
	RM0304	Gn			2.21	1.18	0.62	315	0.2	480	0.03	30	13	2	48	0.01
	RM0305	Gn			0.19	0.18	0.02	30	0.2	10	0.01	5	5	2	6	0.01
	RM0306	Gn			0.86	0.87	0.25	65	0.7	300	0.01	10	9	2	18	0.01
	RM0307	Gn			0.84	1.06	0.17	110	1.0	70	0.03	5	8	12	28	0.01
	RM0308	Gn			0.58	0.43	0.12	90	0.1	80	0.03	30	12	8	24	0.01
	RM0309	Gn			0.38	0.29	0.02	90	0.1	0.5	0.03	5	4	14	14	0.01
	RM0310	Gn			0.19	0.37	0.02	20	0.4	10	0.01	5	4	6	6	0.01
	RM0312	Gn			0.11	0.14	0.01	15	0.3	0.5	0.01	5	2	1	4	0.01
	RM0601	In			1.86	1.04	0.12	295	1.0	570	0.01	100	31	10	82	0.01
	RM0602	In			3.33	1.86	1.09	530	0.9	230	0.03	60	21	10	182	0.01
	RM0607	Gn			0.32	0.46	0.06	390	1.4	10	0.02	5	21	12	24	0.01
	RM0609	Cs			0.77	0.53	0.22	160	0.7	220	0.02	20	18	8	22	0.01
	RM0611	Gn			0.38	0.27	0.05	205	0.2	10	0.02	5	4	16	26	0.01
	RM0901	Gn			0.39	0.61	0.06	75	0.6	50	0.01	5	6	1	12	0.01
	RM0902	Gn			0.86	0.63	0.18	155	0.2	280	0.01	10	9	8	28	0.01
	RM0903	Gn			2.36	4.12	0.27	175	5.2	360	0.01	5	24	10	66	1.30
	RM0904	Gn			0.46	0.53	0.21	60	0.4	50	0.01	10	12	2	12	0.01
	RM0905	In			1.64	0.72	0.30	305	0.4	730	0.02	30	16	8	52	0.01

Abbreviations: Ls=limestone; Gn=gneiss; Cs=calc-silicate rock; In=Inishi rock.

Table 14 *(continued)*

No.	Sample No.	Rock type	$\delta^{18}O$ (‰)	$\delta^{13}C$ (‰)	Fe %	Al %	Mg %	Mn ppm	Ca %	P ppm	Na %	Ba ppm	Sr ppm	Pb ppm	Zn ppm	S (%)
	RM0906	Gn			0.22	0.15	0.03	100	0.5	0.5	0.01	5	14	6	10	0.01
	RM0907	Gn			1.05	1.30	0.26	180	1.2	120	0.01	10	18	8	40	0.01
	RM0908	Gn			0.39	0.36	0.04	50	0.2	10	0.01	5	10	12	10	0.01
	RM0909	Gn			0.80	0.86	0.17	130	0.5	200	0.03	10	15	14	26	0.01
	RM0912	In			2.87	2.53	1.26	305	1.8	2400	0.01	10	86	18	130	0.01
	RM0913	Gn			1.03	1.47	0.30	275	1.1	560	0.02	80	47	6	68	0.01
	RM0914	In			1.86	0.93	0.63	235	2.2	1940	0.01	50	72	20	162	0.01
	RM1201	In			4.46	2.34	1.54	905	2.2	550	0.01	60	44	2	90	0.10
	RM1202	Gn			2.49	1.91	0.85	340	1.4	1050	0.05	50	31	4	60	0.02
	RM1203	Gn			0.48	1.53	0.09	200	1.7	90	0.02	20	13	16	14	0.01
	RM1204	Gn			0.28	0.16	0.07	130	1.2	0.5	0.01	20	65	24	8	0.01
	RM1205	In			0.80	1.29	0.19	155	1.8	1090	0.03	10	21	2	40	0.01
	RM1206	Cs			0.40	3.73	0.20	160	6.1	350	0.01	5	53	4	16	0.01
	RM1208	In			0.61	0.38	0.14	95	0.2	50	0.01	10	10	10	20	0.01
	RM1209	In			1.19	1.55	0.44	280	1.6	610	0.03	10	27	14	34	0.01
	RM1210	Gn			0.10	0.19	0.01	40	0.0	0.5	0.01	10	3	8	6	0.01
	RM1211	Gn			1.75	1.09	0.65	250	0.6	310	0.01	20	11	8	40	0.01
	RM1212	Gn			0.50	0.47	0.17	70	1.7	70	0.02	5	32	8	44	0.01
	RM1213	In			2.69	1.93	1.89	625	2.2	1080	0.03	3380	163	6	80	0.02
	RM1401	Gn			0.47	0.33	0.01	135	0.1	10	0.01	20	3	18	18	0.01
	RM1402	Gn			0.64	0.45	0.20	140	0.2	30	0.03	30	8	12	16	0.01
	RM1403	Gn			0.10	0.11	0.01	5	0.0	0.5	0.02	5	3	1	4	0.01
	RM1404	Gn			1.79	2.31	0.73	225	2.7	270	0.01	10	31	8	56	0.01
	RM1405	Gn			0.44	0.23	0.05	85	0.1	0.5	0.01	5	4	12	10	0.01
	RM1501	Gn			0.14	0.13	0.02	70	0.0	10	0.03	5	3	8	4	0.01
	RM1502	Gn			1.01	1.51	0.23	160	1.6	220	0.01	40	21	10	18	0.01
	RM1504	Gn			0.57	4.78	0.06	120	5.9	320	0.01	5	35	2	22	0.01
	RM1505	Gn			0.51	1.67	0.13	150	1.7	20	0.01	20	14	20	14	0.01
	RM2301	Gn			0.48	0.60	0.12	35	0.6	70	0.03	10	15	4	16	0.01
	RM2303	Gn			4.05	2.26	1.20	510	0.4	1560	0.01	60	16	18	94	0.01
	RS0803	Gn			0.28	1.82	0.01	65	3.2	40	0.01	5	21	12	14	0.01
	RS0806	Gn			2.33	1.15	0.65	415	1.1	600	0.01	30	29	6	68	0.01
	RS1108	Gn			0.30	2.65	0.09	65	3.1	0.5	0.03	5	79	10	16	0.01
	RCK0701	Gn			1.22	0.82	0.20	70	1.2	950	0.06	10	42	2	18	
	RCK0702	Gn			3.27	1.46	0.31	170	1.1	1230	0.08	40	69	8	136	
	RCK0703	Gn			3.75	1.57	0.99	180	0.9	1040	0.04	10	26	2	36	
	RCK1002	Gn			2.72	1.95	1.42	255	1.7	830	0.16	70	47	1	64	
	RCK1006	Gn			1.33	1.17	0.27	170	1.2	1090	0.06	30	44	2	42	
	RCK2103	Gn			4.97	2.05	0.89	260	1.6	1530	0.06	60	34	1	98	
	RCK3101	Gn			2.58	1.14	0.46	500	2.0	90	0.01	940	45	42	396	
	RCK3102	Gn			1.62	0.82	0.38	290	1.5	560	0.05	60	37	26	60	
	RCK3106	Gn			0.52	0.62	0.52	235	2.8	310	0.05	50	54	2	32	
	RCK1001	In			0.95	1.10	0.15	240	2.4	710	0.06	50	60	1	50	
	RCK1003	In			1.32	1.30	0.50	150	2.3	2510	0.07	60	119	1	30	
	RCK1004	In			2.49	1.63	0.95	325	2.2	3520	0.06	40	89	2	54	
	RCK1005	In			1.85	4.74	0.83	230	4.6	1510	0.03	10	49	1	42	
	RCK1007	In			1.53	1.53	0.33	390	1.5	1070	0.06	70	68	4	52	
	RCK1008	In			3.40	1.44	0.26	400	0.3	820	0.06	230	22	4	80	
	RCK2101	In			2.80	5.13	0.37	290	5.7	1060	0.03	<10	39	6	62	
	RCK2104	In			5.01	2.71	1.65	775	2.1	1440	0.07	120	75	1	86	
	RCK3111	In			1.51	3.97	0.13	285	6.1	1150	<.01	10	44	10	72	

Abbreviations: Ls=limestone; Gn=gneiss; Cs=calc-silicate rock; In=Inishi rock.

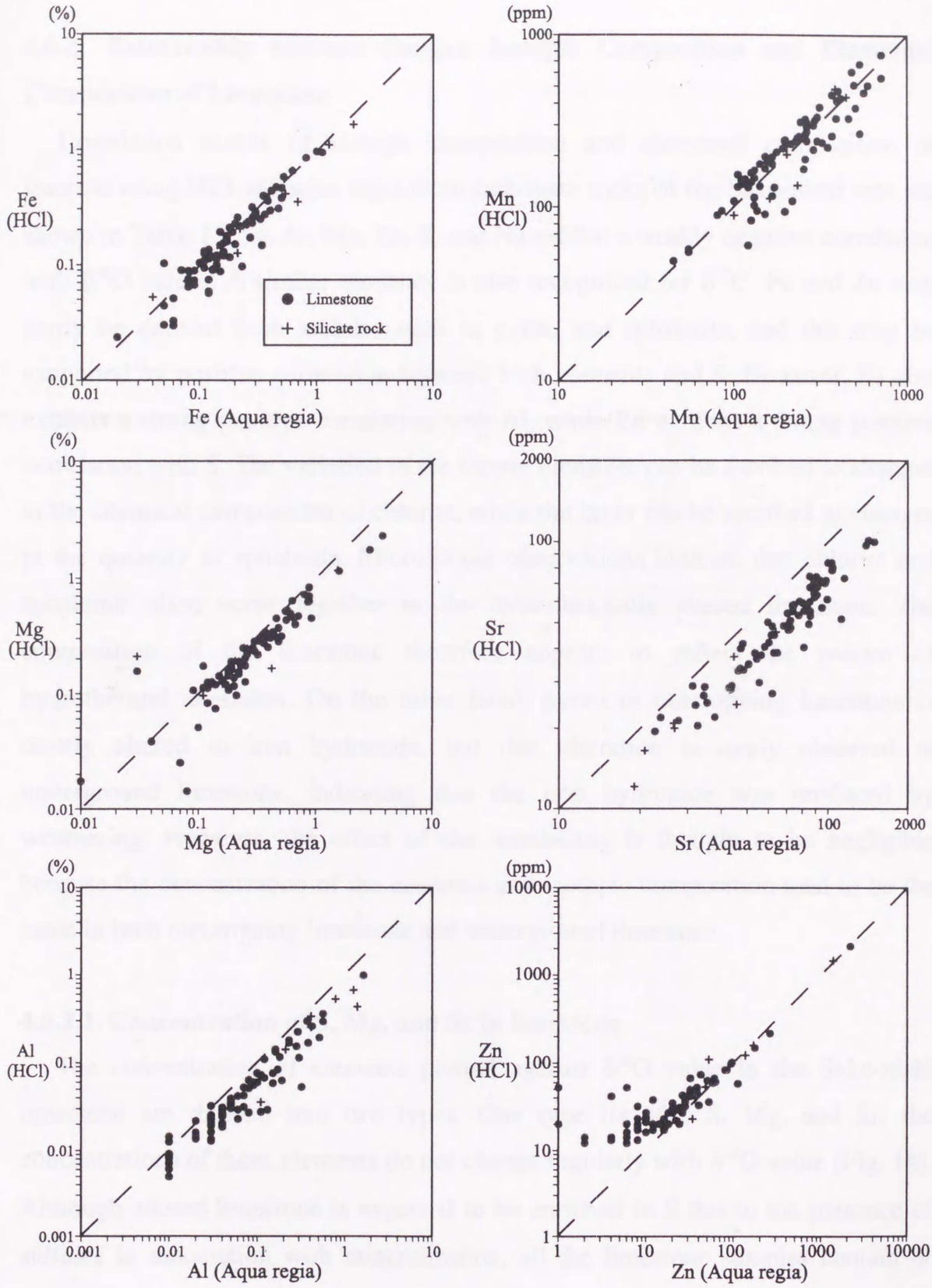

Fig.13. Concentrations of Fe, Mn, Mg, Sr, Al, and Zn in hydrochloric acid (HCl) leachate versus aqua regia leachate for carbonate and silicate rocks in the Sako-nishi area. Note that data are plotted along a 1:1 line.

4.6.2. Relationship between Oxygen Isotopic Composition and Elemental Composition of Limestone

Correlation matrix of isotopic composition and elemental composition of leachate using HCl and aqua regia from carbonate rocks of the Sako-nishi area are shown in Table 15. Fe, Al, Mn, Zn, S, and Na exhibit a weakly negative correlation with $\delta^{18}O$ values. A similar tendency is also recognized for $\delta^{13}C$. Fe and Zn may partly be derived from sulfides such as pyrite and sphalerite, and this may be supported by positive correlation between both elements and S. However, Fe also exhibits a strong positive correlation with Al, while Zn exhibits a strong positive correlation with S. The variation in the former elements can be ascribed to changes in the chemical composition of chlorite, while the latter can be ascribed to changes in the quantity of sphalerite. Microscopie observations indicate that chlorite and sphalerite often occur together in the hydrothermally altered limestone. The composition of the limestone therefore appears to reflect the pattern of hydrothermal alteration. On the other hand, pyrite in outcropping limestone is mostly altered to iron hydroxide, but that alteration is rarely observed in underground limestone, indicating that the iron hydroxide was produced by weathering. However, the effect of the weathering is thought to be negligible because the concentration of the elements and isotopic composition tend to be the same in both outcropping limestone and underground limestone.

4.6.2.1. Concentration of S, Mg, and Sr in limestone

The concentration of elements plotted against $\delta^{18}O$ value in the Sako-nishi limestone are divided into two types. One type includes S, Mg, and Sr; the concentrations of these elements do not change regularly with $\delta^{18}O$ value (Fig. 14). Although altered limestone is expected to be enriched in S due to the presence of sulfides in association with mineralization, all the limestone samples contain of <0.1% S, suggesting negligible amounts of sulfides. This is supported by the low concentrations of Zn (<100 ppm) in most samples. Because calcite and limestone can contain certain amounts of Zn from a few ppm to several hundred ppm (Brand

Table 15 Correlation coefficients among isotopic and elemental compositions of limestone in the Sako-nishi area.

HCl leachate

	$\delta^{18}O_{SMOW}$	$\delta^{13}C_{PDB}$	Fe	Al	Mg	Mn	Ca	Na	Ba	Sr	Pb	Zn	S
$\delta^{18}O_{SMOW}$	1.00												
$\delta^{13}C_{PDB}$	**0.61**	1.00											
Fe	-0.51	-0.33	1.00										
Al	-0.57	-0.41	**0.85**	1.00									
Mg	-0.06	-0.08	**0.31**	**0.25**	1.00								
Mn	-0.58	-0.44	**0.77**	**0.65**	**0.25**	1.00							
Ca	**0.10**	**0.12**	-0.22	-0.27	**0.07**	-0.12	1.00						
Na	-0.33	-0.47	**0.52**	**0.64**	**0.20**	**0.51**	-0.13	1.00					
Ba	-0.05	**0.03**	-0.03	-0.02	-0.02	**0.17**	**0.16**	**0.05**	1.00				
Sr	**0.14**	**0.38**	0.00	-0.06	-0.09	-0.06	**0.25**	**0.07**	**0.11**	1.00			
Pb	-0.07	**0.01**	**0.09**	**0.01**	**0.18**	**0.23**	**0.24**	**0.04**	**0.65**	**0.01**	1.00		
Zn	-0.11	-0.03	**0.05**	**0.03**	**0.11**	**0.23**	**0.23**	**0.01**	**0.68**	-0.06	**0.94**	1.00	
S	-0.02	-0.01	**0.25**	**0.06**	**0.25**	**0.27**	**0.09**	-0.03	**0.38**	-0.14	**0.42**	**0.44**	1.00

* Number of samples are 80 samples from ground(77) and core(3).

Aqua regia leachate

	$\delta^{18}O_{SMOW}$	$\delta^{13}C_{PDB}$	Fe	Al	Mg	Mn	Ca	Na	Ba	Sr	Pb	Zn	S
$\delta^{18}O_{SMOW}$	1.00												
$\delta^{13}C_{PDB}$	**0.71**	1.00											
Fe	-0.50	-0.54	1.00										
Al	-0.39	-0.42	**0.69**	1.00									
Mg	-0.34	-0.45	**0.84**	**0.47**	1.00								
Mn	-0.39	-0.27	**0.52**	**0.19**	**0.38**	1.00							
Ca	**0.42**	**0.51**	-0.59	-0.52	-0.67	-0.06	1.00						
Na	-0.43	-0.48	**0.53**	**0.38**	**0.60**	**0.31**	-0.70	1.00					
Ba	-0.02	**0.10**	-0.03	-0.11	-0.07	**0.27**	**0.17**	**0.03**	1.00				
Sr	**0.30**	**0.41**	-0.20	-0.37	-0.09	-0.04	**0.40**	-0.23	**0.15**	1.00			
Pb	**0.01**	**0.08**	-0.08	-0.06	-0.05	**0.09**	**0.06**	-0.07	**0.53**	**0.04**	1.00		
Zn	-0.18	-0.03	**0.06**	**0.01**	**0.06**	**0.29**	-0.04	**0.02**	**0.55**	-0.11	**0.70**	1.00	
S	-0.17	-0.20	**0.30**	**0.45**	**0.27**	**0.15**	-0.36	**0.16**	**0.31**	-0.31	**0.20**	**0.27**	1.00

* Number of samples are 123 samples from ground(78) and core(45).

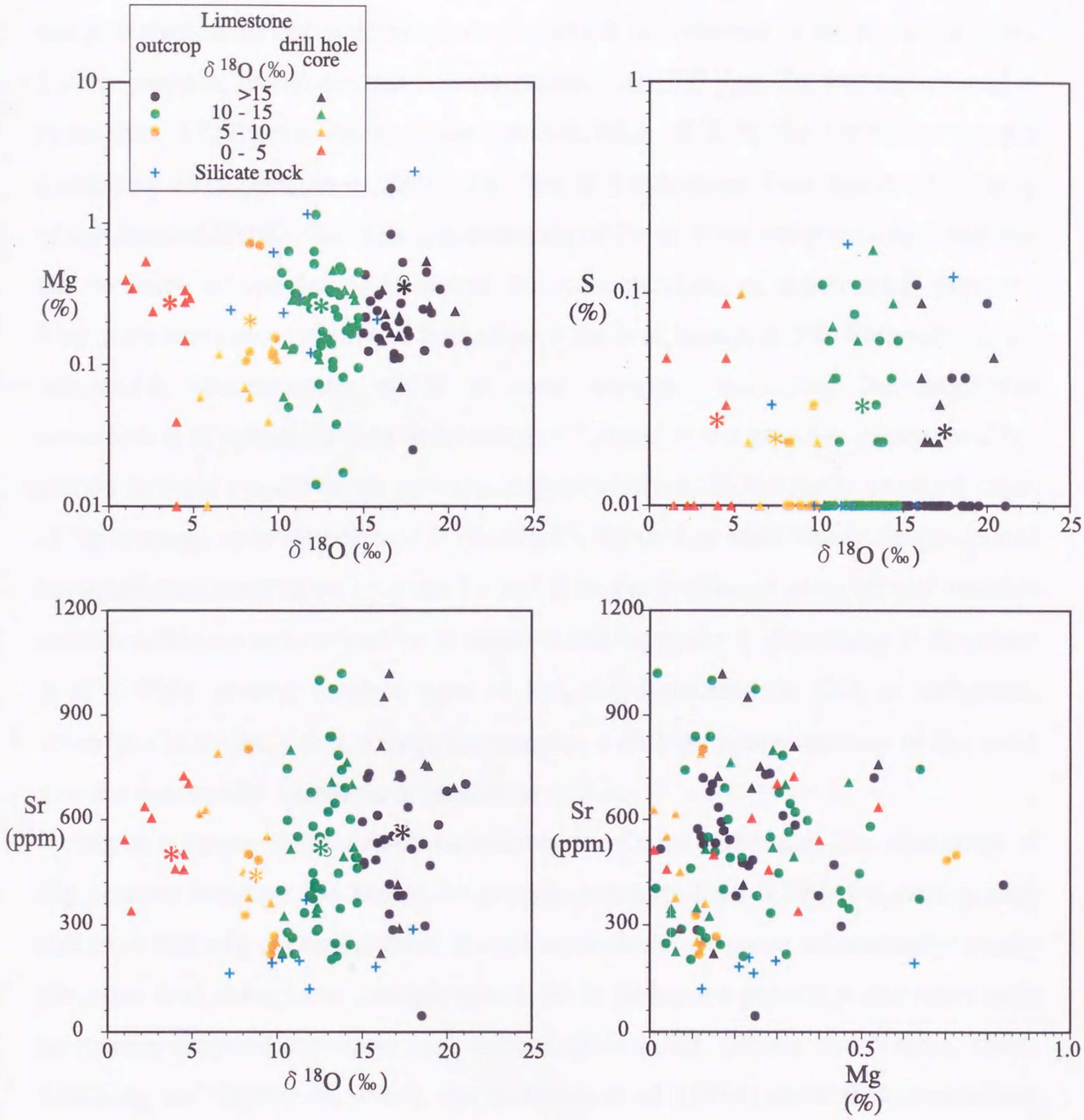

Fig. 14. Scatter plots of Mg, S, and Sr against $\delta^{18}O$ and Mg against Sr for limestones and silicate rocks from the Sako-nishi area. The concentrations of Mg, S, and Sr are for the HCl-leachates. The oxygen and carbon isotopic data are taken from MITI (1998a).

and Veizer, 1980; Calderoni and Ferrini, 1984; Reeder, 1996), it is likely that many samples studied do not contain sphalerite, which is dominant in the Kamioka mine. Twelve samples from core and contain greater than 100 ppm Zn, and three samples more than 1000 ppm. Because the concentration of S in the limestone sample containing 1815 ppm Zn is identical to that of S calculated from the stoichiometry of sphalerite (0.09%), the high concentration of Zn in these samples would indicate the presence of sphalerite. However, the concentration of sphalerite-S expected from a concentration of several tens of ppm Zn is at most 0.005%. This value is far below the concentration of S in most samples, indicating the negligible contribution of sphalerite S in most samples. Likewise, the possible presence of Fe-sulfide (mostly pyrite) is not strongly supported from (1) the fairly constant value of the average concentration of S (0.02-0.03 %) within each limestone group and no significant correlation between Fe and S in the limestone, although all samples contain sufficient amounts of Fe to compensate for pyrite S. According to Pingitore et al. (1995), several hundred ppm of SO_4 can substitute for CO_3 in carbonate. Therefore, it is likely that, except for samples with high concentrations of Zn, most S in the Sako-nishi limestone is present as sulfate.

Mg is a major cation which substitutes for Ca in carbonate. The similarity of Mg content between the limestone groups (average: 0.18-0.29% for each group) indicates that Mg accommodated in carbonate does not move substantially during alteration and changes in isotopic ratios. Sr in limestone generally decreases with increasing diagenetic process and metamorphic grade (Brand and Veizer, 1980; Schuiling and Oosterom, 1966), but Ballanca et al. (1984) show that mineralized limestone in hydrothermal fluorite deposits of northwestern Sicily become enriched in Sr. However, the Sako-nishi limestone shows neither remarkable enrichment nor depletion of Sr with $\delta^{18}O$. It is notable that the Sr content of the Sako-nishi limestone (average: 417-559 ppm for each group) is distinctly higher than that of vein carbonates (58-195 ppm). Fujinuki (1973) and Musashino (1973) document that limestones in Japan with high carbon content are enriched in Sr (>500 ppm), partly due to the adsorption of Sr on graphite or organic carbon.

Therefore, the high concentration of Sr in the Sako-nishi limestone can be attributed to its high graphite content.

The similarity of the concentrations of S, Mg, and Sr among individual limestone groups seems to indicate that these elements, which dominantly substitute for Ca or CO_3 in the carbonate lattice, do not exchange with associated hydrothermal solutions which resulted in the carbon and oxygen isotope alteration. As a result, the isotopically-altered limestone in the Sako-nishi area cannot be identified by a combination of these elements. One example, the Mg-Sr relation, is illustrated in Fig. 14.

4.6.2.2. Concentration of Al, Fe, Mn, P, and Zn in limestone

In contrast to S, Mg, and Sr, the concentrations of Al, Fe, Mn, P, and Zn tend to increase with decreasing in $\delta^{18}O$ value (Fig. 3). The concentration of these elements in limestone, although it varies widely within each group, is 2 to 5 times higher in group-C and 3 to 7 times higher in group-D than in group-A. Of these, the concentration of Al is relatively constant within each limestone group and shows a good correlation with variations in $\delta^{18}O$ value. The altered limestone (groups B, C, and D) can be separated from the original limestone (group-A) at about 0.1% Al (Fig. 3B). Most of the strongly ^{18}O -depleted limestones have more than 0.3% Al. However, the combination of Al, Mn, P, and Zn is ineffective in distinguishing unaltered from altered limestones because the individual groups overlap on the binary diagrams for these elements.

On the other hand, the ratio of Mg to Fe tends to change with $\delta^{18}O$ value (Fig. 15A). Group-C and group-D limestones have Mg:Fe ratios lower than 1.0, while group-A limestones have Mg:Fe ratios greater than 1.0. Furthermore, there is a positive correlation between Fe and Mn (Fig. 15B). Consequently, the ratio of Mg:(Mg+Fe+Mn), designated hereafter as Mg*, can be utilized as an indicator for the classification of the Sako-nishi limestone in terms of the degree of alteration. The altered limestones are discriminated from those of group-A in the Mg* versus $\delta^{18}O$ value diagram (Fig. 16).

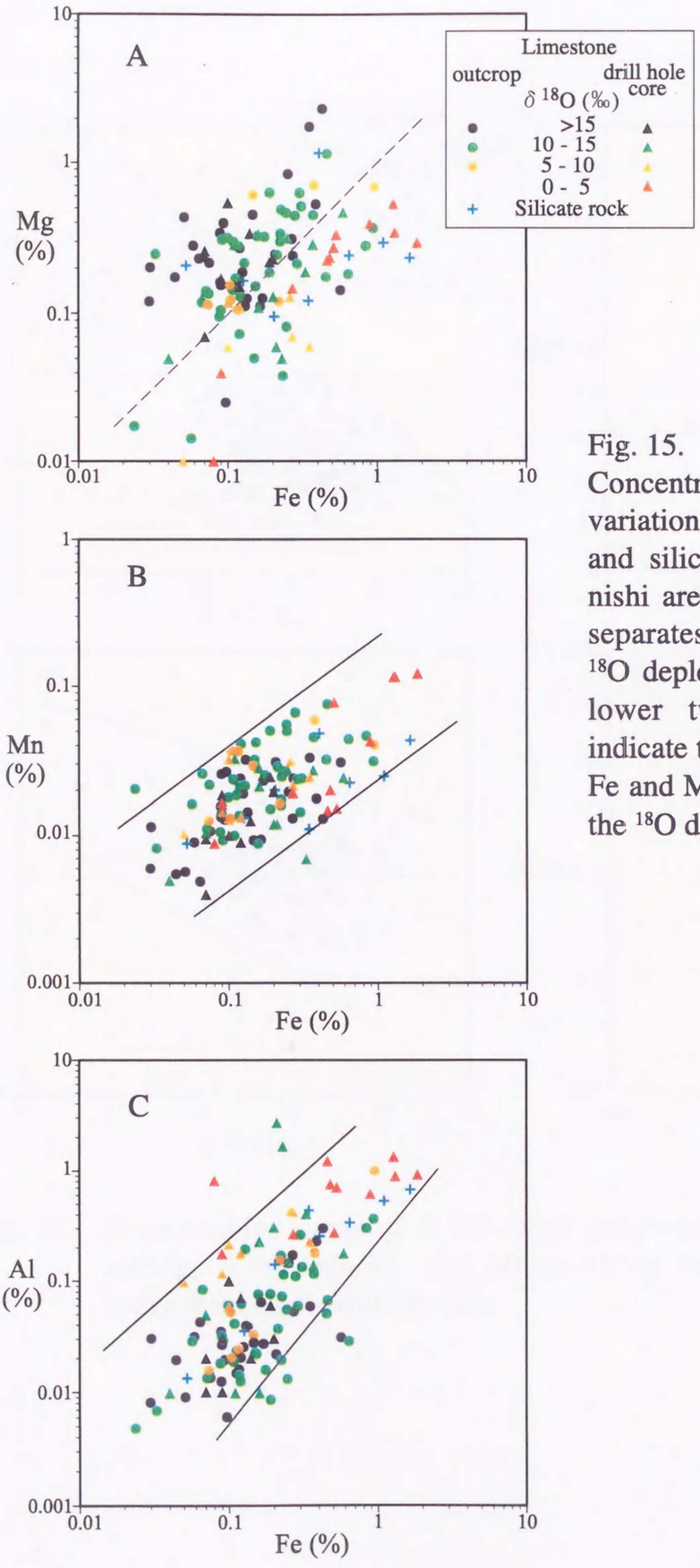

Fig. 15.
Concentrations of Mg, Mn, and Al variations versus Fe for limestones and silicate rocks from the Sako-nishi area. Broken line in Fig.15A separates original limestone from ^{18}O depleted one. Solid line in the lower two figures (B and C) indicate the compositional range of Fe and Mn and that of Fe and Al of the ^{18}O depleted limestone.

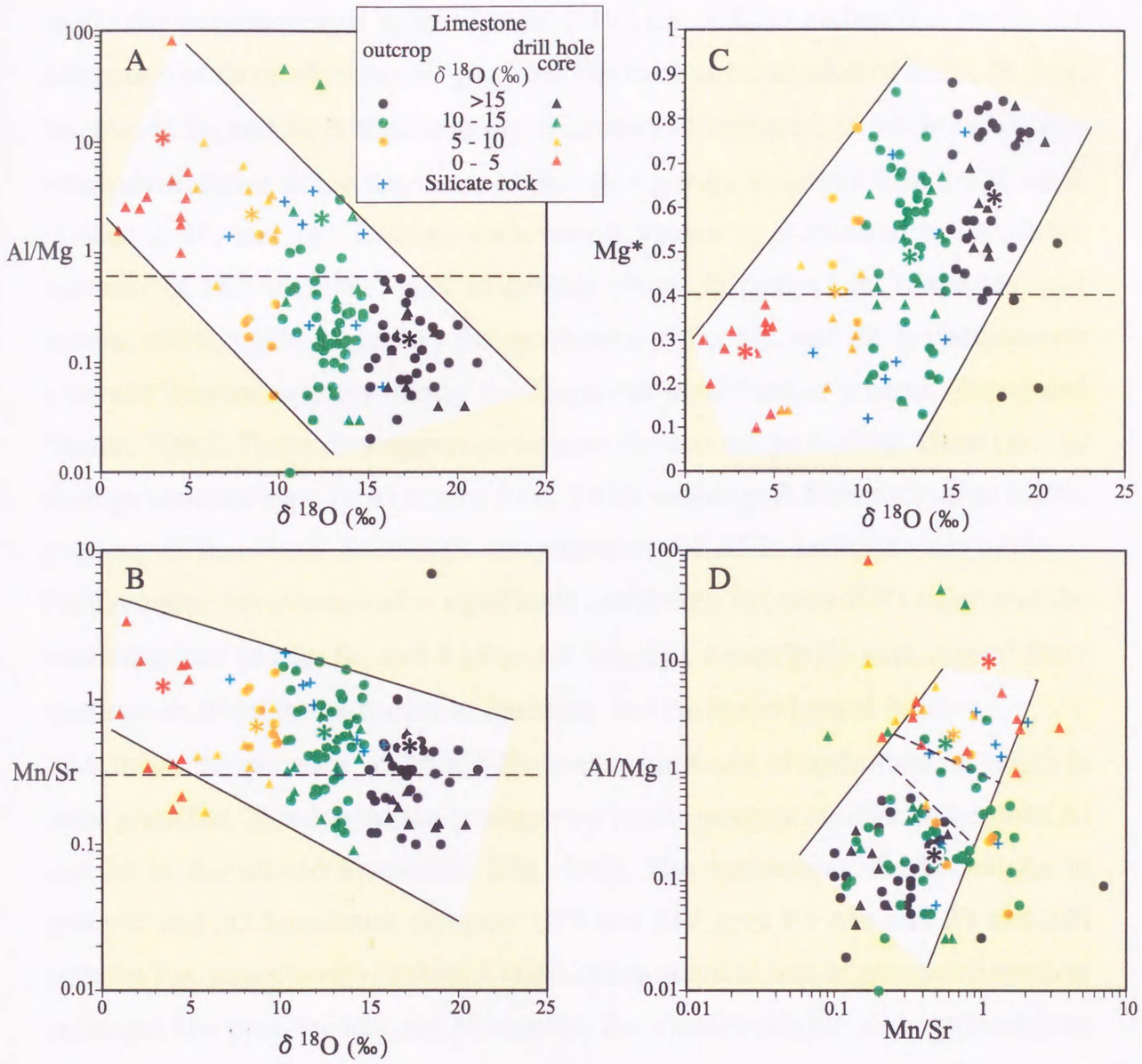

Fig. 16. Relationships between $\delta^{18}O$ -Mg* [Mg*=Mg/(Mg+Fe+Mn)], $\delta^{18}O$-Al/Mg, $\delta^{18}O$ -Mn/Sr, and Mn/Sr-Al/Mg for limestones and silicate rocks from the Sako-nishi area.

The enrichment of Al, Fe, Mn, P, and Zn in the altered limestone is ascribed to (1) the formation of Al and Fe bearing minerals such as chlorite and skarn silicates or (2) the substitution of these elements into Ca or C in carbonates, or (3) the adsorption of these elements on graphite. The total concentration of S, Al, Fe, Mg, Na, Mn, P, Sr, and Zn is high in group-D limestone (average 1.86 wt.%), while it is relatively constant in the limestone of the other groups at around 0.58 ± 0.38 wt.% (Tables 2, 10, and 14). Calcium carbonate is known to accommodate significant amounts of Fe^{2+} and Mn^{2+} and to contain about 30 ppm of Al (Calderoni and Ferrini, 1984), while a tendency for enrichment of Fe, Mn, and Zn in carbonates is generally known to occur during the diagenetic equilibration process (Brand and Veizer, 1980). These data appear to support the second possibility. However, the average concentration of Al ranges from 0.17% in group-B limestone up to 0.69% in group-D limestone. Such high concentrations of Al in carbonate are unlikely. Furthermore, the absence of a significant correlation between $\delta^{18}O$ value and the concentrations of Mg, Sr, and S (Fig. 14) suggests a negligible exchange of these elements between the carbonate in limestone and the hydrothermal fluid.

Instead, the presence of Al and Fe bearing minerals of hydrothermal origin is more probable. This conclusion is supported by the positive correlation between Al and Fe in the altered limestones (Fig. 15C). The enrichment of Mn and Zn in group-C and -D limestones (average: 255 and 562 ppm for Mn and 29 and 236 ppm for Zn, respectively) (Tables 2 and 10) compared to that in group-A limestone (average: 164 ppm for Mn and 32 ppm for Zn, respectively) is also attributable to mafic silicates in group-C and -D limestones, although carbonate can contain several hundred ppm of Zn (Reeder, 1996). Skarn pyroxenes of the Pb-Zn type are generally enriched in Mn and contain 300-400 ppm of Zn (Einaudi and Burt, 1982; Nakano et al., 1994). However, there is no data on the widespread presence of skarn pyroxene in the Sako-nishi altered limestone. The high concentrations of Al, Fe, Mn, and Zn in the altered limestone is more likely attributable to chlorite because this mineral is dominant in the altered silicate rocks and mineralized zone (Hirokawa et al., 1995; MMAJ, 1996) and can contain sufficient amounts of Zn

(Nakano et al., 1991). Likewise, epidote may partly account for the high concentration of Al and Fe in the altered limestone due to its common occurrence in hydrothermally altered silicate rock. This is consistent with the petrographical observation that one mineralized limestone in the Sako-nishi area contains plagioclase, epidote, chlorite, sericite, calcite, and quartz as secondary minerals (MMAJ, 1996).

4.6.2.3. Potential indicator for the determination of hydrothermally altered limestone

The elemental composition of isotopically altered limestone in the Sako-nishi area strongly suggests the presence of Al-Fe bearing minerals, mainly chlorite and epidote. As the $\delta^{13}C$ and $\delta^{18}O$ values of carbonates in group-D limestone partly overlap with those of the skarn calcites of the Kamioka mine (Fig. 3A). These carbonates may have crystallized through a reaction of limestone with the skarn-forming fluid. In contrast, it is assumed that Mg, Sr, and S accommodated in carbonates did not exchange with the fluid. Therefore, it appears that the isotopic halo of the $\delta^{13}C$ and $\delta^{18}O$ values in the Sako-nishi limestone resulted from the isotopic exchange of C and O between the limestone and hydrothermal fluid in association with the formation of Al-Fe minerals as the fluid percolated through the grain boundary and/or small cracks in the limestone.

Figures 3 and 14 show that the group-D limestone plots largely in a region of above 0.3% Al, 0.3% Fe, 300 ppm Mn, 200 ppm P, and 50 ppm Zn, suggesting that these values can be used as potential criteria for focusing on potential areas of mineralization. In contrast, weakly to moderately altered limestones (groups B and C) can be discriminated from group-A limestone by 0.1% Al, while the discrimination is not fully achieved with other elements (Fe, Mn, P, and Zn) (Fig. 3).

The elemental composition of some impure limestones plot in or close to the region of altered limestones (Figs. 3 and 14), implying that they contain increasing amounts of hydrothermal minerals rather than originating from limestone with high

concentrations of detrital minerals. This indicates that it is difficult to use the concentration data alone to distinguish whether the elemental composition of altered limestone is due to the presence of hydrothermal minerals or detrital minerals. For example, if the original limestone is enriched in detrital Al minerals, Al content cannot be applied for the determination of ^{18}O-depleted limestone. This is likely to occur because the Sako-nishi limestone contains thin beds of Inishi rock and gneiss. The contamination of limestone is dependent on the large difference between the $\delta^{18}O$ value of hydrothermal fluid and that of limestone. The ICP-OES method has an advantage over the isotope method owing to its rapidity and convenience of analysis, but has a disadvantage due to its sensitivity to the chemical heterogeneity of the original limestone.

I expect that elemental ratios will be more effective for the identification of altered limestone than the element concentration data because the ratios are less affected by the amounts of non-carbonate minerals. As the element patterns of the Sako-nishi limestone can be divided into 2 types, it appears that element ratios of the 2 types are potentially useful for the classification of limestone. Fig. 16 shows the relationship between the $\delta^{18}O$ value of Sako-nishi carbonate rocks and Mg*, Al/Mg, and Mn/Sr. Note that the Al/Mg ratios in limestone, similar to Mg*, change regularly with $\delta^{18}O$ value. Furthermore, some impure limestones are distinguished from limestone and vein carbonates in the binary diagrams using ratios of Mg*, Al/Mg, and Mn/Sr. Group-A limestone and altered-limestone are roughly divided by values of 0.4 for Mg*, 0.6 for Al/Mg, and 0.3 for Mn/Sr. Heavily-^{18}O depleted limestones (groups C and D) are clearly separated in the Al/Mg-Mn/Sr diagram. Mn/Sr ratios tend to be high in strongly ^{18}O depleted limestone, indicating their usefulness as a supplement to the classification of altered limestone. Figures 3 and 16 demonstrate the effectiveness of Al content and the ratios of Mg*, Al/Mg, and Mn/Sr in limestone as a tool for the exploration of skarn deposits.

4.7. Bulk Chemical Composition of Inishi-rock and Gneiss

Inishi-rock and gneiss are mainly composed of plagioclase, clinopyroxene,

titanite, and quartz with variable modal compositions (Table 3). They are more or less subjected to hydrothermal alteration, in which plagioclase is replaced by prehnite and epidote, and clinopyroxene by actinolite and chlorite (Fig. 6). The elemental compositions of Inishi rocks and gneisses are given in Table 16 and those of their leachates using aqua-regia are in Table 17. Although the concentrations of all elements in bulk rock samples are higher than those in leachate ones, this tendency is more pronounced in Na and Al (Fig.17); the concentration of Na in aqua regia leachate of Inishi rocks (average=0.08 wt.%) is very low compared with that of whole rock (average=2.43 wt.%). A positive correlation between Na and Al in bulk rock samples indicates that the two elements are mainly contained in plagioclase, which is predominant in the silicate-rocks. In contrast, a strong positive correlation among Ca, Fe, Mn, and Mg of bulk rock samples (Table 18) is attributable to clinopyroxene which is a major constituent of Inishi rock, although a part of Ca is present in plagioclase since plagioclase in un-altered Inishi rock contains 32-38 mol% anorthite (Takeno and Iiyama, 1983).

4.7.1. Relationship between Oxygen Isotopic Composition and Elemental Composition of Aqua-regia Leachates in Inishi rock and gneiss

It is notable in Table 17 that the chemical compositions of aqua regia leachates of these silicate rocks change widely compared to those of limestone, in accordance with their complex mineral assemblage. Table 19 shows the correlation coefficients among the concentrations of elements of silicate rocks and the values of $\delta^{18}O$ and $\delta^{13}C$ of limestones in their vicinity. Figures 18 and 19 show the concentrations of Ca, Sr, Fe, Mn, Zn, S, Al, Mg, K, and Na of aqua-regia leachates of Inishi-rock and gneiss plotted against $\delta^{18}O$ value. The variation patterns of the elements are divided into three groups (I, II, and III). Group-I is composed of Ca, Sr, Fe, and Mn, whose concentrations increase with the decrease of $\delta^{18}O$ value. Group-II is composed of K and Na, whose concentrations increase with increasing $\delta^{18}O$ value. Group-III is composed of Zn, S, Al, and Mg, whose concentrations are less dependent on the $\delta^{18}O$ value.

Table 16 Chemical compositions for aqua regia digestion of silicate rock in the Sako-nishi area.

Sample No	Rock type	G	$\delta^{13}C$* ‰	$\delta^{18}O$* ‰	Fe %	Al %	Mg %	Mn ppm	Ca %	Na %	Ba ppm	Sr ppm	Pb ppm	Zn ppm
56HI-1 278.60m	In	B	0.1	12.5	1.73	1.56	0.42	345	2.28	0.11	20	69	10	54
56HI-1 283.70m	In	B	0.1	12.5	1.57	2.32	0.33	275	3.64	0.1	20	76	10	78
56HI-1 292.30m	In	C	-0.3	7.9	1.77	4.3	0.56	375	7.92	0.01	5	67	2	254
56HI-1 314.60m	In	C	-2.3	9.1	0.9	1.6	0.23	150	3.7	0.05	20	95	4	120
56HI-1 351.90m	In	B	-1.5	11.2	0.27	0.73	0.08	55	1.47	0.13	40	76	2	20
56HI-1 393.80m	In	B	-0.7	12.5	0.34	0.89	0.08	105	2.19	0.13	70	93	14	68
56HI-1 452.20m	In	B	3.4	14.8	0.57	1.06	0.19	65	1.88	0.17	20	145	1	22
56HI-1 503.00m	In	A	3.9	15.8	0.4	0.63	0.11	90	1.94	0.15	40	83	2	20
56HI-1 534.60m	Gn	D	2.1	3.6	0.22	0.43	0.06	195	1.87	0.07	130	160	26	8
56HI-1 537.70m	Gn	D	0.7	1.2	0.2	0.26	0.04	130	1.54	0.08	210	107	16	4
2HI-1 25.00m	In	B	2.8	12.8	0.69	1.19	0.38	210	5.84	0.05	100	88	6	30
2HI-1 60.40m	In	C	0.6	9.3	1.92	1.54	0.69	435	4.58	0.01	150	89	20	54
2HI-1 127.40m	In	B	1.1	12.5	4.35	1.83	0.78	455	5.03	0.07	40	74	6	174
2HI-1 180.30m	In	B	1.6	11.8	2.18	1.2	0.34	345	2.61	0.06	20	68	2	90
2HI-1 378.85m	In	B	-4.2	10.5	2.48	1.83	1.21	470	3.62	0.09	40	93	6	86
2HI-1 688.10m	Gn	C	-2.8	5.5	6.79	3.96	2.58	1505	8.08	0.01	120	380	8	180
3HS-3 101.50m	In	C	1.1	7.9	0.82	1.02	0.33	265	13	0.01	5	147	4	48
3HS-3 140.60m	In	B	0.3	10.4	1.25	1.91	0.38	255	3.37	0.11	10	43	8	60
3HS-3 155.50m	In	A	1.2	16.1	1.27	1.26	0.46	240	2.64	0.12	50	161	6	52
3HS-3 363.30m	In	D	-4.0	4.6	1.01	1.76	0.1	250	4.73	0.02	100	92	12	62
3HS-3 366.80m	In	D	-4.0	4.6	1.32	0.7	0.35	330	2.6	0.07	70	109	6	132
3HS-3 426.90m	In	C	-3.1	8.4	1.23	1.37	0.33	605	4.42	0.01	50	188	2	58
3HS-3 515.55m	In	D	-3.9	1.8	0.47	1.02	0.08	85	1.48	0.13	30	69	2	22
3HS-3 584.50m	Gn	C	-5.7	5.2	1.51	0.84	0.25	805	30	0.05	80	1185	152	9250
3HS-3 636.40m	Gn	D	-6.3	2.5	5.3	2.86	1.84	1165	5.42	0.04	30	356	6	110
3HS-3 697.40m	Gn	D	-6.5	4.1	4.77	3.07	2.03	1130	8.56	0.01	40	338	1	92
4HS-5 113.30m	In	C	2.2	8.5	0.76	0.76	0.28	150	14.1	0.02	20	403	6	44
4HS-5 117.40m	In	D	0.6	4.5	2.52	2.01	0.98	400	8.55	0.07	80	355	8	100
4HS-5 123.80m	In	D	-1.0	4.9	0.75	0.6	0.19	160	1.18	0.06	110	33	14	20
4HS-5 600.70m	Gn	C	0.2	5.4	1.19	0.95	0.5	325	2.27	0.12	50	98	8	42
4HS-5 605.30m	In	C	-0.3	6.9	0.46	1.42	0.17	190	7.31	0.05	10	112	4	68
4HS-6 44.00m	Gn	B	3.6	14.8	1.22	1.32	0.44	135	2.9	0.2	20	157	2	60
4HS-6 120.80m	In	B	3.6	13.8	0.68	2.37	0.33	170	4.05	0.41	100	224	6	64
4HS-6 169.00m	In	B	2.4	11.5	0.85	1.84	0.39	185	3.8	0.25	120	181	6	60
4HS-6 309.50m	Gn	B	1.5	11.3	1.65	1.03	0.56	260	1.67	0.04	50	38	8	34
4HS-6 530.90m	In	B	-0.4	11.2	2.25	2.16	0.77	120	3.2	0.13	30	133	1	66
4HS-6 622.60m	Gn	C	2.2	6.7	4.75	2.75	1.92	695	3.44	0.04	160	214	14	92
4HS-6 672.70m	In	C	-0.9	7.4	2.37	1.18	0.41	285	3.92	0.03	170	99	8	186
4HS-6 786.40m	In	B	-2.5	11.6	0.82	1.17	0.26	125	1.57	0.13	50	59	8	24
5HS-7 74.50m	In	A	3.9	17.2	1.89	1.21	0.75	260	5.24	0.1	60	142	8	144
5HS-7 92.80m	Gn	B	3.3	13.3	0.63	0.54	0.13	145	1.03	0.06	50	24	12	20
5HS-7 131.70m	In	C	0.0	6.7	4.62	2.18	0.94	740	3.41	0.05	50	72	2	136
5HS-7 326.50m	In	D	2.3	4.5	10.2	1.01	0.59	7200	11.9	0.04	350	433	8	630
5HS-7 329.70m	In	D	2.3	4.5	3.51	1.47	0.82	930	4.17	0.08	80	202	2	114
5HS-7 394.60m	In	D	-2.4	1.4	3.6	1.7	0.39	2010	4.3	0.01	40	228	38	104000
5HS-7 411.70m	In	D	-2.0	2.1	3.1	2.27	0.54	1595	6.37	0.01	40	365	4	96
5HS-9 525.20m	Gn	B	1.1	11	2.15	1.78	0.74	150	2.58	0.15	20	131	2	56
5HS-9 566.80m	In	B	3.5	14.1	1.64	1.01	0.85	355	5.08	0.05	30	115	18	250
5HS-9 591.20m	In	A	4.3	16.5	1.99	1.86	1.03	245	4.04	0.06	90	137	6	64
5HS-9 603.20m	In	A	3.9	17.1	1.39	0.89	0.44	215	2.62	0.06	50	87	10	108
7KK-1 204.80m	In	B	1.0	11.7	0.54	1.06	0.18	110	1.67	0.13	30	57	6	24
7KK-1 283.40m	In	B	1.2	12.2	0.83	0.99	0.2	210	1.7	0.12	30	87	2	42
7KK-1 302.90m	In	C	2.3	7.2	0.46	3.16	0.13	110	6.43	0.06	30	66	10	60
7KK-1 315.10m	In	D	-2.6	1.6	1.51	1.13	0.37	755	3.49	0.03	10	149	1	54
7KK-1 391.20m	In	D	1.9	2.7	2.1	1.28	0.52	910	5.36	0.04	10	264	2	54
7KK-1 430.60m	In	D	-1.3	4.6	3.03	0.47	0.2	6510	30	0.01	30	418	8	24
7KK-1 447.20m	In	A	-0.7	16.4	1.26	0.78	0.33	205	5.68	0.06	20	122	1	48
7KK-1 525.50m	In	C	-0.4	6	3.76	1.55	0.7	2040	5	0.01	50	325	4	90

Abbreviations: G=group of alteration; Gn=gneiss; In=Inishi rock.

* $\delta^{18}O$ and $\delta^{13}C$ value based on average of the $\delta^{18}O$ values of limestone layer intercalating silicate rocks.

Table 17 Whole rock chemical compositions of silicate rock in the Sako-nishi area.

Sample No	Rock type	G	$\delta^{13}C$* ‰	$\delta^{18}O$* ‰	SiO_2 (%)	TiO_2 (%)	Al_2O_3 (%)	Fe_2O_3** (%)	MgO (%)	MnO (%)	CaO (%)	Na_2O (%)	K_2O (%)	P_2O_5 (%)	Total (%)	S (%)	Zn ppm	Rb ppm	Sr ppm	Zr ppm	Nb ppm	Ba ppm
56HI-1 278.60m	In	B	0.1	12.5	56.73	0.24	18.08	4.15	1.42	0.10	6.37	6.71	0.95	0.28	95.04	0.01	67	23	901	85	4	262
56HI-1 283.70m	In	B	0.1	12.5	54.20	1.30	19.21	3.81	1.13	0.08	11.04	5.31	1.10	0.38	97.56	0.08	80	24	931	123	37	478
56HI-1 292.30m	In	C	-0.3	7.9	47.70	0.15	15.84	6.02	3.30	0.13	23.54	0.20	0.01	0.46	97.35	0.03	154	0	85	30	3	163
56HI-1 314.60m	In	C	-2.3	9.1	49.63	1.39	13.67	9.57	3.11	0.16	18.75	2.22	0.39	0.45	99.34	0.01	269	8	549	101	35	126
56HI-1 351.90m	In	B	-1.5	11.2	56.22	0.62	19.58	3.48	1.59	0.06	10.46	5.45	0.96	0.28	98.69	0.01	67	12	1289	130	11	540
56HI-1 393.80m	In	B	-0.7	12.5	54.26	1.07	19.41	3.67	1.40	0.08	11.60	4.13	1.98	0.45	98.05	0.01	109	31	1111	114	22	1167
56HI-1 452.20m	In	B	3.4	14.8	53.43	1.24	19.99	3.44	2.15	0.05	12.10	4.56	0.45	0.48	97.90	0.03	51	5	1734	182	19	382
56HI-1 503.00m	In	A	3.9	15.8	56.08	1.60	19.29	2.73	1.12	0.06	10.34	5.49	0.83	0.43	97.96	0.04	51	12	1162	143	41	772
56HI-1 534.60m	Gn	D	2.1	3.6	77.00	0.03	14.35	0.68	0.35	0.03	2.70	3.40	2.88	0.01	101.42	0.01	22	122	342	45	2	379
56HI-1 537.70m	Gn	D	0.7	1.2	71.53	0.03	15.22	0.67	0.20	0.03	2.69	6.25	1.10	0.01	97.71	0.07	19	46	451	52	1	535
2HI-1 25.00m	In	B	2.8	12.8	55.71	0.41	15.56	2.83	1.61	0.07	12.31	2.05	5.96	0.21	96.72	0.05	38	102	506	190	14	1971
2HI-1 60.40m	In	C	0.6	9.3	59.01	0.29	14.89	2.88	1.82	0.07	7.37	0.45	9.93	0.28	97.00	0.04	44	174	293	51	8	2376
2HI-1 127.40m	In	B	1.1	12.5	52.53	0.96	13.34	8.15	2.15	0.10	10.30	4.46	0.20	0.27	92.46	0.19	190	4	363	136	26	221
2HI-1 180.30m	In	B	1.6	11.8	52.74	0.84	12.37	11.63	2.88	0.25	14.35	3.48	0.40	0.06	99.01	0.03	253	8	726	84	23	278
2HI-1 378.85m	In	B	-4.2	10.5	52.88	1.12	14.29	6.76	4.72	0.14	10.44	4.21	0.71	0.08	95.35	0.05	119	9	726	120	32	559
2HI-1 688.10m	Gn	C	-2.8	5.5	35.84	1.37	19.54	12.93	5.28	0.24	13.85	0.48	3.96	0.24	93.72	0.13	213	135	404	99	4	1725
3HS-3 101.50m	In	C	1.1	7.9	51.89	0.86	6.33	3.99	2.12	0.11	29.66	0.27	0.01	0.34	95.58	0.24	37	1	111	75	49	286
3HS-3 140.60m	In	B	0.3	10.4	59.03	0.68	17.16	2.85	1.24	0.07	8.15	6.67	0.71	0.20	96.76	0.01	60	15	619	147	35	384
3HS-3 155.50m	In	A	1.2	16.1	53.78	0.29	17.53	5.03	2.57	0.12	10.59	4.91	1.19	0.76	96.76	0.02	88	30	1248	321	3	626
3HS-3 363.30m	In	D	-4.0	4.6	69.74	0.23	13.34	2.21	0.41	0.06	8.34	0.47	7.27	0.04	102.11	0.03	51	120	223	5	8	1530
3HS-3 366.80m	In	D	-4.0	4.6	60.20	0.43	15.65	3.40	1.23	0.08	6.55	3.86	4.94	0.13	96.46	0.02	115	84	857	82	14	1948
3HS-3 426.90m	In	C	-3.1	8.4	54.94	0.57	16.75	5.68	1.23	0.13	15.55	0.99	1.37	0.09	97.28	0.01	50	51	646	93	21	339
3HS-3 515.55m	In	D	-3.9	1.8	57.52	0.52	19.03	3.94	0.86	0.09	8.50	6.23	1.15	0.23	98.08	0.06	69	25	1141	236	9	698
3HS-3 584.50m	Gn	C	-5.7	5.2	43.05	0.24	7.42	2.57	0.92	0.13	29.61	0.90	1.56	0.06	86.46	1.13	1177	33	780	102	2	1524
3HS-3 636.40m	Gn	D	-6.3	2.5	43.11	1.11	14.25	9.82	4.90	0.21	11.14	3.37	0.66	0.25	88.82	0.58	117	29	777	148	5	440
3HS-3 697.40m	Gn	D	-6.5	4.1	43.49	0.65	10.77	9.42	6.12	0.21	18.93	0.37	0.88	0.15	91.00	0.05	82	26	732	123	5	1377
4HS-5 113.30m	In	C	2.2	8.5	42.39	0.38	10.17	1.92	1.16	0.05	27.87	1.25	3.79	0.20	89.18	0.09	23	54	454	72	28	2185
4HS-5 117.40m	In	D	0.6	4.5	49.12	0.13	15.95	4.23	2.68	0.07	15.19	1.80	2.66	0.34	92.18	0.02	72	80	551	63	1	872
4HS-5 123.80m	In	D	-1.0	4.9	69.70	0.21	14.79	1.75	0.79	0.04	2.69	2.93	7.32	0.11	100.33	0.03	31	117	512	161	2	2762
4HS-5 600.70m	Gn	C	0.2	5.4	56.08	0.93	15.60	5.62	3.02	0.14	10.34	5.02	0.74	0.33	97.81	0.05	84	21	1083	223	23	397
4HS-5 605.30m	In	C	-0.3	6.9	54.32	0.15	14.91	1.86	1.04	0.06	18.07	3.82	0.42	0.03	94.67	0.01	38	8	595	112	8	459
4HS-6 44.00m	Gn	B	3.6	14.8	53.74	1.52	18.90	3.70	2.10	0.05	11.34	4.90	0.65	0.55	97.45	0.01	69	13	1537	172	23	388
4HS-6 120.80m	In	B	3.6	13.8	51.92	1.32	18.92	3.66	1.86	0.07	13.01	3.75	1.66	0.27	96.45	0.01	82	47	1054	150	31	643
4HS-6 169.00m	In	B	2.4	11.5	54.26	0.92	16.47	5.09	2.83	0.09	14.12	3.23	1.09	0.69	98.78	0.01	100	28	985	121	17	786
4HS-6 309.50m	Gn	B	1.5	11.3	66.62	0.48	14.42	2.52	1.42	0.05	3.64	3.44	4.16	0.26	97.02	0.01	34	76	587	166	6	1915
4HS-6 530.90m	In	B	-0.4	11.2	49.36	3.52	17.79	6.52	3.46	0.08	11.40	3.72	0.90	1.07	97.81	0.16	80	15	1454	127	15	411
4HS-6 622.60m	Gn	C	2.2	6.7	49.53	0.77	15.50	8.02	4.70	0.12	6.05	2.90	2.09	0.40	90.06	0.01	108	62	903	194	4	906
4HS-6 672.70m	In	C	-0.9	7.4	56.72	0.56	13.95	6.69	1.30	0.10	13.31	2.79	0.68	0.18	96.28	0.2	195	19	695	137	8	1049
4HS-6 786.40m	In	B	-2.5	11.6	57.49	0.52	18.83	3.26	1.56	0.07	7.43	6.26	1.50	0.20	97.13	0.01	49	25	1186	423	6	661
5HS-7 74.50m	In	A	3.9	17.2	49.65	1.13	15.93	5.16	3.30	0.07	13.56	3.35	1.22	0.69	94.07	0.15	156	21	1067	118	11	787
5HS-7 92.80m	Gn	B	3.3	13.3	77.17	0.13	14.06	0.93	0.30	0.03	1.61	3.31	4.85	0.02	102.40	0.01	23	119	241	88	5	521
5HS-7 131.70m	In	C	0.0	6.7	55.00	0.75	14.44	8.21	2.40	0.19	6.72	2.48	2.21	0.11	92.51	0.11	142	66	423	204	6	871
5HS-7 326.50m	In	D	2.3	4.5	39.24	0.05	4.04	21.85	1.81	1.30	23.40	0.31	0.11	0.03	92.13	0.17	778	11	436	27	2	545
5HS-7 329.70m	In	D	2.3	4.5	51.09	0.93	15.17	6.47	2.05	0.16	9.38	4.87	0.63	0.18	90.94	0.01	113	18	1185	112	24	472
5HS-7 394.60m	In	D	-2.4	1.4	36.05	1.09	11.51	10.17	1.11	0.33	15.44	3.20	0.35	0.12	79.38	10	61759	10	490	63	21	2
5HS-7 411.70m	In	D	-2.0	2.1	49.26	0.73	15.28	8.27	1.64	0.26	17.48	0.29	1.19	0.19	94.60	0.01	45	78	764	104	23	177
5HS-9 525.20m	Gn	B	1.1	11	50.04	1.26	16.74	6.58	5.07	0.08	12.86	3.17	0.84	0.89	97.55	0.4	77	14	1159	116	3	284
5HS-9 566.80m	In	B	3.5	14.1	54.12	0.74	15.48	3.06	2.34	0.07	11.83	3.57	2.21	0.25	93.66	0.14	154	67	736	134	21	715
5HS-9 591.20m	In	A	4.3	16.5	51.52	1.21	18.42	3.13	2.55	0.05	8.57	5.10	1.43	0.70	92.67	0.01	48	55	1881	170	16	612
5HS-9 603.20m	In	A	3.9	17.1	59.53	1.39	14.29	5.31	2.02	0.09	10.20	3.63	2.14	0.24	98.83	0.03	153	35	908	122	37	1000
7KK-1 204.80m	In	B	1.0	11.7	61.04	0.14	18.90	2.55	1.06	0.06	6.94	5.89	1.20	0.10	97.88	0.01	43	22	1073	124	2	482
7KK-1 283.40m	In	B	1.2	12.2	57.39	0.84	17.09	5.33	1.25	0.12	9.31	6.08	1.07	0.45	98.94	0.01	87	26	911	116	39	469
7KK-1 302.90m	In	C	2.3	7.2	52.90	1.04	16.36	4.56	1.55	0.10	18.80	2.66	0.87	0.18	99.02	0.03	66	17	227	80	44	599
7KK-1 315.10m	In	D	-2.6	1.6	64.42	0.42	10.43	6.50	2.23	0.23	14.66	1.62	0.22	0.14	100.86	0.01	73	5	531	150	16	145
7KK-1 391.20m	In	D	1.9	2.7	52.60	1.61	12.26	7.39	2.21	0.20	17.50	2.21	0.13	0.30	96.41	0.01	71	3	835	151	57	188
7KK-1 430.60m	In	D	-1.3	4.6	39.91	0.02	3.56	4.92	0.68	1.02	34.38	0.26	0.02	0.02	84.80	0.85	21	1	273	41	2	321
7KK-1 447.20m	In	A	-0.7	16.4	49.84	0.86	15.19	5.15	1.87	0.09	16.75	3.64	0.79	0.26	94.43	0.08	72	15	699	116	28	494
7KK-1 525.50m	In	C	-0.4	6	46.80	0.35	9.67	14.51	4.05	0.73	20.97	0.24	0.02	0.14	97.48	0.03	139	2	636	126	4	122

Abbreviations: G=group of alteration; Gn=gneiss; In=Inishi rock.
* $\delta^{18}O$ and $\delta^{13}C$ value based on average of the $\delta^{18}O$ values of limestone layer intercalating silicate rocks.
**Tatal Fe as Fe_2O_3.

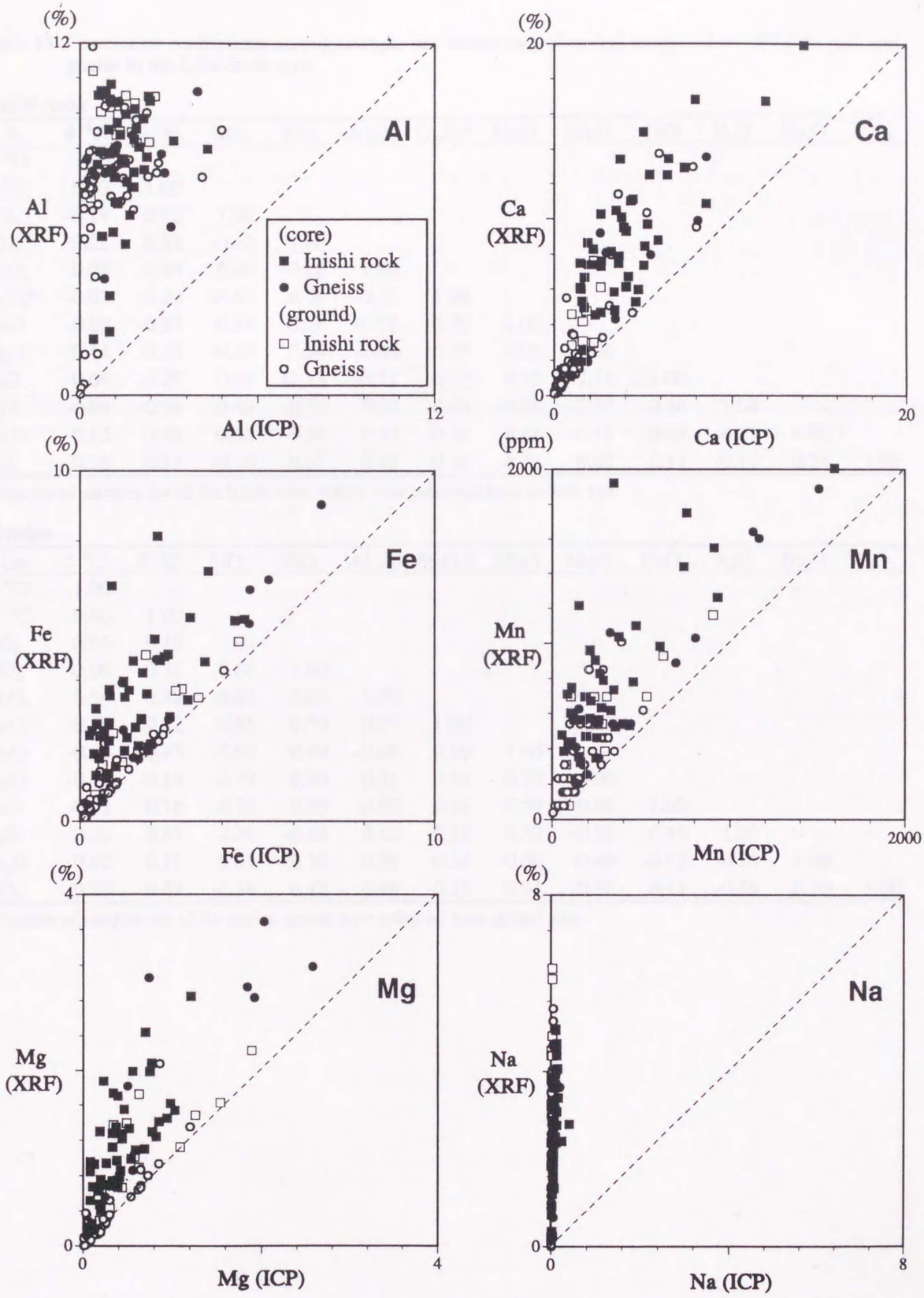

Fig. 17. Comparison of Al, Ca, Fe, Mn, Ti, and Na contents between whole rock and aqua regia leachates of Inishi rocks and gneisses in the Sako-nishi area

Table 18 Correlation coefficients among isotopic and whole rock chemical compositions of Inishi rock and gneiss in the Sako-nishi area.

Inishi rock

In	$\delta^{18}O$	$\delta^{13}C$	SiO_2	TiO_2	Al_2O_3	Fe_2O_3*	MnO	MgO	CaO	K_2O	Na_2O	P_2O_5
$\delta^{18}O$	1.00											
$\delta^{13}C$	0.59	1.00										
SiO_2	-0.19	0.12	1.00									
TiO_2	0.23	0.32	-0.12	1.00								
Al_2O_3	0.08	0.49	0.44	0.28	1.00							
Fe_2O_3*	-0.03	-0.29	-0.53	0.02	-0.55	1.00						
MnO	-0.05	-0.37	-0.56	-0.26	-0.73	0.75	1.00					
MgO	0.14	0.22	-0.28	0.34	-0.06	0.39	0.05	1.00				
CaO	0.06	-0.29	-0.69	-0.13	-0.71	0.32	0.55	0.11	1.00			
K_2O	-0.09	-0.04	0.49	-0.26	0.09	-0.40	-0.28	-0.30	-0.38	1.00		
Na_2O	0.12	0.48	0.30	0.24	0.69	-0.35	-0.44	-0.15	-0.65	-0.21	1.00	
P_2O_5	0.36	0.53	-0.10	0.61	0.42	-0.16	-0.32	0.40	-0.11	-0.14	0.24	1.00

* Number of samples are 45 for Inishi rock, which were collected from drilled core.

Gneiss

Gn	$\delta^{18}O$	$\delta^{13}C$	SiO_2	TiO_2	Al_2O_3	Fe_2O_3*	MnO	MgO	CaO	K_2O	Na_2O	P_2O_5
$\delta^{18}O$	1.00											
$\delta^{13}C$	0.60	1.00										
SiO_2	0.68	0.18	1.00									
TiO_2	-0.08	0.31	-0.68	1.00								
Al_2O_3	0.54	0.32	0.02	0.62	1.00							
Fe_2O_3*	-0.54	-0.22	-0.85	0.70	0.27	1.00						
MnO	-0.80	-0.43	-0.87	0.49	-0.06	0.90	1.00					
MgO	-0.47	-0.14	-0.79	0.70	0.21	0.94	0.79	1.00				
CaO	-0.73	-0.16	-0.76	0.25	-0.50	0.36	0.59	0.35	1.00			
K_2O	0.32	0.31	0.39	-0.34	0.10	-0.18	-0.22	-0.33	-0.41	1.00		
Na_2O	0.62	0.11	0.61	-0.10	0.38	-0.54	-0.66	-0.49	-0.63	-0.25	1.00	
P_2O_5	0.23	0.49	-0.38	0.77	0.49	0.35	0.04	0.52	0.11	-0.38	0.10	1.00

* Number of samples are 12 for gneiss, which were collected from drilled core.

Table 19 Correlation coefficients among isotopic and elemental compositions of Inishi rock and gneiss in the Sako-nishi area.

	$\delta^{18}O$	$\delta^{13}C$	Fe	Al	Mg	Mn	Ca	Na	Ba	Sr	Pb	Zn	K	P	Ti	S
$\delta^{18}O$	1.00															
$\delta^{13}C$	0.59	1.00														
Fe	-0.19	-0.32	1.00													
Al	-0.22	-0.11	0.42	1.00												
Mg	-0.23	-0.13	0.69	0.65	1.00											
Mn	-0.11	-0.35	0.68	-0.03	0.13	1.00										
Ca	-0.24	-0.27	0.24	0.00	0.05	0.56	1.00									
Na	0.34	0.47	-0.35	-0.08	-0.24	-0.30	-0.32	1.00								
Ba	0.11	-0.22	0.44	-0.10	0.12	0.41	0.04	-0.03	1.00							
Sr	-0.33	-0.35	0.36	0.05	0.22	0.42	0.79	-0.18	0.18	1.00						
Pb	-0.26	-0.16	-0.03	-0.15	-0.10	0.04	0.56	-0.11	0.14	0.73	1.00					
Zn	-0.15	-0.23	0.12	0.02	-0.04	0.15	0.03	-0.15	-0.04	0.11	0.27	1.00				
K	0.01	-0.06	0.00	0.03	0.15	-0.16	-0.24	0.09	0.46	-0.02	0.11	-0.02	1.00			
P	0.32	0.52	-0.10	0.17	0.15	-0.29	-0.24	0.43	-0.20	-0.15	-0.20	-0.09	-0.02	1.00		
Ti	0.32	0.48	-0.20	0.03	-0.05	-0.33	-0.33	0.47	-0.36	-0.32	-0.29	-0.17	-0.32	0.51	1.00	
S	-0.17	-0.25	0.15	0.02	-0.03	0.20	0.10	-0.17	-0.05	0.15	0.28	0.99	-0.04	-0.08	-0.18	1.00

* Number of samples are 45 for Inishi rock and 12 for gneiss, which were collected from drilled core.

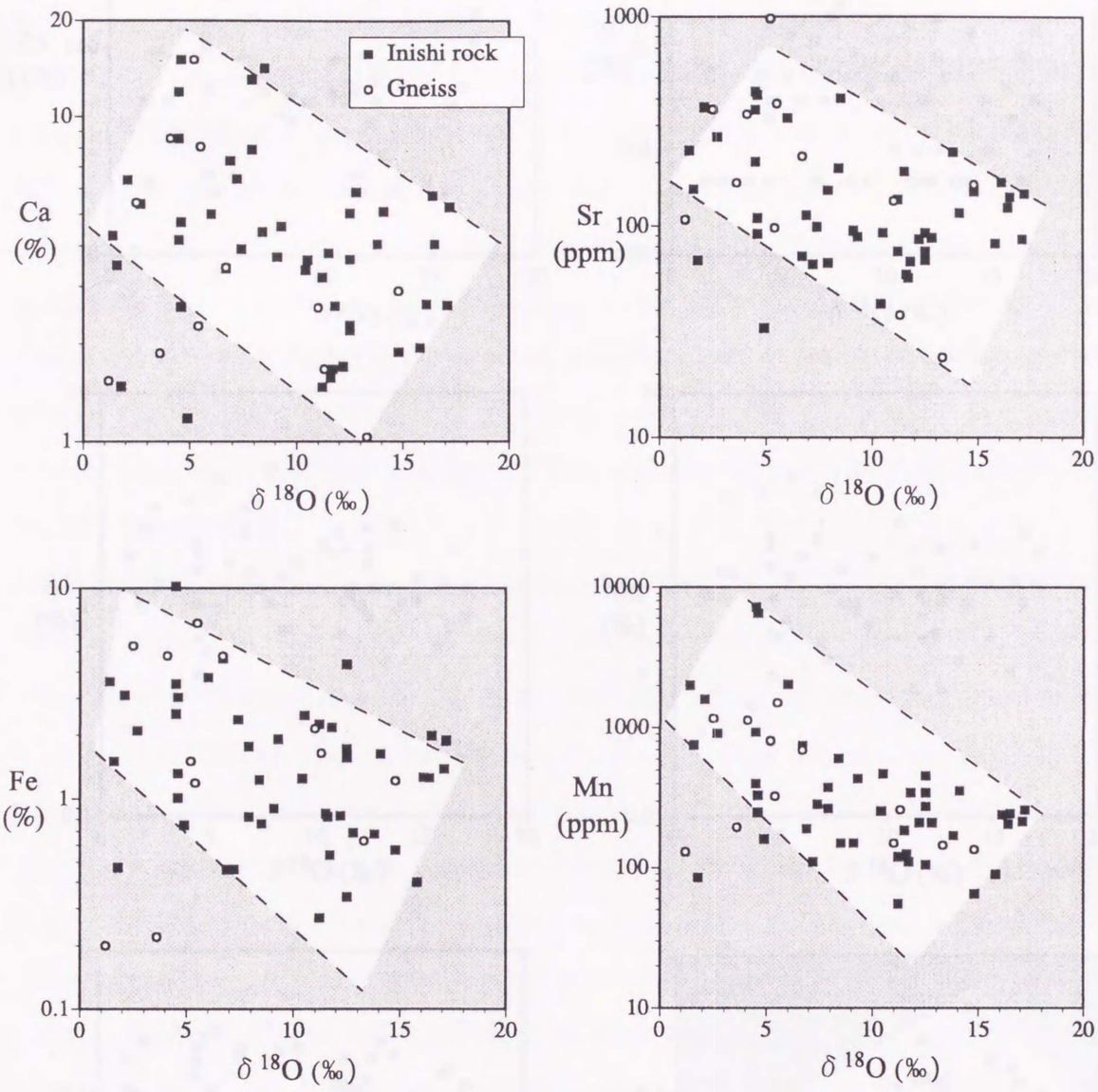

Fig. 18. Scatter plots of Ca, Sr, Fe, and Mn against $\delta^{18}O$ for Inishi rocks and gneisses from the Sako-nishi area.

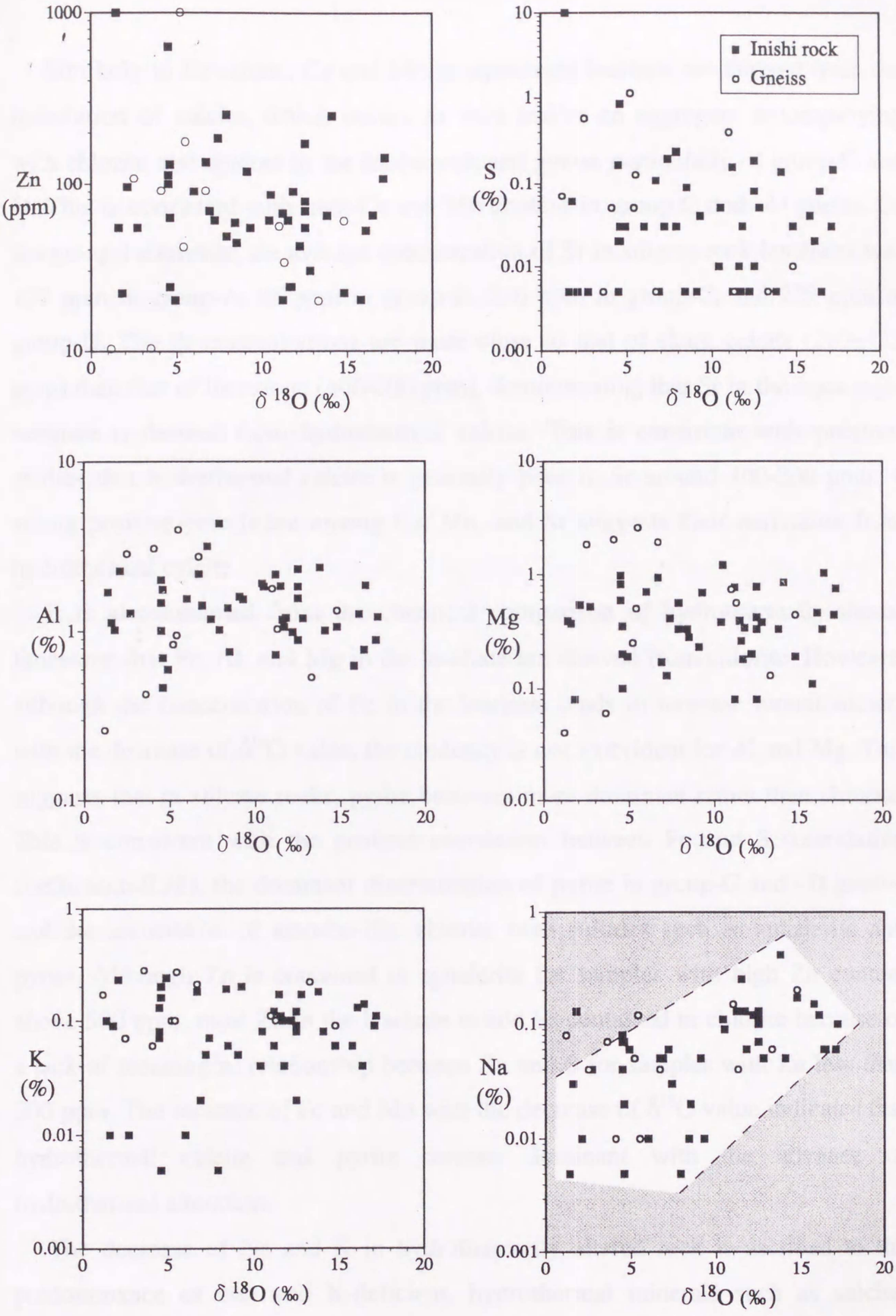

Fig. 19. Scatter plots of Zn, S, Al, Mg, K, and Na against $\delta^{18}O$ for Inishi rocks and gneisses from the Sako-nishi area.

Similarly to limestone, Ca and Mn in aqua-regia leachate are derived from the dissolution of calcite, which occurs as vein and/or an aggregate accompanying with chlorite and epidote in the Inishi-rock and gneiss particularly of group-C and D. This is consistent with high Ca and Mn content in group-C and –D gneiss. Of the group-I elements, the average concentration of Sr in silicate-rock leachates was 122 ppm in group-A, 96 ppm in group-B, 236 ppm in group-C, and 229 ppm in group-D. The Sr concentrations are more close to that of skarn calcite (269±113 ppm) than that of limestone (400-600 ppm), demonstrating that Sr in the aqua-regia leachate is derived from hydrothermal calcite. This is consistent with previous studies that hydrothermal calcite is generally poor in Sr around 100-200 ppm. A strong positive correlation among Ca, Mn, and Sr suggests their derivation from hydrothermal calcite.

It is also assumed from the chemical comparison of hydrothermally-altered limestone that Fe, Al, and Mg in the leachate are derived from chlorite. However, although the concentration of Fe in the leachate tends to increase monotonically with the decrease of $\delta^{18}O$ value, the tendency is not so evident for Al and Mg. This suggests that in silicate rocks, pyrite becomes more dominant rather than chlorite. This is consistent with the positive correlation between Fe and S (correlation coefficient=0.38), the dominant dissemination of pyrite in group-C and –D gneiss, and the association of amoeba-like chlorite with sulfides such as sphalerite and pyrite. Although Zn is contained in sphalerite for samples with high Zn content above 500 ppm, most Zn in the leachate would be contained in chlorite because of a lack of meaningful relationship between Zn and S for samples with Zn less than 500 ppm. The increase of Fe and Mn with the decrease of $\delta^{18}O$ value indicates that hydrothermal calcite and pyrite become dominant with the advance of hydrothermal alteration.

The decrease of Na and K in hydrothermally altered rock is ascribed to the predominance of Na- and K-deficient, hydrothermal minerals such as calcite, chlorite, pyrite, quartz, epidote, and prehnite.

4.7.2. Potential indicator for the determination of hydrothermally altered silicate rock

Although the ICP-OES method has an advantage over the isotope method owing to its rapidity and convenience of analysis, but has a disadvantage due to its sensitivity to the chemical heterogeneity of the original rock. Further there is no element which can separate group-A silicate rock from group-D one mainly due to the wide variation of elemental concentrations. I expect that elemental ratios will be more effective for the identification of altered rock than are the concentration data. Several relationships between the ratios of group-I elements to group-II or -III ones are plotted against $\delta^{18}O$ value (Fig. 20). The Al/Mg and Mn/Sr ratios were useful for classifying limestone but not for the silicate rocks. The low effectiveness of Al/Mg seems to result from that chloritization in the silicate rocks is not so intense compared to that in limestone. In contrast, the relative constant of Mn/Sr ratio is due to that the two elements in the silicate rock leachate are derived only from the hydrothermal calcite while there is a large difference in Mn/Sr ratio between the hydrothermal calcite and limestone calcite. In contrast, the group-A silicate rock is separated clearly from the group-D one by using Ca/Na and Ca/K ratios; in particular, the two rocks are separated by Ca/Na ratio of 100 (Fig. 21). Likewise, Mn/Mg and Fe/Al ratios seem effective for the classification of hydrothermally-altered silicate rocks.

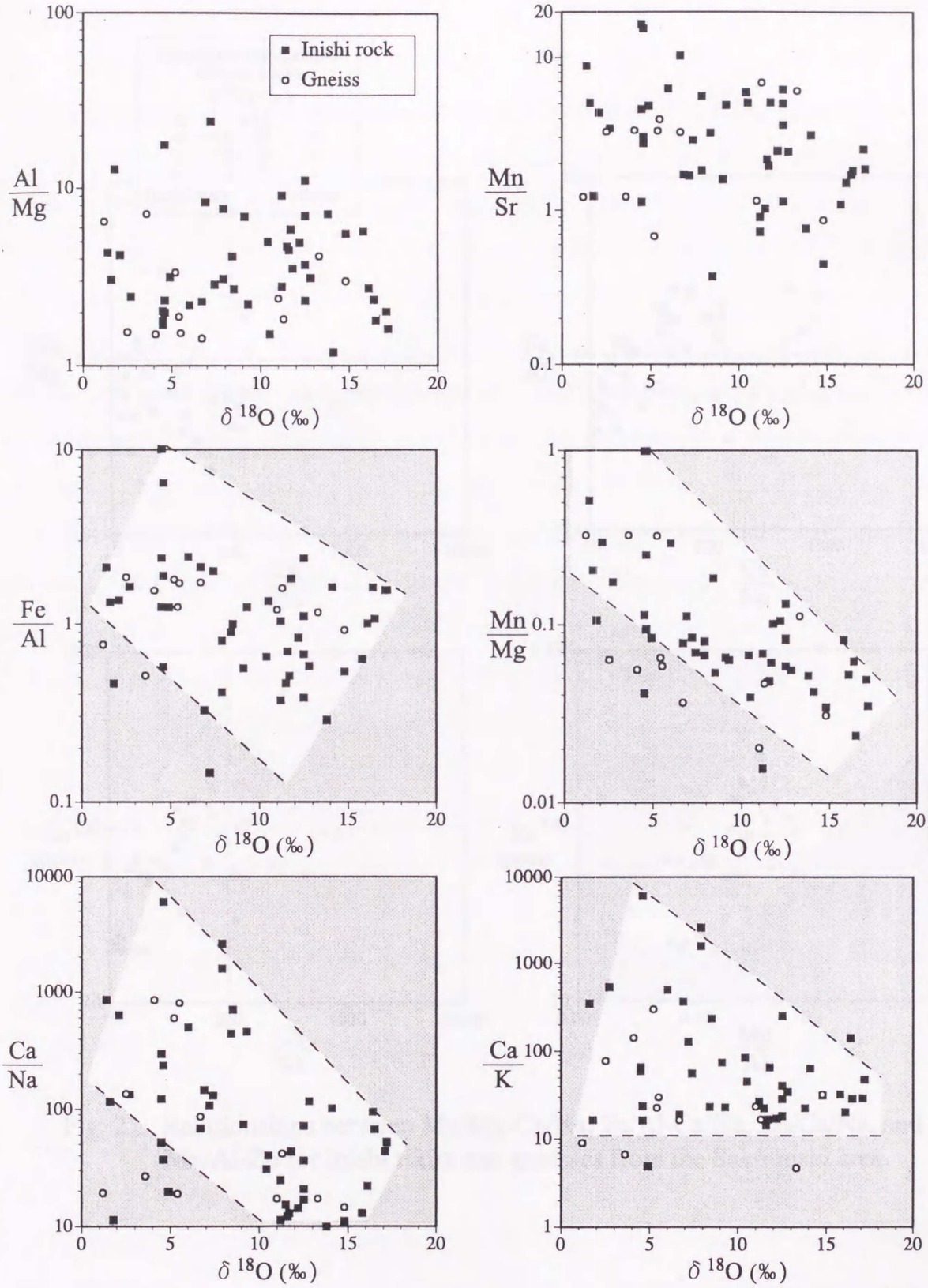

Fig. 20. Scatter plots of Al/Mg, Mn/Sr, Fe/Al, Mn/Mg, Ca/Na, and Ca/K against $\delta^{18}O$ for Inishi rocks and gneisses from the Sako-nishi area.

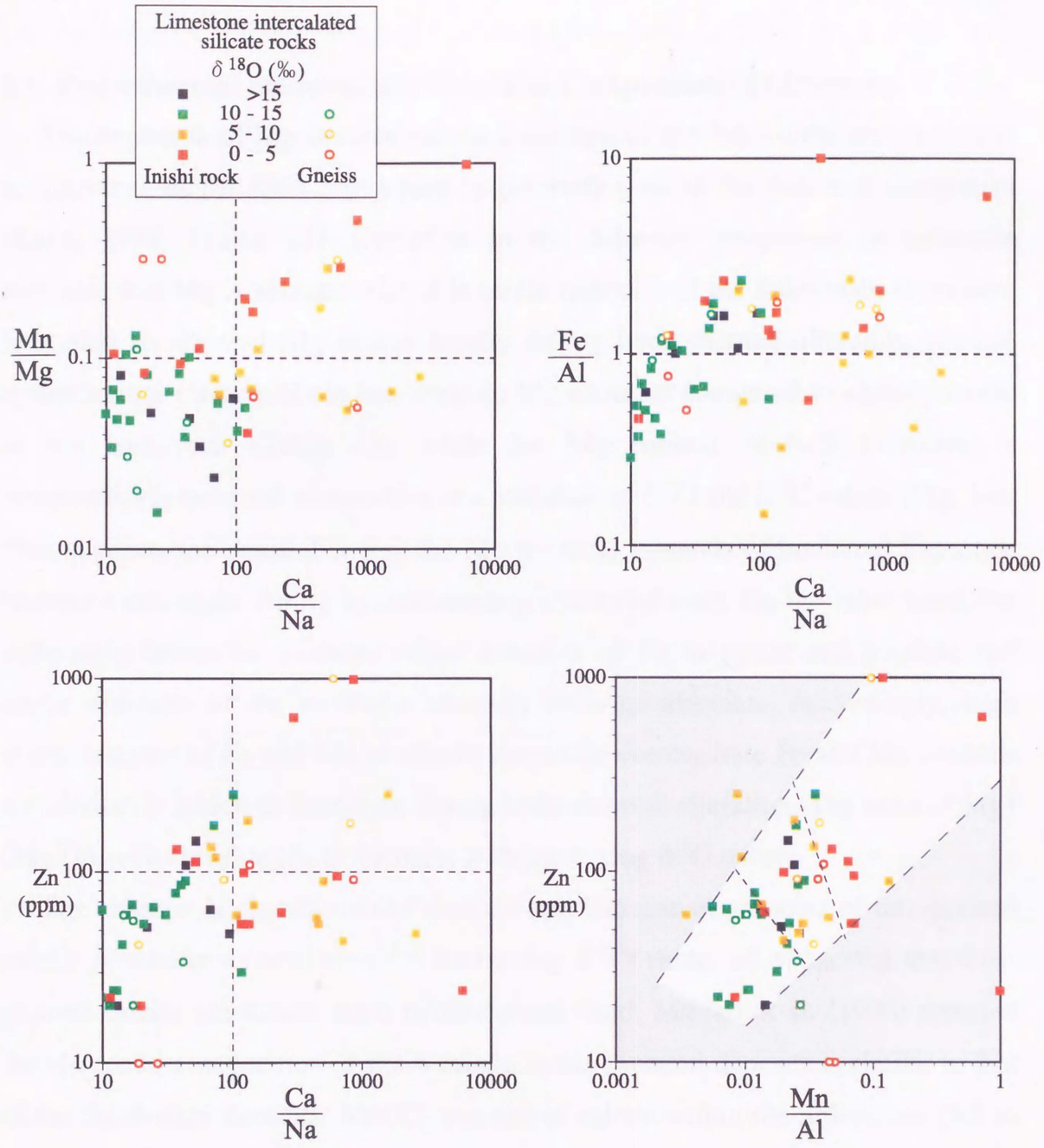

Fig. 21. Relationships between Mn/Mg-Ca/Na, Fe/Al-Ca/Na, Zn-Ca/Na, and Mn/Al-Zn for Inishi rocks and gneisses from the Sako-nishi area.

Chapter 5 DISCUSSION

5.1. Hydrothermal Minerals and Chemical Composition of Limestone

The depletion of Mg in carbonate in limestone of the Sako-nishi area is similar to limestone of the Hida area which is generally poor in the dolomite component (Kano, 1998) (Table 12). Depletion in the dolomite component in carbonate indicates that Mg is accommodated in mafic minerals of the Sako-nishi limestone. It is also shown that Mg moves locally during hydrothermal alteration because hydrothermal Ca-amphibole has variable Mg contents compared to clinopyroxene in the host rock (Table 13), while the Mg content of bulk limestone is comparatively constant irrespective of a variation of $\delta^{18}O$ and $\delta^{13}C$ values (Fig. 14). This suggests the possibility that the Mg in mafic minerals of unaltered limestone became fixed again during hydrothermally altered process. On the other hand, the Sako-nishi limestone contains minor amounts of Fe in pyrite and goethite and major amounts of Fe in mafic minerals such as chlorites. Accordingly, high concentrations of Fe and Mn in altered limestone demonstrate Fe and Mn contents are obviously added to limestone during hydrothermal alteration. The ratio of Mg* (Mg/(Mg+Fe+Mn)) tends to decrease with increasing $\delta^{18}O$ value.

The absence of significant deformation and increase of amounts of fine-grained calcite occurring as veinlets with decreasing $\delta^{18}O$ value, all suggested that fine-grained calcite precipitate from hydrothermal fluid. Mariko et al. (1996) reported the elemental composition of skarn calcite in the Mozumi deposits is similar to that of the Sako-nishi deposits. $MnCO_3$ content of calcite within the Shiroji ore (6.5 to 11.5 mol.%) is extraordinarily high compared to that within the Mokuji ore (0.5 to 4.5 mol.%). $MnCO_3$ content of skarn calcite in the Mozumi and Tochibora deposits (1.0 to 7.1) is enriched compared to the limestone of group-D. The Mn to Fe ratio in hydrothermal chlorite is low compared to the ratio in hydrothermal calcite (Tables 12 and 13). This could reflect Mn and Fe contents derived mainly from chemical composition of calcite and chlorite in limestone, respectively. It is supposed that the low Mn to Fe ratio in chlorite was controlled by a chemical

distribution in which chlorites were enriched through Fe fractionation rather than Mn fractionation relative to calcite (Iiyama and Tamura. 1981). It is interpreted that the positive Mn-Fe correlation within the Sako-nishi limestone (Fig. 15) may have been caused largely by the presence of hydrothermal chlorite and calcite which increased with the advance of alteration. Furthermore, the altered limestone (group-C and -D limestone) plots in a region of high concentrations of Fe and Mn (Fig. 15). This correlates with the observed hydrothermal alteration mineral assemblage in limestone. Mn and Sr are mainly distributed in calcite. The average concentration of Sr in limestone of group-A is 559 ± 201 ppm.

In contrast, the average concentration of Sr in skarn calcite is 269 ± 113 ppm, less significant than that in limestone. Barbieri et al. (1984) reported that the concentration of Sr in hydrothermal calcite is in general low, around 200 ppm. Skarn calcite is enriched in Mn and depleted in Sr compared to limestone (Table 4) resulting in a high Mn/Sr ratio for the hydrothermal calcite. Accordingly, I attribute the tendency for Sr depletion to correspond to increasing $\delta^{18}O$ values in the Sako-nishi limestone to the presence of hydrothermal calcite. In addition to the concentration of Sr and Mn continuously change with isotopic shift of limestone (Fig. 15). Consequently, this tendency suggests that the fluid that participated in the hydrothermal alteration of the limestone was originally the same as fluid responsible for skarnization-mineralization. The high concentrations of Fe, Mn Al, and Zn in the HCl-leachate of altered limestone demonstrate that these elements were obviously added to the limestone during hydrothermal alteration. As a result, the ratio of Mg* in the HCl-leachate of limestone tends to decrease (Fig. 16C), while the Al/Mg and Mn/Sr ratios tend to increase (Fig. 16A,B), with decreasing $\delta^{18}O$ values due to the increasing amounts of Fe and Al derived from chlorite and those of Mn from calcite.

5.2. Geochemical Mapping of Limestone

The distribution of the $\delta^{18}O$ value of carbonates in the Sako-nishi outcropping rocks is shown in Figure 22A. It is seen that the $\delta^{18}O$ value tends to be low within

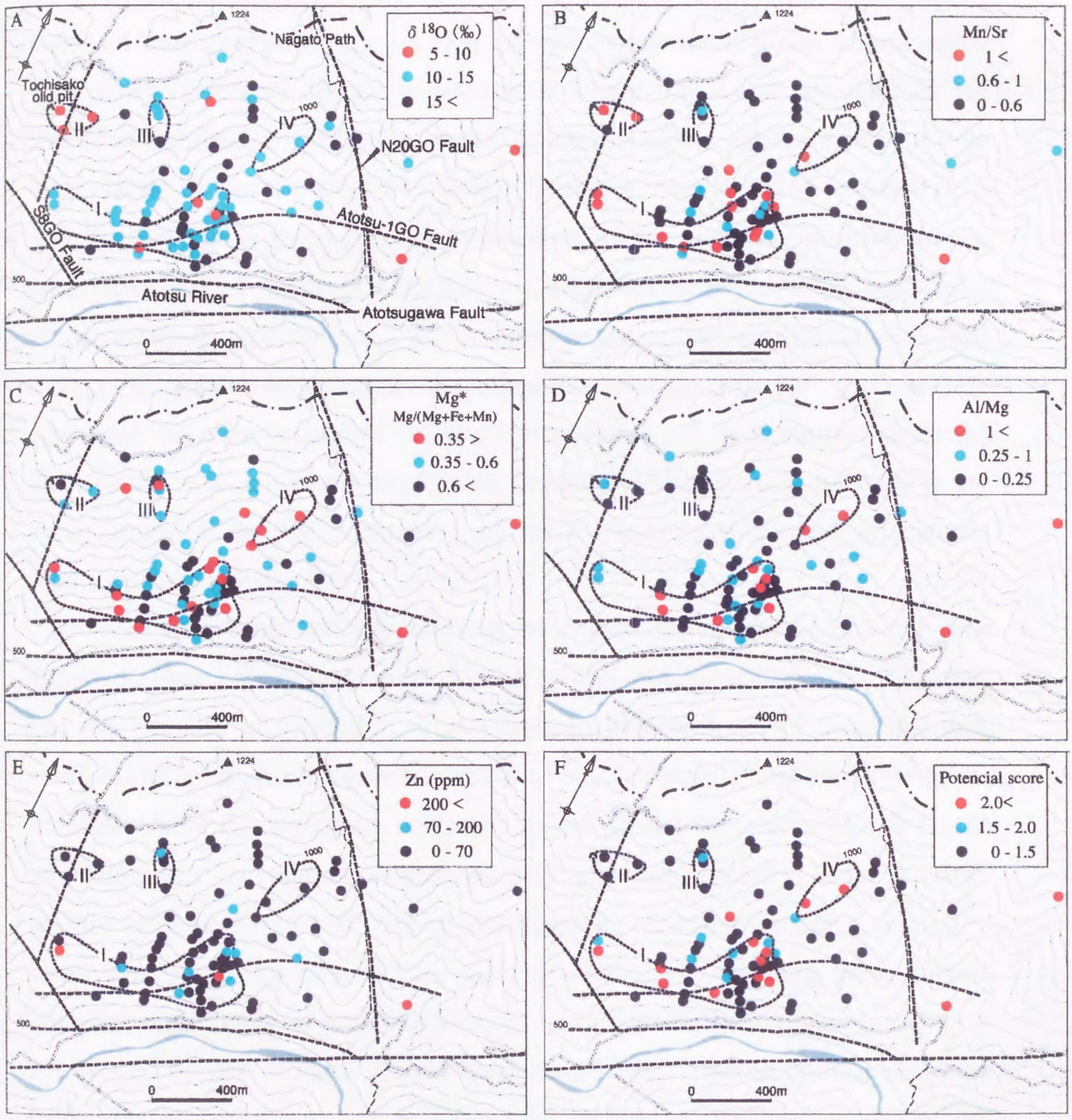

Fig. 22. Map of $\delta^{18}O$, Al/Mg, Mn/Sr, Mg*, Zn content, and PS (potential score: see text) of limestones and silicate rocks in the Sako-nishi area.

the mineralized zone (Fig. 22A). However, it is also recognized that some limestone with low $\delta^{18}O$ values was barren. This result shows that the oxygen isotopic composition in the outcropping carbonate does not always correspond to the hydrothermal alteration zones because the isotopic composition of carbonates does not only depend on the oxygen isotopic composition of the hydrothermal fluid alone, but also on the water/rock ratio and on the temperature of the hydrothermal fluid. In particular, the oxidation of pyrite to goethite indicates the involvement of surface-water with low $\delta^{18}O$ values. As a result of the interaction with surface-water, the outcropping limestone in the non-mineralized area may have variable $\delta^{18}O$ values. It is notable, however, that the Mg*, Al/Mg, and Mn/Sr ratios and the Zn content in the HCl-leachate of limestones and silicate rocks tend to show anomalous values within the mineralization zone (Fig. 22B, C, D, and E). An index of these elements reflects the presence of hydrothermal minerals, because the variation in the Mg* value and Zn content of mafic minerals is not conspicuous during the weathering of mafic minerals to secondary minerals (Nakano et al., 1991)..

In order to reliably identify mineralized zones, the weight of potential was determined using the ratios of Mg*, Mn/Sr, Al/Mg, and Zn content, and $\delta^{18}O$ value. For this purpose of weighting, it was assumed that each set of analytical data consisted of a complex population and that the elements in unaltered crystalline limestone were homogeneous compared to the altered limestone. The threshold was determined by splitting the data into more than one population units. The steps in this construction are as follows: (1) plotting of the cumulative frequency distribution curves for each element analysis value, (2) by replacing the arithmetic ordinate scale with a probability scale, the cumulative frequency curve is represented by one or more straight lines, and (3) the threshold of each analytical value for the population unit is determined by reading the intersections of the distribution lines directly from a probability plot (Lepeltier, 1969; Otsu et al., 1984). Using the above method, each element-analysis data set was partitioned into six population units for Mg* and Mn/Sr and four population units for Al/Mg

and Zn content, and then each unit was substituted for a point in ascending order from 0 to 1 at 0.2 intervals (Table 20). The potential score (termed PS hereafter) of the limestone is the total number of points for each data. The distribution map of PS is given in Figure 22F.

Among the four zones, only zones I and IV had high scores (Fig. 22F). Although zones II and III showed an excess relative to the background $\delta^{18}O$ value (Fig.22A), PS mapping indicates that they are not potentially mineralized. This is consistent with that concealed ore bodies have not been identified in the two zones during past exploration. The mineralized zone I with high PS score is distributed along the Atotsu-1GO fault. This is consistent with indications from mapping of the isotopic zonation of wall rocks owing to hydrothermal activity (Naito et al., 1995). High PS score in zone IV suggests the presence of promising mineralized zone in the underground. This result is consistent with the widespread occurrence of hydrothermal minerals in the Inishi rock and gneiss in this zone. The elemental ratios of the altered limestone zones indicate not only the existence of an area of hydrothermal activity related to mineralization, but also indicate directly the presence of hydrothermal minerals such as chlorite and calcite. This elementary scaling method yields better results than the isotopic zonation mapping.

5.3. Hydrothermal Alteration Accompanied with Chlorite

Chlorite is a common mineral in low-grade metamorphic rocks and hydrothermal deposit, and many as such numerous studies have documented the characteristics and habit of this mineral. Figure 10 shows the relationship between the ratio of Fe# value (Fe/(Fe+Mg)), and the tetrahedral site of Al value of chlorite in limestone in the Sako-nishi area, compared with chlorite of hydrothermal deposits. The Fe# value of chlorite from Kuroko deposits and epithermal gold-silver deposits is low, however that of polymetallic vein deposits is high (Shikazono and Kawahata, 1987; Nagasawa et al., 1976). On the other hand, the Fe# value of chlorite from epithermal Pb-Zn vein deposits has an intermediate range compared with other deposits (Nagasawa et al, 1976). It is therefore evident

Table 20 Threshold values (score points from 0 to 1 at 0.2 interval) of Mg*, Mn/Sr, Al/Mg, and Zn in limestones from the Sako-nishi area.

Point	Mg*	Mn/Sr	Al/Mg	Zn
0	> 0.75	< 0.2	< 0.35	< 40
0.2	0.6 - 0.7	0.2 - 0.4	0.35 - 0.60	40 - 70
0.4	0.5 - 0.6	0.4 - 0.55	0.60 - 1.2	70 - 200
0.6	0.4 - 0.5	0.55 - 0.85	> 1.2	> 200
0.8	0.3 - 0.4	0.85 - 1.5		
1.0	< 0.3	> 1.5		

that the chemical composition of hydrothermal chlorite has a wide compositional range. The Fe# value of chlorite from the Kamioka deposits is high, similar to that of polymetallic vein deposits. It is known that in vein type deposits, the Fe# value of chlorite from hydrothermally altered rock (0.3-0.5) is low, the same as that of primary mafic minerals, but that from hydrothermal veins (0.3-0.7) is relatively high (Shikazono and Kawahata, 1987). In the propylitic alteration zone of Toyoha (Sawai, 1984, 1986) and Hosokura (Takahashi, 1988) vein type deposits, the Fe# value of chlorite increases as the center of the alteration zone is approached. The Fe# value of chlorite from the Sako-nishi limestone does not vary with decreasing oxygen and carbon isotopic composition, but is distinctly low compared to that from skarn deposits. This tendency is similar to the relationship of chlorite between hydrothermally altered rocks and hydrothermal veins.

It is reported by Yoneda (1989) that the MnO content of chlorite from vein-type deposits in Japan has a wide ranges from 1.1 wt% to 17.5 wt% (Fig. 10A). The MnO content of chlorite from the Kamioka deposits ranges from 0 wt% to 1.0 wt%, which is similar to the variation observed in the Toyoha Zn-Pb-Ag deposit (Sawai, 1984, 1986, 1988). In addition, the relationship between Mn and Fe of chlorite from the Kamioka deposits is also recognized in that of chlorite from the Toyoha deposits (Sawai, 1986). On this basis, the relationship in the chemical composition of chlorite between skarn ore bodies and the Sako-nishi limestone bears a close resemblance to vein type deposits. This indicates that hydrothermal alteration of limestone can be attributed to hydrothermal fluids having common condition to vein type deposits such as the Toyoha deposits.

Generally, chlorite is found as a retrograde alteration mineral in skarn deposits, and is a particularly abundant and widespread product of alteration in Zn-Pb type skarn deposits (e.g., Einaudi et al., 1981). In the Kamioka deposits, the Shiroji ore (containing calcite-quartz) formed during the later retrogressive stage compared to the Mokuji ore (containing hedenbergitic clinopyroxene) based on evidence from the filling temperature of fluid inclusions and mode of occurrence (Mariko et al., 1996). According to Takeno and Iiyama (1983), in the Tochibora and Maruyama

deposits, clinopyroxene skarn and Inishi rocks have been altered to assemblages containing actinolite, and hastingsite or chlorite, respectively, associated with granitic porphyry magmatizm. In the Mozumi deposits, large amounts of chlorite and sericite occur (Nagasawa and Shibata, 1986). The formation of actinolite and chlorite in the Mozumi deposits corresponds to the Shiroji ore stage (Mariko et al., 1996). It is reported that disseminated Pb-Zn type deposit exhibiting fissure control and containing epidote and chlorite is found in the Sako-nishi area and Atotsu area in the western area of the Sako-nishi and Mozumi deposits. (Sakurai et al., 1993; Hirokawa et al., 1995). The formation temperature of disseminated Pb-Zn type ore vary from 100 to 200 ℃ and are lower than that of the Mokuji ore. It is therefore suggested that silicate minerals which were rich in iron, such as actinolite, hastingsite, and chlorite in the Kamioka ore deposits, were formed together with calcite which is rich in Mn in the Shiroji ore during almost the same stage. It is considered that hydrothermal alteration of limestone can be attributed to series of hydrothermal fluids which were also responsible for mineralization of the Mokuji and Shiroji ores, and were rich in Fe and Mn.

Study concerning the fractionation of Fe, Mg and Mn between chlorite and hydrothermal fluid is important to estimate the nature and physical and chemical environment of the hydrothermal fluids which participated in chlorite formation. Temperature is the most important factor influencing chlorite composition. Theoretical prediction using solid solution models (Sverjensky, 1985; Walshe, 1986) and thermometry utilized tetrahedral site of aluminum which was demonstrated from the relationship between filling temperature data and chemical composition of chlorite in geothermal system (Cathelineau and Nieva, 1985) has been advocated.

Figure 23 shows plot of the Kamioka chlorite data in two thermometers. Temperature of formation for chlorite in limestone is 50 ℃ lower than that in skarn, however having error among thermometers. The alteration zone within limestone, formed during a retrogressive of stage, is therefore considered to have developed at a lower temperature comparison than that of the skarn. Thermodynamic data of

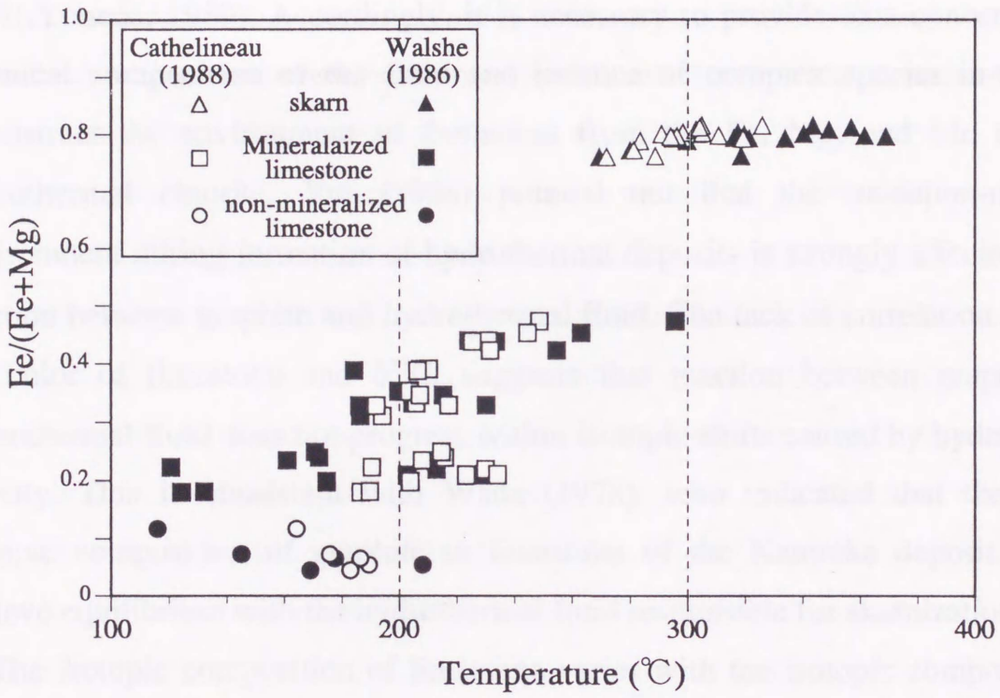

Fig. 23. Plot of chlorite composition in the Sako-nishi limestone on two chlorite geothermometers by Walshe (1986) and Cathelineau (1988).

Sverjensky (1985) shows the Fe/Mn ratio of chlorite is dependent on temperature. Bottrell and Yardley (1991) reported that this relationship applies in the oxidizing environment, but not in the reducing environment from an examination of chlorite from low grade metamorphic rocks. If Fe and Mg in chlorite is assumed to be in equilibrium with a fluid phase and pyrite, the exchange of Fe^{2+}, Mg^{2+}, and Mn^{2+} between chlorite and the hydrothermal fluid may be related to factors such as pH, oxygen fugacity, temperature, and total dissolved sulfur (Shikazono and Kawahata, 1987; Yoneda, 1989). Accordingly, it is necessary to provide data concerning the chemical composition of the fluid and balance of complex species in order to reconstruct the environment of formation from the Fe, Mg, and Mn ratios of hydrothermal chlorite. Yui (1968) pointed out that the oxidation-reduction environment during formation of hydrothermal deposits is strongly affected by the reaction between graphite and hydrothermal fluid. The lack of correlation between the color of limestone and $\delta^{13}C$, suggests that reaction between graphite and hydrothermal fluid does not progress within isotopic shifts caused by hydrothermal activity. This is consistent with Wada (1978), who indicated that the carbon isotopic composition of graphite in limestone of the Kamioka deposit did not achieve equilibrium with the hydrothermal fluid responsible for skarnization.

The isotopic composition of limestone varies with the isotopic composition of the hydrothermal fluid, temperature, and water/rock ratio. No systematic correlation exists between the estimated temperature from chlorite thermometry and oxygen isotopic composition of limestone. This may suggest that the oxygen isotopic composition and water/rock ratio of hydrothermal fluid varied during alteration. Information on temperature, fluid composition which is estimated from the chemical composition of chlorite coexisting with carbonate minerals and the fluid inclusion data, all may provide further strong constraints on the isotopic shifts in carbonate rocks.

5.4. Application to Exploration for Zn-Pb Hydrothermal Deposit

Zn type skarn deposits which contain mainly Zn-Pb-Ag ore is characterized by

their distinctive manganese-rich mineralogy which can be correlated with prograde clinopyroxene and retrograde chlorite and calcite (Einaudi et al., 1981). This tendency has been further clarified by Meinert (1992). Nakano (1998) demonstrated that skarn deposits in Japan are classified into Zn-Pb and Cu-Fe types. It is pointed out that the Zn-Pb type of Nakano (1998) contains clinopyroxene and sphalerite with high Mn/Fe ratio and resembled the Zn type of Einaudi et al (1981). The Zn-Pb type skarn deposit of Nakano (1998) exhibits characteristic Mn-rich carbonate and silicate, respectively including kutnahorite (Hoei mine, Miyahisa et al., 1975) and rhodochrosite (Nakatatsu mine, Shimizu and Iiyama, 1982; Nakamura and Shimazaki, 1987; Chichibu mine, Miyazawa, 1958), and epidote (Nakatenjo area in the Nakatatsu mining district, Nakamura and Shimazaki, 1987). Amounts of high Mn carbonates increase commonly away from a center of skarn and ore body, and in the retrograde stage. Shiroji ore occurs near the limestone contact. The Mn content in hydrothermal calcite of limestone tends to increase with in a relatively altered limestone, such as group-D, occurring near the skarn zone associated with hydrothermal alteration. The chemical variation in the Sako-nishi hydrothermally-altered limestone (Figs. 3 and 14) is different from those of carbonates related to diagenesis and other hydrothermal alteration. During diagenesis, carbonates tend to become enriched in Sr and Mg and depleted in Fe (Brand and Veizer, 1980). According to Bellanca et al. (1984), the characteristic of mineralized limestone of fluorite and barite in northwestern Sicily become enriched in Sr and Fe, and depleted in Mg. The elemental variation of the Sako-nishi limestone is regarded as typical among Zn-Pb type skarn deposits (Figs 3, 9 and 10).

A mineral assemblage of chlorite-carbonate-quartz-pyrite, which is often observed in limestone of group-C and -D, is an assemblage which characterizes chloritization. The hydrothermal alteration of limestone except lack of an assemblage of zeolite-albite-K-feldspar is closely similar to propylitic alteration and mineralization overlapped propylitic alteration. When the original rock is a silicate rock in the Kamioka mine, the alteration zone associated with disseminated

Zn-Pb-Ag mineralization is also characterized by a mineral assemblage typical of propylitic alteration (Machida et al., 1987; Sakurai et al., 1993; Hirokawa et al., 1995). In the Nakatatsu mine, a Zn-Pb skarn deposit the same as Kamioka, a similar alteration mineral assemblage is reported where the original rock was a volcanic rock of basaltic to andesitic composition (Nishikawa and Tochimoto, 1985). In the Kamioka skarn deposit, most of the original rock is limestone, not containing silicates such as plagioclase. This suggests that the lack of silicate minerals in limestone results in a difference in the mineral assemblage from a typically propylitic alteration assemblage which characterizes igneous rocks such as andesites and dacites. Propylitic alteration is characterized by conspicuous depletion and addition, respectively of Ca and K content without removal of Mg, however variation of Ca and K is not found in the Sako-nishi limestone. This is consistent with the analysis of silicate rocks.

On the contrary, chlorite and carbonate minerals are universally produced in not only skarn deposits but also hydrothermal deposits and peripheral hydrothermally altered rock. In particular, chlorite and carbonate minerals enriched in Fe and Mn are dominant in and around base metal deposit. Accordingly, Al, Fe, and Mn contents and the Mg* value of hydrothermal minerals such as chlorite and carbonate minerals may be indicative of the proximity to hydrothermal mineralization. Hydrochloric acid selectively dissolves chlorite and calcite. It is likely that the leaching method studied herein using hydrochloric acid and a combination of hydrochloric acid and acetic acid provides an application useful in the detection of geochemical anomalies around hydrothermal deposits.

Chapter 6 CONCLUSIONS

Detailed investigations on the mineralogy, petrography, and geochemistry on the limestone and intercalated silicate rocks in the Sako-nishi area of the Kamioka Zn-Pb-Ag mine, central Japan, yielded the following results:

1. The $\delta^{18}O$ and $\delta^{13}C$ values of the Sako-nishi limestone ranged widely between -2.5 and +21.1‰ and between -5.9 and +5.3‰, respectively, due to interaction with hydrothermal fluids with a dominant meteoric water component. It was classified into four groups as A, B, C, and D in 5‰ interval by oxygen isotopic composition.
2. With a decrease of $\delta^{18}O$ value, the amount of hydrothermal calcite increased. The calcite is transparent under the microscope and occurs as fine-grained and veinlets calcite increased. It is enriched in Mn, depleted in Sr, and has bright cathodoluminescence image.
3. Clinopyroxene of original limestone altered into actinolite within weakly altered zone, while it is altered into chlorite within strongly altered zone. The hydrothermal chlorite becomes dominant in altered limestone whose $\delta^{18}O$ value is less than 10‰. It is enriched in Fe and contains small amounts of Mn compared to mafic minerals within unaltered limestone.
4. Calcite and chlorite in skarn deposits is highly enriched in Mn and Fe. Skarn calcite showing a bright luminescence image contains Mn of 2 wt.% or greater and is also characterized by low Sr content (300 ± 100 ppm). Chlorite geothermometer yielded the formation temperatures of about 200-250 ℃, which is compatible with the homogenization temperature of fluid inclusion and is lower than the formation temperature of skarn clinopyroxene around 300-350 ℃.
5. The occurrence and chemical composition of hydrothermal minerals in the limestone, skarn, and ore indicate that the ^{18}O-depleted zones were formed in the later stage from fluids, which were responsible for mineralization and

skarnization, and for Fe and Mn enrichment.

6. Dissolution experiments on limestone showed that acetic acid can dissolve carbonate while hydrochloric acid and aqua-regia acid can dissolve the carbonate and chlorite selectively.
7. As the $\delta^{18}O$ value decreases, the concentrations of Al, Mn, Fe, and Zn in hydrochloric and aqua-regia acid leachate increase, while only slight changes are observed in Mg and Sr, owing to the dissolution of hydrothermal chlorite and calcite. The Al content (~ 0.1%), Mn content (~ 300ppm), Fe content (~ 0.3%), Fe/Mg ratio (~ 2.0) and Al/Mg ratio (~ 1.0) of the acid leachate are effective for identifying altered limestone in the Sako-nishi area.
8. Four mineralization zones are known in the outcrop of the Sako-nishi area. Although these zones do not always correspond to the $\delta^{18}O$-depleted value possibly due to weathering or isotope fractionation at low temperature, hydrochloric acid leachate of limestone from these areas has a high Mn/Sr ratio and low Mg value.
9. An index which combines elemental composition with stable isotopic composition was introduced. This index proved to be effective for specification of mineralization, because it was clearly anomalous along the 7-GOHI fault and the Atotsu-1GO faults, which are thought to have played a major role in facilitating the passage of hydrothermal fluid responsible for mineralization. This structure indicates that the skarn deposits of the Sako-nishi area belong to Mozumi-type Zn-Pb skarn deposits.
10. It is suggested that isotope alteration zones are produced by rapid precipitation of fine-grained calcite from the hydrothermal fluid in the minute cracks which developed in limestone, and isotope exchange reaction between limestone and Mn-Fe rich hydrothermal fluid which developed during the latter stages of skarnization.
11. Inishi-rock and gneiss are subjected to hydrothermal alteration whose mineral assemblage is similar to the altered limestone. The concentrations of Ca, Sr, and Mn of aqua-regia leachates of these silicate rocks increase systematically

with the decrease of $\delta^{18}O$ value of associated limestone, due to the presence of hydrothermal calcite and pyrite. The Al/Mg and Mn/Sr ratios were effective for the separation of hydrothermally-altered silicate rocks from unaltered ones.

12. Mineral assemblages observed in altered rock of the Sako-nishi area closely resemble chloritic and propylitic alteration hosted by silicate rocks recognized in Zn-Pb type vein deposits. Analysis of acetic acid and hydrochloric or aqua-regia acid leachate in addition to cathodoluminescence image provides an effective tool for identifying hydrothermally altered rock of Zn-Pb type deposits including skarn type because it makes possible the detection of the elemental composition of hydrothermal minerals such as chlorite and carbonate and because of the rapidity and convenience of analysis.

ACKNOWLEDGEMENTS

I would like to express my gratitude to Professors Y.Kajiwara, and T. Miyano, Assoc. Prof. T. Nakano, and Asst. Prof. K. Komuro of Institute of Geoscience, the University of Tsukuba. I am very grateful to the following for assistance of various kinds: T. Sakasegawa, K. Nakayama, and Dr. C. A. Feebrey of Metal Mining Agency of Japan. Dr. K. Yokoyama has been of great help in providing EDX technical assistance. I thank Dr. A. Kano of University of Hiroshima for using cathodoluminescence equipment, and Dr. T. Yoneda of University of Hokkaido for useful suggestions with respect to chlorite geochemistry. Thanks are due to Mrs. Y Takeuchi for assistance of analysis by ICP.

Special thanks to Mr. M. Yamanaka, Mr. Y. Horikawa, Dr. Y. Yokoo, Dr. S. R. Jeon, and colleagues in our laboratory of Institute of Geoscience, the University of Tsukuba for giving me continuous encouragement.

REFERENCES

Abe, H. (1957) On the chlorite associated with gold ores. Jour. Japan. Assoc. Mineral, Petrol. Econ. Geol., 41, 192-198 (in Japanese with English abstr.).

Akiyama, S. (1980) Geological structure of the Hida metamorphic belt and mineralization of the Kamioka-type ore deposits: Studies on regional geology and mineralization in the Kamioka district. Mining Geol., 30, 345-362 (in Japanese with English abstr.).

Akiyama, S. (1981) Recent information about the mineralization in the Kamioka mining area: Studies on regional geology and mineralization in the Kamioka district. Mining Geol., 31, 157-168 (in Japanese with English abstr.).

Arita, Y. and Wada, H. (1990) Stable isotopic evidence for migration of metamorphic fluids along grain boundaries of marbles. Geochem. Jour., 24, 173-186.

Ballanca, A., Cenisi, P., Salvo, P. Di. and Neri, R. (1984) Textural, chemical and isotopic variations induced by hydrothermal fluids on Mesozoic limestones in northwestern Sicily. Mineral. Deposita, 19, 78-85.

Barbieri, M., Masi, U. and Tolomeo, L. (1984) Strontium geochemical evidence for the origin of the barite deposits from Sardinia, Italy. Econ. Geol., 79, 1360-1365.

Black, M. P. (1984) Oxygen isotope study of metamorphic rocks from the Ouegoa district, New Caledonia. Contrib. Mineral. Petrol., 47, 197-206.

Bottrell, S. H. and Yardley, B. W. D. (1991) The distribution of Fe and Mn between chlorite and fluid: Evidence from fluid inclusions. Geochim. Cosmochim. Acta, 55, 241-244.

Brand, U. and Veizer, J. (1980) Chemical diagenesis of a multicomponent carbonate system - 1: trace elements. Jour. Sediment. Geol., 50, 1219-1236.

Calderoni, G. and Ferrini, V. (1984) Abundances and chemical fractionation of Al, Fe, Mn, Zn, Pb, Cu and Tl in Cretaceous-Paleocene limestones from Gubbio (Central Italy). Geochem. Jour., 18, 31-41.

Cathelineau, M. and Nieva, D. (1985) A chlorite solid solution geothermometer. The Los Azufres (Mexico) geothermal system. Contrib. Mineral. Petrol., 91, 235-244.

Criss, R, E., Fleck, R. J. and Taylor, H. P. J., (1991) Tertiary meteoric hydrothermal systems and their relation to ore deposition, northwestern United States and southern British Columbia. Jour. Geophy. Res., 94, 13335-13356.

Einaudi, M. T. and Burt, D. M. (1982) Introduction, terminology, classification and composition of skarn deposits. Econ. Geol., 72, 764-783.

Einaudi, M. T., Meinert, L. D. and Newberry, R. J. (1981) Skarn deposits: Econ. Geol. 75th Anniv. vol. 317-391.

Faure, G. (1986) Principles of Isotope Geology. Second ed. John Wiley & Sons, New York, 589 p.

Frank, J, R., Carpanter, A.B. and Oglesby, T. W. (1982) Cathodluminescence and composition of calcite cement in Taum Sauk Limestone (Upper Cambrian), southeast Missouri. Jour. Sediment. Petrol., 52, 631-638.

Fu, M., Changkakoto, A., Krouse, H. R., Gray, J. and Kwak, T. A. P. (1991) An oxygen, hydrogen, sulfur, and carbon isotope study of carbonate-replacement (skarn) tin deposits of the Dachang tin field, China. Econ. Geol., 86, 1683-1703.

Fujinuki, T. (1973) Trace elements in carbonate rocks. Mining Geol., 23, 295-306 (in Japanese).

Hama, H., Hashimoto, M. and Doi, S. (1975) The zonal distribution of lead and zinc in the Mozumi mining area, Kamioka mine. Mining Geol., 25, 83-92 (in Japanese with English abstr.).

Hayashi, H. (1961) Mineralogical study on alteration products from altered aureole of some "Kuroko" deposits. Jour. Mineral. Soc. Japan, 5, 101-125 (in Japanese).

Hirokawa, M., Hayashi, K. and Machida, M. (1995) On the exploration of the Sakonishi district in the Kamioka mining area, Gifu Prefecture. Resource Geol., 45, 157-168 (in Japanese with English abstr.).

Iiyama, J. T. and Tamura, M. (1981) Partition of Mg and Fe between chlorite and

hydrothermal solution. Mining Geol., 31, 43 (in Japanese).

Kano, T. (1973) Geological study of the Hida metamorphic belt in the eastern part of Toyama prefecture, central Japan (part1) - On the tectonic division, the characteristics of the Funatsu stage plutonism, and the lithostratigraphic division of the metamorphic rocks.-. Jour. Geol. Soc. Japan., 79, 407-421 (in Japanese with English abstr.).

Kano, T. (1982) Jour. Geol. Soc. Japan., 21, 9-24 (in Japanese with English abstr.).

Kano, T. (1998) Crystalline limestone in the Hida metamorphic complex, central Japan - Geological characteristics, mineral composition, texture and mode of occurrence of dolomite-. Resource Geol., 48, 77-92 (in Japanese with English abstr.).

Kawasaki, M., Yashiro, K. and Yoshimura, F. (1985) Recent exploration of the Mozumi ore deposits in the Kamioka mine - Especially on the relation between fissures and mineralization -. Mining Geol., 35, 145-159 (in Japanese with English abstract).

Keith, M. L. and Weber, J. N. (1964) Isotopic composition and environmental classification of selected limestones and fossils. Geochim. Cosmochim. Acta, 28, 1787-1816.

Keith, M. L., Anderson, G. M. and Eichler, R. (1964) Carbon and oxygen isotopic composition of mollusk shells from marine and fresh-water environments. Geochim. Cosmochim. Acta, 28, 1756-1786.

Kim, K. H. and Nakai, N. (1980) Carbon and oxygen isotope studies of the carbonate rocks from the Shinyemi zinc-lead ore deposits Western Taebaegsan metallogenic belt, Korea. J. Earth Sci. Nagoya Univ., 28, 57-74.

Kitano, Y., Sakata, M. and Matsumoto, E. (1981) Partitioning of heavy metals into mineral and organic fractions in a sediment core sample from Osaka Bay. Jour. Ocean. Soc. Japan. 37, 259-266.

Lepeltier, C. (1969) A Simplified Statistical Treatment of Geochemical Data by Graphical Representation. Econ. Geol., 64, 538-550.

Machida, M., Otsubo, T. and Furuyado, A. (1987) Disseminated type

mineralization in the Tochibora ore deposits, Kamioka mine, Gifu prefecture, Japan. Mining Geol., 37, 119-131 (in Japanese with English abstr.).

Mariko, T., Kawada, M., Miura, M. and Ono, S. (1996) Ore Formation Process of the Mozumi Skarn-type Pb-Zn-Ag Deposits in the Kamioka Mine, Gifu Prefecture, Central Japan - A Mineral Chemistry and Fluid Inclusion Study -. Mining Geol., 46, 337-354.

Marshall, D. J. (1988) Cathodoluminescence of Geological Materials. Allen & Unwin, Winchester, 128p.

Matsuda, T. and Okada, A. (1968) Active fault. Quat. Research., 7, 188-199.

Matsuhisa, Y., Imaoka, T. and Murakami, N. (1980) Hydrothermal activity indicated by oxygen and hydrogen isotopes of rocks and minerals from a Paleogene cauldron, Southwest Japan. Mining Geol., Spec.Issue, 8, 49-65.

Meinert, L. D. (1992) Skarn and Skarn Deposit. Geoscience Canada, 19, 145-162.

MMAJ (1994) Report for detailed Geological Survey "Hida region" during the 1993 Fiscal Year. 105 p. (in Japanese).

MMAJ (1996) Report for detailed Geological Survey "Hida region" during the 1995 Fiscal Year. 158 p. (in Japanese).

MITI. (1978) Report on the Regional Geological Survey "Hida region" during the 1977 Fiscal Year. 104p . (in Japanese).

MITI (1982) Report on the Regional Geological Survey "Hida region" during the 1981 Fiscal Year. 38 p. (in Japanese).

MITI (1996) Report on the Regional Geological Survey "Hida region" during the 1995 Fiscal Year: Projects for Structural Analysis. 158 p. (in Japanese).

MITI (1997) Report on the Regional Geological Survey "Hida region" during the 1996 Fiscal Year. 127 p. (in Japanese).

MITI (1998a) Report on the Regional Geological Survey "Hida region" during the 1997 Fiscal Year: Projects for Structural Analysis. 198 p. (in Japanese).

MITI (1998b) Report on the Regional Geological Survey "Hida region" during the 1997 Fiscal Year. 45 p. (in Japanese).

Miyahisa, M., Harada, S., Ishibashi. K., Shibuya, G. and Motomura, Y. (1975)

Kutnahorite from Hoei tin mine, with special concern to its chemical composition and mineral paragenesis. Mining Geol. 25, 347-357 (in Japanese with English abstr.).

Miyazawa, T. (1958) Occurrence and characteristics of Mn-Fe dolomite in the Daikoku deposit of the Chichibu mine. Memorial volume dedicated to Prof. Fujimoto, N. on the occasion of his retirement. 467-477 (in Japanese).

Musashino, M., (1973) Lithofacies and chemical composition of the Carboniferous Nagaiwa limestone, northeast Japan. Jour. Geol. Soc. Japan. 79, 481-492 (in Japanese with English abstr.).

Nagasawa, K., Shirozu, H. and Nakamura, T. (1976) Clay minerals as constituents of hydrothermal metallic vein-type deposits. Mining Geol. Spec. Issue, 7, 75-84 (in Japanese with English abstr.).

Nagasawa, K. and Shibata, K. (1986) K-Ar ages of sericites from the Kamioka mine and its significance in geochronology of the Kamioka deposits. Mining Geol., 35, 57-65 (in Japanese with English abstr.).

Naito, K., Fukahori, Y., He, P. M., Sakurai, W., Shimazaki, H. and Matsuhisa, Y. (1995) Oxygen and carbon isotope zonations of wall rocks around the Kamioka Pb-Zn skarn deposits, central Japan: Application to prospecting. Jour. Geochem. Exploration, 54, 199-211.

Nakamura, K. and Shimazaki, H. (1987) Geology and mineralization of the Nakatenjo ore deposit in the Nakatatsu area - zonal arrangement of skarn and ore minerals-. Mining Geol., 37, 237-252 (in Japanese with English abstr.).

Nakano, T. (1998) Pyroxene geothemistry as an indicator for skarn metallogenesis in Japan. Mineral. Assoc. Canada Short Course vol. 26, 147-167.

Nakano, T., Yoshino, T. and Nishida, N. (1991) Rapid analytical method for trace Zn contents in some mafic silicates using the electron microprobe: Potential utility as a metallogenetic and petrogenetic indicator. Chemical Geol., 89, 379-389.

Nakano, T., Yoshino, T. and Shimazaki, H. and Shimizu, M. (1994) Pyroxene composition as an indicator in the classification of skarn deposits. Econ. Geol.,

89, 1567-1580.

Nesbitt, B. E. (1996) Applications of oxygen and hydrogen isotopes to exploration for hydrothermal mineralization. SEG Newsletter, 27, 1-13.

Nishikawa, Y. and Tochimoto, K. (1985) Pb-Zn mineralization controlled by geological features in the Nakatatsu skarn-type ore deposit, Fukui Prefecture. Mining Geol., 35, 161-177 (in Japanese with English abstr.).

Nitta, T., Fukabori, Y. and Mishima, H. (1971) On the successful exploration at the lower part of the Mozumi mining area, the Kamioka mine (No.2). Mining Geol., 21, 20-32 (in Japanese with English abstr..

Nozawa, T., Kawata, K. and Kawai, M. (1975) Quadrangle series, geology of the Hida-Furukawa district. Geological Surv. Japan (in Japanese with English abstr.).

Oinuma, K. and Kobayashi, K. (1965) Some problems concerning clay mineralogical study on sedimentary rocks. Nendokagaku no Shinpo, 5, 77-84 (in Japanese with English abstr.).

Otsu, H., Kubota, R. and Matsuda, Y. (1984) Partition of statistical frequency distribution of geochemical data. Mining Geol., 34, 51-56 (in Japanese with English abstr.).

Pingitore, N. E., Merrzner, G. and Love, K. M., (1995) Identification of sulfate in natural carbonates by X-ray absorption spectroscopy. Geochim. Cosmochim. Acta, 59, 2477-2482.

Reeder, R. J. (1996) Interaction of divalent cobalt, zinc, cadmium, and barium with the calcite surface during layer growth. Geochim. Cosmochim. Acta, 60, 1543-1552.

Sakai, S. (1963) Study on zonal distribution of ore deposits in Kamioka. Mining Geol., 13, 115-120 (in Japanese with English abstr.).

Sakamoto, T. and Sudo, T. (1956) Magnesium-rich chlorite from the Wanibuchi mine, Shimane Prefecture. Mineral. Jour., 1, 348-358.

Sakurai, W. and Shimazaki, H. (1993) Exploration of blind skarn deposits based on the mineralization model of the Kamioka Mine, Gifu Prefecture, central Japan.

Resource Geol. Special Issue, 16, 141-150.

Sakurai, W. and Shiokawa, S. (1993) K-Ar ages of the dike rocks in the Kamioka Pb-Zn skarn deposits in the Hida terrain, Japan. Resource Geol., 43, 311-319 (in Japanese with English abstr.).

Sakurai, W., Nishida, Y. and Mizuyachi, O. (1993) On the exploration of the Atotsugawa district in the Kamioka mining area, central Japan. Resource Geol., 43, 79-91 (in Japanese with English abstr.).

Sasaki, A., Sato, K. and Cumming, L. G. (1982) Isotopic composition of ore lead from the Japanese islands. Mining Geol., 32, 457-474 (in Japanese with English abstr.).

Sato, K. and Uchiumi, S. (1990) K-Ar ages and mineralization of the Kamioka Pb-Zn skarn deposit in the Hida terrain, Japan. Mining Geol., 40, 389-396 (in Japanese with English abstr.).

Savard, M. M., Veizer, J. and Hinton, R. (1995) Cathodluminescence at low Fe and Mn concentrations. A SIMS study of zones of natural calcite. Jour. Sediment. Res., A65, 208-213.

Sawai, O. (1984) Wall rock alteration around the Motoyama deposits, Toyoha mine, Hokkaido, Japan. Mining Geol., 34, 173-186 (in Japanese with English abstr.).

Sawai, O. (1986) The distribution of alteration zones in the eastern area of the Toyoha mine, Hokkaido, Japan. Mining Geol., 36, 273-288 (in Japanese with English abstr.).

Sawai, O. (1988) Wall rock alteration of the Chiemon vein in the Akenobe mine, Hyogo Prefecture. Mining Geol., Spec. Issue, 12, 23-35.

Schuiling, R. D. and Oosterom, M. G. (1966) The metamorphic complex on Naxos (Greece) and the strontium and barium content of its carbonate rocks. Proc. Kon. Ned. Akad. Wetensch. B69, 166-175.

Shieh, Y. N. and Taylor, H. P. Jr. (1969) Oxygen and carbon isotope studies of contact metamorphism of carbonate rocks. Jour. Petrol., 10, 307-331.

Shikazono, N. and Kawahata, H. (1987) Compositional differences in chlorite from

hydrothermally altered rocks and hydrothermal ore deposits. Canadian Mineral., 25, 465-474.

Shimazaki, H. (1984) Genesis of so-called Inishi rock in the Kamioka mining area, Gifu Prefecture (abstract). Mining Geol., 34, 70-71 (in Japanese).

Shimazaki, H., Shimizu, M. and Nakano, T. (1986) Carbon and oxygen isotopes of calcites from Japanese skarn deposits. Geochem. Jour., 20, 297-310.

Shimazaki, H. and Kusakabe, M. (1990a) Oxygen isotope study of the Kamioka Zn-Pb skarn deposits, central Japan. Mineral. Deposita, 25, 221-229.

Shimazaki, H. and Kusakabe, M. (1990b) D/H ratios of sericites from the Kamioka Mining Area. Mining Geol., 40, 385-388 (in Japanese with English abstr.).

Shimizu, M. and Shimazaki, H. (1981) Application of the sphalerite geobarometer to some skarn-type ore deposits. Mineral. Deposita, 16, 45-50.

Shimizu, M. and Iiyama, J. T. (1982) Zinc-lead skarn deposits of Nakatatsu mine, central Japan. Econ. Geol., 77, 1000-1012.

Shiobara, K. (1961) Decrepitation temperatures and chemical characteristics of the mineral species from the Kamioka mine. Mining Geol., 11, 344-349 (in Japanese with English abstr.)

So, C., Yum, S. and Koh, Y. (1993) Mineralogy, fluid inclusion, and stable isotope evidence for the genesis of carbonate-hosted Pb-Zn(-Ag) orebodies of the Taebaek deposit, Republic of Korea. Econ. Geol., 88, 855-872.

Sohma, T. and Akiyama, S. (1984) Geological structure and lithofacies in the central part of the Hida metamorphic belt. J. Geol. Soc. Japan, 90, 609-628 (in Japanese with English abstr.).

Sverjensky, D. A. (1985) The distribution of divalent trace elements between sulphides, oxides and hydrothermal solution: I Thermodynamic basis. Geochim. Cosmochim. Acta, 49, 853-864.

Takahashi, H. (1988) Wall-rock alteration and ore-formation model of Hosokura Pb-Zn ore deposits, Japan. Mining Geol., 38, 335-346 (in Japanese with English abstr.).

Takeno, N. and Iiyama, J. T. (1983) Alteration around granite porphyry in the

Tochibora and Maruyama deposits, Kamioka mine. Mining Geol., 33, 305-316 (in Japanese with English abstr.).

Taylor, B. E. and O'Neil, J. R. (1977) Stable isotope studies of metasomatic Ca-Fe-Al-Si skarn and associated metamorphic and igneous rocks, Osgood Mountains, Nevada. Contrib. Mineral. Petrol., 63, 1-49.

Taylor, H. P. Jr. (1973) $^{18}O/^{16}O$ evidence for meteoric-hydrothermal alteration and ore deposition in the Tonopah, Comstock lode, and Goldfield mining district, Nevada. Econ. Geol., 68, 747-764.

Wada, H. (1978) Carbon isotopic study on graphite and carbonate in the Kamioka mining district, Gifu prefecture, central Japan, in relation to the role of graphite in the pyrometasomatic ore deposition. Mineral. Deposita, 13, 201-220.

Walshe, J. L. (1986) A six-component chlorite solid solution model and the conditions of chlorite formation in hydrothermal and geothermal systems. Econ. Geol., 81, 681-703.

Yokoyama, K., Matsubara, S., Saito, Y., Chiba, T. and Kato, A. (1993) Analyses of Natural Minerals by Energy-dispersive Spectrometer. Bull. Nation. Sci. Museum, Tokyo, Ser. C, 19, 115-126.

Yoneda, T. (1989) Chemical composition of chlorite with special reference to the iron vs. manganese variation, from some hydrothermal vein deposits, Japan. Mining Geol., 39, 393-401.

Yui, S. (1968) Results of equilibrium calculations on the reaction between graphite and a H_2O-CO_2 fluid at 300-500°C and 100-2000 bars, and its implication to relict graphite in pyrometasomatic ore deposits. J. Mining Coll. Akita Univ., Series A, IV, 29-39.

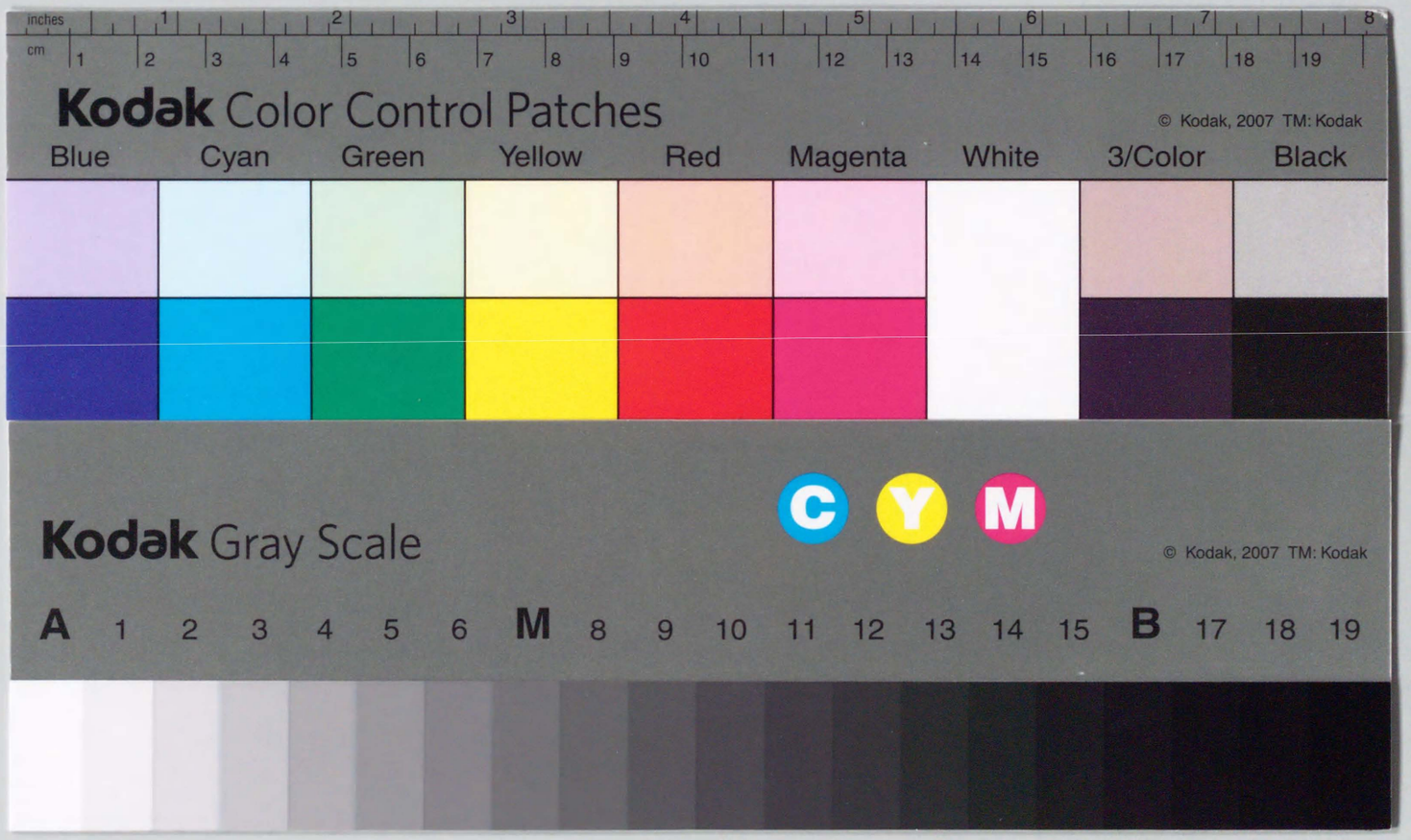
inches
cm
Kodak Color Control Patches
© Kodak, 2007 TM: Kodak
Blue
Cyan
Green
Yellow
Red
Magenta
White
3/Color
Black
Kodak Gray Scale
C
Y
M
© Kodak, 2007 TM: Kodak
A 1 2 3 4 5 6 M 8 9 10 11 12 13 14 15 B 17 18 19